

 Open access • Journal Article • DOI:10.1021/CR500488P

Theoretical Chemical Kinetics in Tropospheric Chemistry: Methodologies and Applications — [Source link](#)





Luc Vereecken, David R. Glowacki, Michael J. Pilling

Institutions: Max Planck Society, University of Leeds

Published on: 06 Apr 2015 - Chemical Reviews (American Chemical Society)

Related papers:

- [Direct Kinetic Measurements of Criegee Intermediate \(CH₂OO\) Formed by Reaction of CH₂I with O₂](#)
- [Theoretical studies of atmospheric reaction mechanisms in the troposphere](#)
- [The M06 suite of density functionals for main group thermochemistry, thermochemical kinetics, noncovalent interactions, excited states, and transition elements: two new functionals and systematic testing of four M06-class functionals and 12 other functionals](#)
- [The gas-phase ozonolysis of unsaturated volatile organic compounds in the troposphere.](#)
- [Direct measurements of conformer-dependent reactivity of the Criegee intermediate CH₃CHOO](#)

Share this paper:    

View more about this paper here: <https://typeset.io/papers/theoretical-chemical-kinetics-in-tropospheric-chemistry-2fj0c3sq9y>



Vereecken, L., Glowacki, D. R., & Pilling, M. J. (2015). Theoretical chemical kinetics in tropospheric chemistry: methodologies and applications. *Chemical Reviews*, 115(10), 4063-4114.
<https://doi.org/10.1021/cr500488p>

Peer reviewed version

Link to published version (if available):
[10.1021/cr500488p](https://doi.org/10.1021/cr500488p)

[Link to publication record in Explore Bristol Research](#)
PDF-document

This is the accepted author manuscript (AAM). The final published version (version of record) is available online via American Chemical Society at <http://dx.doi.org/10.1021/cr500488p>. Please refer to any applicable terms of use of the publisher.

University of Bristol - Explore Bristol Research

General rights

This document is made available in accordance with publisher policies. Please cite only the published version using the reference above. Full terms of use are available:
<http://www.bristol.ac.uk/red/research-policy/pure/user-guides/ebr-terms/>

Theoretical Chemical Kinetics in Tropospheric Chemistry: Methodologies and Applications

Luc Vereecken,¹ David R. Glowacki^{2,3,4,5} and Michael J. Pilling⁶

1. Max Planck Institute for Chemistry, 55218 Mainz, Germany
2. PULSE Institute and Dept of Chemistry, Stanford University, Stanford, CA 94305, USA
3. SLAC National Accelerator Laboratory, Menlo Park, California 94025, USA
4. School of Chemistry, University of Bristol, Bristol, BS8 1TS, UK
5. Department of Computer Science, University of Bristol, BS8 1UB, UK
6. School of Chemistry, University of Leeds, Leeds, LS2 9JT, UK

Table of Contents

1. Introduction	5
2. Methodologies for Theoretical Kinetics.....	8
2.1. Overview	8
2.2. Electronic Structure Calculations.....	12
2.2.1. Basis Sets.....	14
2.2.2. Single Reference <i>Ab Initio</i> Methods	16
2.2.3. Multi-reference <i>Ab Initio</i> Methods.....	19

2.2.4. Density Functional Methods	22
2.2.5. Semi-empirical Methods	24
2.2.6. Composite Methods.....	26
2.2.7. Excited State Electronic Structure Methodologies.....	28
2.3. Statistical Rate Theories	32
2.3.1. Molecular Degrees of Freedom.....	35
2.3.1.1. Molecular translation and rotation	36
2.3.1.2. Vibrational Modes	37
2.3.1.3. Treating Internal Rotations.....	40
2.3.2. Canonical Transition State Theory	44
2.3.3. Microcanonical Transition State Theory	48
2.3.4. Variational Calculations	50
2.3.5. Tunneling.....	54
2.3.6. Multi-surface Reactions	56
2.4. Pressure-dependent Reactions	59
2.4.1. Interaction of Reaction and Collisional Energy Transfer.	59
2.4.2. Modelling Collisional Energy Transfer	60
2.4.3. Modelling Pressure Dependent Reactions.....	63
2.5. Dynamics.....	76
2.6. Product Energy Distributions	82
2.7 State of the Art.....	83
3. Thermodynamics.....	85

4. Reactions of OH Radicals	87
4.1. OH + H ₂ , CH ₄	88
4.2. OH + CO	89
4.3. OH + C ₂ H ₄	90
4.4. OH + (CH ₃) ₂ CO, CH ₃ OH.....	93
4.5. OH + Terpenoids	95
5. Peroxy Radical Chemistry.....	96
5.1. Peroxy Radicals in Atmospheric Chemistry and Combustion	96
5.2. Oxidation of Acetylene.....	102
5.3. Residual Energy in Reactions of Peroxy Radicals with NO	107
5.4. Peroxy Radicals from Aromatics.....	108
5.5. Isoprene	113
5.6. Formation of Secondary Organic Aerosol.....	116
6. Criegee Intermediates.....	119
6.1. Carbonyl Oxide Wavefunction	119
6.2. Sources of CI.....	120
6.2.1. Ozonolysis	121
6.2.2. Other Sources of CI.....	123
6.3. Criegee Intermediate Spectra	124
6.4. Criegee Intermediate Unimolecular Reactions	125
6.4.1. <i>Syn/Anti</i> Isomerisation.....	125
6.4.2. Acid/Ester Channel.....	128

6.4.3. Vinylhydroperoxide Channel	129
6.4.4. Other Unimolecular Reactions	130
6.5. Criegee Intermediate Bimolecular Reactions.....	132
6.5.1. The Reaction with SO ₂	132
6.5.2. The Reaction with H ₂ O and (H ₂ O) ₂	133
6.5.3. The Reaction with Organic Acids and Carbonyl Compounds	135
6.5.4. The Reaction with Alkenes.....	137
6.5.5. The Reaction with NO _x	138
6.5.6. The Reaction with CO	138
6.5.7. The Reaction with RO ₂ and HO ₂	138
6.5.8. The Reaction with O ₃	139
6.5.9. The CH ₂ OO+CH ₂ OO Reaction	140
6.6. The Fate of CI in the Atmosphere	140
7. Predictive Correlations and Structure-Activity Relations.....	141
8. Construction of Oxidation Mechanisms.....	144
9. Automated Chemical Process Discovery	146
10. Future Directions.....	147
Author Information	149
Acknowledgements	151
References	152

1. Introduction

Chemical kinetics is central in much of tropospheric chemistry and in modelling tropospheric chemical processes. Chemical reaction rate coefficients and product yields have traditionally been obtained experimentally,^{1,2} have been estimated using structure activity relations³ or have simply been guessed. The large number of organic compounds emitted to the atmosphere and the massive number of reactions involved in their oxidation makes experimental measurement of even a small fraction of them a daunting task. In recent years, theoretical chemistry has begun to contribute substantially to our understanding of a number of important reactions and reaction sequences in the atmosphere. These contributions have, at their heart, the use of electronic structure calculations to determine the energies and other characteristics (geometries and vibrational frequencies) of transition states (TS) in reactions, which are then used in theoretical frameworks, such as transition state theory, to determine rate coefficients. The main factor limiting the accuracy of this process is the uncertainty in the transition state energy: for small molecules with reasonably well-behaved wave functions, it is becoming increasingly common for this to be on the order of “chemical accuracy” – i.e., 1 kcal mol⁻¹, or ~ 4 kJ mol⁻¹. When incorporated in the Arrhenius expression, this translates to an uncertainty of a factor of 5 in the rate coefficient at 298K. Much greater accuracies are possible with higher levels of theory, but are generally restricted to reactions of small molecules, with less than 6 to 8 non-hydrogen atoms. A second important factor affecting the uncertainty is the prediction of the change of entropy, in particular for molecules that cannot be described in terms of simple harmonic oscillators, owing, for example, to the presence of internal rotors or other anharmonicities as discussed later in this review. Transition states are generally harder to describe adequately, and unfortunately benchmark calculations and comparison to reference experimental data is mostly performed on stable species, such that it is not

always clear how accurately the TS is described.

Predictive accuracy is, therefore, limited, especially for reactions of larger molecules having 10 or more non-hydrogen atoms such as biogenic hydrocarbons; here, the barrier height accuracies can be considerably worse than 4 kJ mol^{-1} , and often extensive non-harmonic effects on the entropy are at play. Nevertheless theory plays an increasingly important and central role in atmospheric chemical kinetics. It can provide a route to improved structure activity relations⁴ especially when combined with experiment to adjust transition state energies. It can give new and quantitative insights into reaction mechanisms, especially when stimulated by results of field experiments and combined with laboratory experiments as in the recent developments in our understanding of isoprene oxidation.⁵

There are close relations between the oxidation of organic compounds in the atmosphere and in combustion. The experimental techniques used to measure rate coefficients are similar, at least up to $\sim 1000 \text{ K}$, but the conditions of temperature and pressure required for combustion applications can be difficult to reproduce in the laboratory, so that some form of extrapolation is frequently needed to provide the rate data needed. As a result, theory coupled to experiment is often more necessary in combustion than in atmospheric chemistry. The role of theory in combustion is further strengthened by the higher temperatures involved: at 1000 K the Arrhenius uncertainty is only $\sim 60\%$. This closer and longer-standing involvement of theoretical kinetics in combustion has resulted in the development of a range of techniques and of chemical understanding⁶ that are proving beneficial in atmospheric chemistry. Indeed the realization that there is a continuum of mechanistic understanding and quantitative kinetics across combustion and atmospheric chemistry is an important thread in the development of both areas. Recent advances in the experimental and theoretical understanding of Criegee intermediates derive from important instrumental developments at the Advanced Light Source

in Berkeley, aimed initially at combustion chemistry.^{7,8} The assessment and tuning of calculated rate coefficients, e.g for H abstraction by OH, invariably span low temperature atmospheric conditions and high temperature combustion conditions. New understanding of peroxy radical chemistry in the atmosphere builds on developments in combustion chemistry.⁹

We have aimed, in this review, to provide an understanding of the basis of theoretical chemical kinetics in an atmospheric, and primarily tropospheric, context. We have deliberately avoided mathematical developments; rather we have stressed the physicochemical foundation in qualitative terms, emphasizing the basis of the techniques used and their limitations. The review is far from exhaustive in its coverage, or in its selection of topics, because of these objectives. For example, we have not included any discussion of photochemistry.

At the heart of the review is an outline of the underlying theory. We first discuss electronic structure calculations, concentrating on *ab initio* and density functional theories (Section 2.2). We examine the basis, applicability and accuracy of the methods available and explain the origins and uses of the sometimes bewildering array of acronyms and methods. We then summarise the basis of statistical rate theories (Section 2.3) including transition state theory and RRKM theory, briefly extending the basic theories to include variational effects, quantum mechanical tunnelling and reactions on multiple potential energy surfaces. Pressure dependent reactions and the use of master equation methods are discussed in Section 2.4 followed by brief sections on dynamics, an important complement to statistical rate theories with the potential, not yet fully realized and still in its initial stages, for application in atmospheric chemistry (2.5). Dynamics are also well-suited to studying product energy distributions (2.6), which are often more accessible to theory than to experiment.

The rest of the review is devoted to applications. The accuracy of thermodynamic quantities, such as enthalpies of formation has been revolutionised, especially for relatively small molecules, by *ab initio* calculations and by the use of thermochemical networks (Section 3). The determination of rate coefficients for reactions of OH with organic compounds (Section 4) is a natural home for many of the techniques discussed in Section 2. Our understanding of peroxy radical chemistry (Section 5) has become much richer in recent years, although many uncertainties and areas of potential development remain. Carbonyl oxides (Criegee intermediates, Section 6) provide another topic in which current interest is intense and in which theory has helped to reveal the detail of the chemistry. The development of structure activity relations (Section 7) and the construction of oxidation pathways, where we concentrate on terpene chemistry, (Section 8) are outlined. The review ends with very brief comments on automatic process discovery (Section 9) – methods for automatically generating oxidation mechanisms or components of them – and on future directions in theoretical kinetics (Section 10).

2. Methodologies for Theoretical Kinetics

2.1. Overview

The theoretical prediction of rate coefficients and product distributions, as a function of the reaction conditions such as temperature, pressure, and reaction mixture, requires linking of the fundamental, microscopic molecular properties to the macroscopic, phenomenological world. The kinetic characterization of a reaction thus requires a number of steps which together allow a quantification of the rate parameters; the accuracy of these predictions depends on the computational rigor applied to each individual step.

Overall, we distinguish the following methodological stages in a theoretical kinetic

investigation: (a) characterization of the molecules at a fundamental level involving a quantum chemical description of the potential energy surface (PES) and yielding relative energies, the characteristics of the molecular degrees of freedom, and other fundamental properties; (b) a quantification of the quantum state density of reactants and transition state(s), by an energy-dependent description of the molecular degrees of freedom and their interaction; (c) calculation of the energy- or temperature-dependent rate coefficients, incorporating quantum effects like tunneling and potential energy surface crossings; (d) temperature- and pressure-dependence of the overall, macroscopic rate coefficients as determined by the interaction of the microscopic, energy-specific reaction rates against the macroscopic reaction environment including effects of collisional energy transfer, the reaction initiation process, loss processes, etc. For tropospheric chemistry, a temperature range from 200 to 400K is sufficient, and a pressure range from 1 atm down to 0.2 atm, although it is often useful to extend calculations outside this range.

From the four stages above, we aim to obtain an in-depth understanding of the reaction process, and provide a theory-based set of kinetic parameters that allow facile incorporation of the individual reactions into larger kinetic models describing a practical chemical system. Each of the stages is described in more detail below, emphasizing the state of the art and current challenges. It is worth noting that there are two main approaches in theoretical kinetics: a statistical approach which typically derives kinetic parameters from the characterization of the critical points on the PES, i.e. reactants, transition states, intermediates and occasionally reaction products, and a dynamical approach that describes the time-dependent movements of the reaction ensemble across the PES. In fact, the two approaches are linked, with the statistical approach making the assumption that both energy and molecular motion are suitably randomized on the dynamical timescales which characterize typical

reactive events.¹⁰ Both the dynamical and the statistical approaches have their strengths and weaknesses, which will be briefly discussed. In the dynamical approach, the different stages described above are blended together; we first describe the statistical approach where each step is more separable.

To guide the readers' thoughts we will use two example reactions throughout this methodology section; these reactions illustrate most of the challenges encountered in a theoretical kinetic analysis, while still being relevant in practical atmospheric applications. The first reaction is the H-abstraction from glycolaldehyde by OH radicals. A stylized PES is shown in Figure 1, where the main features are (a) the formation of a pre-reactive complex, (b) reaction via a TS that is either protruding or submerged, i.e. it lies respectively above or below the energy level of the free reactants, (c) tunneling of the H-atom during the H-abstraction process, and finally (d) further reaction by dissociation of one (or more) of the reaction products. A second example is the reaction of Criegee intermediates with SO₂ molecules, of importance in the formation of aerosol seed particles in the troposphere. A stylized PES is shown in Figure 2, where the main features are (a) a barrierless entrance channel, (b) the possibility for collisional energy loss of intermediates that affect the impact of competing exit channels, and (c) internal rotations in the intermediates.

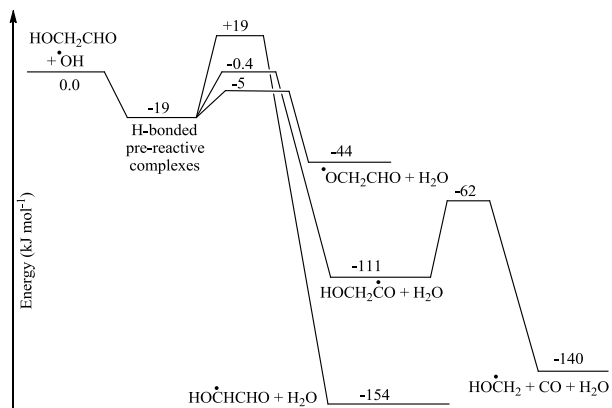


Figure 1. Simplified potential energy surface for the reaction of glycolaldehyde with OH radicals, based on Galano *et al.*,¹¹ Méreau *et al.*,¹² and Viskolcz and Bérces.¹³

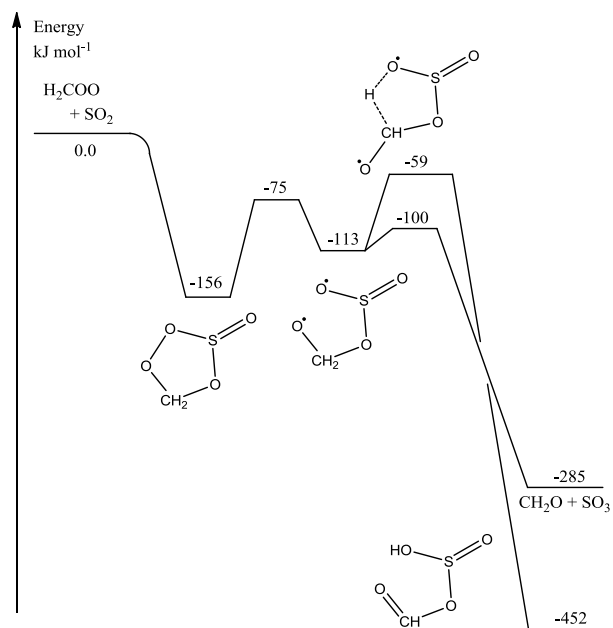


Figure 2. Simplified potential energy surface for the reaction of carbonyl oxides, CH₂OO, with

SO₂, based on Vereecken *et al.*¹⁴

2.2. Electronic Structure Calculations

The quantum chemical characterization of potential energy surfaces (PES) is a mature but active field of research, whose in-detail discussion is outside the scope of this review. Here, we will only touch upon the principal aspects of this PES characterization in as much as they are relevant to theoretical kinetics; the reader is referred to the many excellent books and reviews on quantum theory for further information.^{15–26}

Quantum chemical calculations can typically be divided into three categories: (a) *ab initio* calculations based on a wavefunction description of the molecules, (b) Density Functional Theory (DFT) based on a description of the electron density in a molecule, and (c) semi-empirical calculations that involve using parameterized force fields. *Ab initio* calculations which utilize sophisticated treatments of electronic correlation provide the most accurate results and support the widest set of chemical problems, but often carry a high computational cost. DFT methods are less costly to execute, and in recent years their accuracy has improved dramatically, but DFT methods tend to be highly parametrized because they rely on a so-called 'exchange-correlation' functional, the exact form of which is unknown. Finally, semi-empirical calculations are very fast, but are typically only valid for description of the properties to which the force field has been designed. Within each of these categories, a plethora of methodologies exists, each balancing computational cost against rigor, generality, and completeness of the description of the quantum system as a function of the desired properties. There is a hierarchy in these methodologies, allowing progressive and systematic

improvements on the quality of the predictions, though often at increasing computational cost; for DFT methods this hierarchy was dubbed Jacob's Ladder by Perdew *et al.*²⁷ To keep the calculations tractable, virtually all methodologies rely on the Born-Oppenheimer approximation, where the time-dependent Schrödinger equation is approximated by separating the electronic equation from the nuclear equations, effectively describing the adjustments of the electronic wavefunction as instantaneous compared to the timescale of the motion of the atom nuclei.

Pragmatically, theoretical kinetic studies use a combination of the available methodologies, dependent on the problem at hand, and aiming to provide the best estimates possible within the available time and computational capabilities. Statistical rate theory applications usually choose DFT for most properties (geometries, vibrational frequencies) enhanced with *ab initio* calculations for more accurate estimates of e.g. relative energies. Molecular dynamics studies typically employ semi-empirical and recently more DFT-based approaches to offset the computational cost of their highly detailed description of the reaction dynamics.

Quantum chemical theories yield the properties of a single structure at a time. To obtain the critical points on a potential energy surface, i.e. reactants, TS and products, the geometries are optimized from a starting guess by optimizing this geometry with respect to the predicted energy (e.g. minimization of energy for reactants and products) and shape of the PES (1st order saddle points for TS). First-order (gradient), second order (hessian) and higher-order derivatives of the potential energy surface give information on the shape of the PES around the geometry studied. Typically, one obtains the harmonic frequencies for molecular vibrations from the hessian, anharmonicity constants from 3rd- and 4th-order derivatives of the PES, and information on hindered internal rotors by projection of the hessian on appropriate internal rotation coordinates. This is usually sufficient to describe the

rovibrational characteristics for statistical analysis.

If a reactant or a TS has multiple conformers, isomers, or enantiomers, these need to be characterized individually, though for statistical rate analysis one can also approximate their properties by extrapolation from a (set of) reference structures. For some types of kinetic calculations, including for more elaborate treatments of tunneling, it is necessary to have information on geometries along the reaction coordinate of a reaction. These minimum-energy paths (MEP) are obtained from quantum chemical intrinsic reaction coordinate (IRC) calculations^{28,29} which follow a steepest descent path on the PES from the TS down towards reactants and products (and thereby also confirm the start- and endpoints of the reaction); the geometries encountered along this MEP can then be further analyzed quantum chemically and incorporated in the rate theory.

Some reactions proceed by so-called “surface hopping”, where the reacting ensemble does not stay on a single adiabatic PES, but rather transfers from one surface to another. Examples include intersystem crossing (ISC) between singlet and triplet potential energy surfaces, or transitions between electronic states in photochemical relaxation processes. To calculate the probability of non-adiabatic surface hopping, multi-state calculations are necessary that characterize the coupling at the minimum energy crossing point (MECP) of the crossing seam or the conical intersection between the two surfaces involved (see section 2.2.7).

2.2.1. Basis Sets

To represent the electronic wavefunction in *ab initio* calculations, or the electron density in DFT calculations, quantum chemical programs use linear combinations of a set of orthonormal functions, called basis functions, in a predefined basis set. The number of basis functions in a basis set

can range from only a handful to hundreds per atom. In principle, the functions can take any of a variety of forms, but for computational chemistry on molecules it is convenient and more efficient to use basis functions that mimic atomic orbitals. The higher the number of basis functions in a basis set, the more flexibly the electron positions can be described, reaching the infinite basis set limit when the basis set no longer imposes restrictions on the description of the electronic wavefunction or density. To obtain the wavefunction, one optimizes the coefficients in the linear combination of basis functions such that the electronic energy is minimized. Obviously, the larger the basis set, the better the description, but the more computationally costly the optimization process and any further energy corrections based on this wavefunction. Using too small a basis set can induce a so-called basis set superposition error (BSSE).³⁰ For example, when CH₂OO intermediates react with SO₂ forming a cyclic adduct, the electrons in the previously separated CH₂OO and SO₂ moieties have access to the basis functions of the other moiety. This allows additional optimization of the wavefunction, thus inducing an additional lowering of the predicted adduct energy by enlargement of the accessible set of basis functions.

Many basis sets are available; the choice of basis set should balance computational cost against accuracy consideration. An early choice of basis functions were the Slater-type orbitals, which show radial behavior similar to H-atom atomic orbitals, but have no angular dependence. Later, it was realized that large gains in computational efficiency could be made by using Gaussian functions; these Gaussian type orbitals are the most common choice in current quantum chemical programs. Pople basis sets, such as 6-31G(d,p) or 6-311++G(2df,2pd),^{17,31} predefine combinations of Gaussian functions which describe for each atom type their core orbitals, valence orbitals, and optionally polarization orbitals, and diffuse orbitals for long-range interactions. Dunning correlation-consistent basis sets,³²⁻³⁶

e.g. cc-pVDZ or aug-cc-pVTZ, are furthermore designed to converge to the complete basis set limit in a systematic series; here too,^{34,37,38} one can optionally add diffuse functions for long-range interactions. Other basis set types exist but are in less common use in theoretical atmospheric chemistry.

For basis sets designed to systematically converge to the complete basis set (CBS) limit, it is possible to estimate the CBS limit by an extrapolation of the results for two or more basis sets in the series.^{25,39-47} How quickly a series converges to the CBS limit depends not only on the basis sets but also on the methodology used; asymptotic convergence is typically of the third order, $\sim l^3$, of the highest orbital angular momentum quantum number l in the basis set.

2.2.2. Single Reference *Ab Initio* Methods

The most basic approach for *ab initio* calculations is the Hartree-Fock (HF) method, which approximately accounts for the potential and kinetic energy of the electrons in a multi-electron system around a set of atomic nuclei, as well as the exchange energy induced by the quantum chemical Fermion character of electrons. These calculations are straightforward, requiring minimization of the energy of the wavefunction by optimizing the coefficients describing the wavefunction as a linear combination of basis set functions. This optimization is typically done in an iterative manner, leading to a self-consistent field (SCF) where the energetically most favorable spin orbitals contain the electrons, and the remaining linear combinations of the basis set functions are unoccupied, so-called virtual spin orbitals. For computational efficiency, restricted HF (RHF) calculations for closed-shell molecules force the electrons of opposite spin to have the same spatial wavefunction. Unrestricted Hartree-Fock (UHF) allows the α - and β -spin electrons to have a different spatial distribution, which also allows for the description of open-shell species, such as radicals that have a differing number of α - and β -spin

electrons and (singlet) biradicals. Optimization by UHF leads to wavefunctions that are eigenfunctions of the per-electron Hamiltonian, but where the overall wavefunction might not be an eigenfunction of the global spin-operator. In such a case we get spin contamination where the UHF solution is a mixture of the desired spin state (e.g. doublet for a radical) and higher spin states; this leads to inaccuracies in the predictions. Restricted open-shell HF (ROHF) improves upon UHF by restricting overall spin, eliminating the spin-contamination problem. Various quantum chemical methodologies suffer in different degrees from spin-contamination problems; advanced methodologies that build upon a spin-contaminated HF wavefunction might not be able to fully correct for the incorrect reference wavefunction.

The Hartree-Fock method neglects how electrons interact through correlation, i.e. it describes each electron as moving through a mean field created by all other electrons, but not how two electrons interact at each instant, e.g. by Coulomb repulsion causing spatial avoidance. Post-Hartree-Fock methods aim to describe this missing correlation energy. Configuration interaction (CI) allows for a complete description of the correlation energy, within the limits of the Born-Oppenheimer approximation and the size of the basis set. It expands the SCF wave function into a linear combination of configuration state functions, i.e. electronic states where a number of electrons are promoted from their ground state orbital to a virtual orbital. The set of configuration state functions where a single electron is promoted, describe so-called single-excitation determinants, changes of two orbitals describe double excitations, and so on. The coefficients in the CI linear combination are then optimized, such that the additional flexibility in describing the wavefunction allows for the required electron correlation. If all possible excitations are included, we obtain the full-CI result (FCI). Unfortunately, this is computationally prohibitively expensive for all but the smallest of molecules and

basis sets. Because of this, the CI expansion is typically truncated after a few terms, e.g. CISD includes only single and double excitations. Coupled-cluster treatments (CC) such as CCSD,⁴⁸ QCISD(T)⁴⁹ and CCSD(T)^{50,51} represent a similar approach, but generate their excitations based on an exponential operator form. Given that exponential functions can be written as infinite power series, optimizing the coefficients e.g. for the first and second excitations as in CCSD leads to results that already include part of the triple, quadruple and higher excitations through this power expansion, leading to more accurate results than the truncated CI series. A different approach to correlation is the use of perturbation theory, e.g. Møller-Plesset theory (MP), where the missing electron correlation in the HF wavefunction is added as a series of perturbations to this wavefunction. MP2 and MP4 are often used, and truncate the series of perturbations after the second and fourth term, respectively; in terms of CI, these include double and triple excitations, respectively. Configuration interaction and perturbation theory can be applied simultaneously; a commonly used methodology is CCSD(T), calculating coupled cluster configurations with single and double excitations, and a perturbative inclusion of the remaining triple excitations. Another improvement on the methodologies described above are the explicitly correlated R12/F12 methods, which account for the interelectronic distance explicitly; examples include the MP2-F12 or CCSD(T)-F12 methods, which are increasingly popular owing to their high accuracy, and especially their fast convergence with respect to the basis set size.

The most commonly used wave function methodologies can be ranked as a function of their accuracy : HF < MP2 < MP4 < QCISD(T) \leq CCSD(T) < CCSD(T)-F12 < FCI, where the HF solution represents the reference wavefunction used in the correlation methods, and full-CI includes all correlation.

2.2.3. Multi-reference *Ab Initio* Methods

Despite the flexibility and high predictive performance of single-reference *ab initio* methods, some compounds cannot be correctly described based on a single HF reference wavefunction. Archetypical examples⁵² of these are e.g. O₃, carbonyl oxides, and some radicals formed from aromatic and other unsaturated volatile organic compounds (VOCs); another example are singlet biradical intermediates as found in the example CH₂OO + SO₂ reaction or in the wavefunctions that occur in homolytic dissociation of chemical bonds (see Figure 3). While all compounds benefit to some extent from a multi-reference description, we will concisely present the case of singlet diradicals as an example of a system where it is inevitable. Singlet diradicals have two electrons that are present in two nearly degenerate frontier orbitals;⁵³ note that a standard HF solution can not have degenerate frontier orbitals of the same symmetry. With two electrons and two orbitals, 4 different singlet occupations are possible, which are labelled Φ_a through Φ_d (Figure 3).^{53,54} Φ_a and Φ_b describe zwitterionic states of the system, while Φ_c and Φ_d represent singlet diradical states, but the unpaired electrons do not have the same orbital energy and are thus not equivalent. A qualitatively accurate description of the singlet diradical wavefunction with (equivalent) unpaired electrons thus requires a combination of Φ_c and Φ_d , and further improvements may be achieved by additionally including Φ_a and Φ_b .

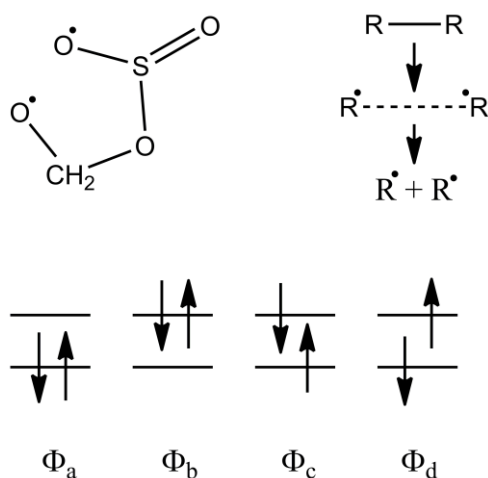


Figure 3. Singlet biradicals, a functionality present in some molecules or in the transition states of homolytical dissociation, are two-electron two-orbital systems that require multireference wavefunctions consisting of multiple configurations Φ to describe the ground state wavefunction.

An SCF calculation on these sets of reference configurations is called multiconfiguration SCF (MCSCF) and the resulting multi-reference wavefunction can be used to apply further correlation corrections. One of the most popular MCSCF methods at this time is CASSCF, complete active space SCF,⁵⁵ which generates reference configurations from an “active space”, i.e. all possible combinations of a number of electrons across a set of spin orbitals taken from the occupied and virtual orbitals, and performs an MCSCF calculation across these configurations. In practice only a handful of configurations contribute significantly to the final multi-configuration wavefunction, but using larger active spaces allows for more versatile configuration selection and hence yields more accurate results, at a combinatorially increasing computational cost. The computational cost can be mitigated when one includes only the subset of the active space that is most tailored to the problem, as e.g. in restricted active space (RASSCF)⁵⁶⁻⁵⁸ or correlated participating orbitals (CPO)⁵⁹ selection schemes. To improve

further on the correlation treatment, the MCSCF wavefunction is often used as the basis for a second-order perturbation theory calculation, i.e. perturbation is performed on each configuration. Using a CASSCF wavefunction, this yields the popular CASPT2 methodology. Even higher accuracy for the correlation correction can be achieved by MRCI, the multi-reference variant of CI that includes excited states of the molecule as additional reference configurations to improve the correlation treatment, particularly for these excited states, in truncated basis sets and limited excitation space; this method is computationally very demanding and hence only practical for small systems with up to 5 or 6 non-hydrogen atoms.

In practice, even formally multi-reference systems are often approximated sufficiently well using single-reference theories. Also, sufficiently high levels of correlation can in some cases⁶⁰ overcome even a very poor single-reference wavefunction. Transition states are more likely to have multi-reference character, e.g. the homolytic dissociation of a single bond forming two radical products,⁶⁰ or the addition of O₂ on an alkyl radical. The T₁ and D₁ diagnostic metrics^{61,62} are available to help decide whether a single-reference or multi-reference approach is needed by examining the magnitude of the single-reference CCSD excitation vectors. If these are large, wavefunctions other than the reference HF wavefunction have a large contribution, indicating too high a multi-reference character of the overall wavefunction. For example a single-reference coupled cluster result is considered not reliable if the T₁ diagnostic value is larger than about 0.044,⁶³ but it depends on the specific molecule at which value of the diagnostic multi-reference treatment becomes critical. The D₁ diagnostic is more sensitive to local multi-reference character of the wavefunction, e.g. the active site in a larger molecule.

Again, we can rank the most commonly used methods according to their accuracy: MCSCF <

CASSCF < CASPT2 < MRCI. Compared against single-reference methods, the amount of correlation present in MCSCF and CASSCF is similar to HF, whereas the correlation treatment in CASPT2 is similar to MP2.

2.2.4. Density Functional Methods

Kohn-Sham spin-density functional theory describes the molecule in terms of the electron density, where functionals operating on this density yield the molecular energy and other properties. There are similarities with wavefunction-based *ab initio* methodologies, in the sense that DFT calculations resemble SCF calculations working on Kohn-Sham density orbitals where, instead of a Hartree-Fock operator, density functionals incorporate the electron exchange and correlation. DFT calculations scale very favorably with the size of the calculation, where the use of advanced functionals can yield results approaching chemical accuracy, i.e. relative energies to better than $\sim 4 \text{ kJ mol}^{-1}$ (1 kcal mol^{-1}). Because of this, DFT has become very popular, and is often the tool of choice, especially for larger molecular systems. The Kohn-Sham equations underpinning DFT theory are only valid for the molecular ground state, limiting the direct applicability of DFT. However, it is possible to use time-dependent density functional theory (TD-DFT) to obtain information on excited states and photochemical processes, broadening the appeal of DFT.

As in *ab initio* calculations, there exists a hierarchy in the quality of the DFT functionals, which have been characterized by Perdew et al.²⁷ as rungs on Jacob's Ladder. The simplest functionals are based only on the local spin density approximation (LSDA), followed by generalized-gradient (GGA) functionals also incorporating gradient information, meta-GGA including 2nd derivative information, hyper-GGA introducing exact exchange, and finally the generalized random-phase

approximation (RPA) which additionally accounts for the virtual, unoccupied orbitals. Most functionals in use today use elements out of several of these Ladder rungs. It is possible to derive density functionals purely on *a priori* arguments,^{27,64} where the currently most advanced is the TPSS functional. However, most practical functionals use tunable functions where parameters are optimized by stringent benchmarking against large reference databases containing experimental as well as high-level *ab initio* results. A very large number of functionals have been proposed, often optimized for a specific problem set. The few functionals that are most often employed, e.g. B3LYP, M06-2X, BH&H, aim to be broad-purpose functionals applicable to most chemical problems. Historically, one of the most popular functionals was the B3LYP functional, an 8-parameter functional tuned to experimental reaction energies and molecular enthalpies of formation. It is a GGA functional that also includes an amount of Hartree-Fock exchange. The accuracy and breadth of applicability of B3LYP has been surpassed by more modern functionals, such as M06-2X,⁶⁵ M08, and others. Double-hybrid-GGA functionals, e.g. B2PLYP or PWPB95, which mix in perturbation theory corrections over the occupied and virtual orbitals, remain less used due to their somewhat higher computational cost, though they offer significantly better accuracies than pure-SCF functionals while still remaining well below the computational cost of pure *ab initio* correlation techniques. The accuracy of DFT calculations can be further improved by additional corrections,^{66,67} e.g. DFT-D3 which corrects for London dispersion interactions. Application of DFT to multi-reference systems is discussed in section 2.2.7.

In the theoretical characterization of atmospheric processes, DFT is currently the dominant methodology. It is typically the tool of choice to explore the potential energy surface, characterize all pathways to identify the most important ones, and to provide accurate geometries and rovibrational characteristics of the intermediates; typically, *ab initio* methodologies and/or composite methods are

then applied to the most critical structures to further improve the quality of the thermodynamic and kinetic predictions.

2.2.5. Semi-empirical Methods

Strictly speaking, many of the methods utilized in quantum chemistry are ‘semi-empirical’ in the sense that they contain a number of parameters optimized to give agreement with empirical results.⁶⁸ However, within the more conventional classification scheme of quantum chemistry, semi-empirical methods refer to a class of methods that are effectively simplified *ab initio* molecular orbital treatments. To maintain an acceptable level of accuracy, the cost of simplification results in an increased number of parameters whose values are selected in order to fit a test set of either experimental or higher level theoretical data. The original semi-empirical method was the one-electron Hückel model for π electrons, later extended by Hoffman to include all valence electrons.⁶⁹ With the rise of SCF methods which treat two-electron interactions, the main computational bottleneck lies in treating the two-electron integrals. This led to a hierarchy of semi-empirical approximations aimed at reducing the cost of the two-electron integrals. These included the CNDO (complete neglect of differential overlap), INDO (intermediate neglect of differential overlap), and NDDO (neglect of diatomic differential overlap) approximations, which were aimed at reproducing *ab initio* HF results with simplified integral evaluation schemes.

The MNDO (modified neglect of differential overlap) approach was based on calibration to experimental reference data. Distinct parameterizations of the MNDO approach led to the well-known AM1 and PM3 methods, as well as a host of others.⁶⁸ Beyond MNDO, the OMx methods (OM1, OM2, OM3) include orthogonalization corrections in the one-electron terms of the NDDO Fock Matrix to

account for Pauli exchange-repulsion, leading to an improved description of conformational properties, noncovalent interactions, and electronically excited states.⁶⁸ Recent work has seen the popularization of semiempirical methods which have roots in DFT – namely the non-SCF density functional tight binding (DFTB) approach (which shares many similarities with the extended Hückel approach), and the self-consistent charge density functional tight-binding method (SCC-DFTB).⁷⁰ The SCC-DFTB method arises from neglecting, approximating, or parameterizing many of the interaction integrals in conventional DFT. In this way, the origins of DFTB and SCC-DFTB within DFT are akin to the origins of semi-empirical methods within HF theories.

Owing to their dramatic integral approximations and relatively lightweight computational cost compared to wave function and DFT methods, semi-empirical methods are increasingly becoming a tool of choice for running MD simulations of large systems (i.e., more than 1000 heavy atoms),⁶⁸ where other electronic structure theory methods are generally not tractable. For extremely large systems, molecular mechanics forcefields are often the only tractable way forward. In many cases, the bottleneck of semi-empirical methods is the diagonalization routine, which scales as $O(N^3)$, although there has also been considerable progress toward linear-scaling methods. The most commonly used semi-empirical methods are derivative from MNDO (e.g., AM1, PM3, PM6, PM7) and OMx methods (OM1, OM2, OM3), variants of which invoke different levels of approximation. Both MNDO and OMx methods can be considerably improved by the addition of empirical dispersion corrections of the sort introduced by Grimme.^{e.g. 67} Semi-empirical methods have also been successfully parameterized for a number of specific systems, giving rise to so-called specific reaction parameters (SRP).⁷¹ Such SRP semi-empirical methods can often give excellent agreement with the higher-level calculations to which they are calibrated, at a considerably reduced computational cost. Benchmark tests evaluating the

performance of MNDO, AM1, PM3, OM1, OM2, OM3, and SCC-DFTB methods on ground-state molecular properties suggest an overall trend in accuracy along the lines of AM1 < SCC-DFTB < OM2.⁷² In some cases, the OMx approaches have a similar level of accuracy as DFT-B3LYP approaches.⁷³ This is an encouraging result given that semi-empirical methods often tend to be ~1000 times faster than DFT, but it is nevertheless the case that DFT remains favored over semi-empirical methods for smaller systems where it is tractable.

2.2.6. Composite Methods

In the preceding discussion of the various available methodologies, the computational cost was often mentioned. Atmospheric reactive systems often involve large molecules: the most commonly emitted non-methane VOCs are the terpenoids, i.e. C₅H₈, C₁₀H₁₆ and larger analogues, which during their oxidation cycle often incorporate multiple oxygen atoms or other substituents, and can even accumulate to form aerosol particles. For such species, applying the best levels of theory is often impractical, yet lower-level methodologies do not necessarily provide the required accuracy. A solution is composite methods, which predict the result that would be obtained at an unfeasibly high level of theory, by extrapolating from a set of calculations at more affordable levels of theory chosen to estimate the impact of different aspects of the calculation quality. Typical aspects considered are the basis set, i.e. the impact of (a) valence, diffuse, and/or polarization functions and how they affect convergence to the complete basis set limit, (b) freezing or incorporating correlation for core (non-valence) electrons, (c) better correlation theories, (d) spin orbit coupling, etc. Composite methods typically also define which level of theory is recommended for geometry optimizations, vibrational frequency analysis, and zero point vibrational energy (ZPE) corrections. Often, there is also an

empirical correction included, based on an extensive comparison against a benchmark database of thermodynamic values. As an illustration, we discern the following main steps in a Gaussian-2 (G2) calculation:⁷⁴ (a) the base energy is obtained at MP2/6-311G(d) level of theory; (b) the effect of the basis set size is derived from the energy difference between that base energy and an MP2/6-311+G(2df,2p) energy; (c) the effect of a better correlation treatment is derived from the energy difference between the base MP2/6-311G(d) energy and a QCISD(T)/6-311G(d) calculation; (d) the energy of a high-level QCISD(T)/6-311+G(2df,2p) calculation is then estimated from the base energy and adding the two energy differences obtained.

Many composite methods have been described in the literature. The most commonly applied are the Gaussian-*n* methods, where G2 is historically the most commonly used, though it is nowadays superseded by G3, G3X, and G4 methods,⁷⁵⁻⁷⁸ each again available in a few variants.⁷⁹⁻⁸³ Another often-applied family of composite methods is the CBS series by Petersson *et al.*,⁸⁴⁻⁸⁸ e.g. CBS-QB3 and CBS-APNO, which aim to extrapolate to the basis set limit; these methods are computationally quite affordable but are becoming somewhat dated as better estimates of the basis set limit are feasible nowadays.

For highly accurate thermodynamic estimates, three composite approaches are in common use. The first is the Weizmann-*n* series (W1, W2, W3 and recently W4)⁸⁹⁻⁹² which incorporates corrections even past CCSD(T) correlation. Likewise, HEAT^{93,94} includes coupled-cluster calculations up to CCSDTQ, and corrections for deviations from the non-relativistic Born-Oppenheimer approximation. Finally, focal point analysis^{95,96} entails calculations tracking the convergence towards the complete basis set and towards full CI for a large set of systematically more elaborate calculations. The use of these highly accurate composite methods has enabled prediction of thermochemical properties with

chemical, and even sub-kJ mol⁻¹ accuracies (see section 3).

2.2.7. Excited State Electronic Structure Methodologies

The methods outlined so far have reached a state of maturity where it is possible to calculate energies and molecular properties on the electronic ground states of small to medium-sized molecules, with sufficient accuracy to verify and complement experimental data. Calculating the properties of excited states is a more significant challenge for a number of reasons: (a) excited states tend to have significant multi-reference character; (b) excited state wave functions often lead to charge transfer states, which require an accurate description of both short-range and long-range interactions; and (c) the number of reactive channels which are energetically accessible in an excited state is considerably larger than the number of channels available at ground state energies. A comprehensive review of excited state methods in electronic structure theory is beyond the scope of this review, and for that we refer the reader to other works.⁹⁷⁻¹⁰⁵ In what follows we briefly outline some of the most commonly used methodologies, with some qualitative comments on their performance.

The most straightforward means for calculating electronically excited states is the configuration interaction-singles (CIS) method. The CIS method is based on an expansion of a reference Hartree-Fock wave function which includes all possible single excitation Slater determinants. These are then used to construct a configuration interaction (CI) matrix, diagonalization of which yields the respective state energies, and the corresponding excited state wavefunction. CIS is simple, relatively fast, and usually provides good qualitative insight into the character of excited states. For systems where the reference ground state wave function can describe the ground and excited states, it can sometimes provide reasonable excitation energies. However, there are a limited number of systems where a single

reference wavefunction is appropriate, and in these cases CIS tends to severely overpredict excitation energies by several eV, and often gives incorrect energy ordering.^{97,102}

So-called ‘propagator methods’, which include Green’s function, linear response, and equation-of-motion (EOM) approaches, constitute a second category of single-reference excited-state methods. The idea behind these methods is that, following exposure of a molecular system to a time-dependent electric field oscillating at a certain frequency, the frequency-dependent ground-state polarizability is well approximated by an expression depending on the square of the transition dipole moment, and the difference in the state energies. Using complex function analysis, it is then possible to obtain the poles of the expression: for those values at which the transition dipole moment goes to zero, the excited state energy corresponds to the one-photon absorption matrix elements. Propagator methods are unique insofar as excited state information is derived without the explicit calculation of the excited states, but rather through the response of the ground state wave function.^{102,105,106} In this respect, the quality of results obtained from propagator methods is linked to the quality of the reference wave function. The random phase approximation (RPA) or time-dependent Hartree Fock (TDHF) are propagator methods that use the HF reference wave function. Further improvements on these methods have come in the form of perturbation theory type corrections (e.g., the second order polarization propagator approach, SOPPA, as well as second and third order diagrammatic construction approaches, ADC(2) and ADC(3)). RPA typically gives errors of 1-2 eV in the excitation energies, with oscillator strengths that may differ by an order of magnitude. SOPPA, ADC(2), and ADC(3) typically perform better, with errors in the excitation energies on the order of ± 0.6 eV.¹⁰²

The most accurate class of single-reference excited state methodologies is the coupled-cluster (CC) family of methods. CC methods include a substantial amount of dynamical electron correlation,

which in many cases can compensate the use of a poor reference wave function. Commonly used coupled cluster methods include the EOM-CCSD method (which includes double excitations in the reference wave function), and the family of CCS, CC2, CCSD, CC3, and CCSDT methods, all of which are based on response theory. For cases where the single reference wave function is of reasonable quality, the CC3 method can provide singlet excitation energies that are on the order of ± 0.3 eV, with CC2 giving only slightly worse performance.⁹⁸

The approximation of a single-reference wave function means a neglect of static correlation. For a wide range of systems in excited state chemistry, this is the source of considerable error, even with a CC treatment. This is particularly true for systems that involve bond-breaking, conical intersections, and diradicals, all of which are common features of excited state chemistry. Accurate treatment of such systems can be achieved using previously discussed MRCI methods, although the computational cost of MRCI makes it intractable for all but the smallest systems. More practical are so-called MCSCF approaches, in which the CI coefficients as well as the orbital coefficients are minimized for a given system. The most common MCSCF method is the complete active space (CAS) SCF approach, where the specific orbitals and electrons entering the CI expansion are selected based on chemical criteria. Because the construction of a CAS wave function from constituent orbitals and electrons is usually difficult, there have been attempts to simplify its use. For example, the fractionally occupied molecular orbital (FOMO) CAS CI method attempts to generate the orbital active space by solving a single determinant HF equation with fractional occupation numbers. In the description of excited states, CASSCF wave functions are usually constructed in a state averaged manner, where one optimizes a functional that depends on the energy of n different states, each of which has an associated weight. This yields a wave function whose active space is optimized for the states of interest, and ensures

orthogonality of the wave functions corresponding to each state. MCSCF methods can be considerably improved by adding in dynamical correlation effects. The most common method along these lines is the previously discussed CASPT2 method. CASPT2 is presently the most practical method available for treating excited state problems that require a multi-reference wave function.^{98,101,103} Multi-reference coupled cluster (MRCC) methods have also been proposed and are available, although they are still being refined and tested.

The final excited-state method to be discussed herein is time-dependent density functional theory (TD-DFT), which has become increasingly popular over the past decade.^{102,107,108} TD-DFT is based on the frequency-dependent polarizability equation discussed above. The appeal of TD-DFT methods arises from their relative simplicity, their wide availability, and the fact that they are relatively ‘black-box’ compared to multi-reference approaches. For closed shell species in which the ground and excited states are reasonably well described by a single reference wave function, TD-DFT can provide accuracy on the order of 0.4 – 0.5 eV for excitation energies, though in some cases it fails miserably, with errors of 5 – 6 eV.¹⁰² Compared to the performance of ground state DFT, the performance of TD-DFT for excited states is considerably more erratic and unsystematic: it provides a poor description of charge-transfer (CT) states, it cannot describe biradicals, it suffers massive inaccuracies in describing the valence states of large π -conjugated systems, and it cannot treat degenerate situations like conical intersections owing to the fact that the interaction matrix elements connecting the ground and excited states are not included in the response equations. Improvements in TD-DFT’s treatment of CT states has been achieved by the introduction of range-separated hybrid functionals, in which short-range exchange is treated using a local functional, and long-range exchange is treated using exact exchange. TD-DFT is useful for obtaining a qualitative picture of a system’s excited states, but its accuracy for

describing a particular system should be carefully checked against a range of other methods.

2.3. Statistical Rate Theories

Describing the time-dependence of a bimolecular reaction requires analyzing the dynamics of the reactants as they progress towards the products. Each reactant molecule, however, can be in a different state, e.g. the reactants can have different energies and different distributions of that energy across the degrees of freedom, and a collision between two reactants can occur at any angle and at a wide range of relative velocities. Molecular dynamics calculations (see section 2.5) explicitly trace the trajectories that these molecules, and the component atoms, follow in the reaction. In contrast, statistical rate theories describe an ensemble of molecules and trace the changes in the energy distributions within the ensemble to describe the reaction kinetics. Such statistical rate theories are based on a limited set of assumptions which experiments have shown to be well-founded for a wide range of chemical reactions.

A key concept in statistical rate theories is the transition state (TS), which is defined by a hypersurface in $6n$ -dimensional phase space (i.e., $3n$ -dimensional coordinate space and $3n$ -dimensional momenta space) which separates the reactant phase space from that of the product.¹⁰⁹ Statistical rate theories assume a non-recrossing rule: any reaction trajectory that crosses this hypersurface from reactants to products, does not recross back towards the reactants, i.e. crossing the TS hypersurface constitutes a reaction, and the TS is the kinetic bottleneck for the reaction. Hence, the best TS description is then one that minimizes the number of trajectories that cross it and still lead to reaction (minimal flux). For multidimensional systems, finding the optimum TS hypersurface is generally a computationally intractable problem, so statistical theories approximate this surface to the best of their abilities. A real system always has a number of recrossing trajectories, but minimizing the

reaction flux through the TS surface by varying e.g. the position of the TS along the reaction coordinate, or making the dividing surface non-planar improves the TS description, and thus allows for variational improvement strategies. Practical identification of a TS usually involves neglecting the $3n$ phase space coordinates which involve momenta, and instead carrying out a search in coordinate space: an obvious first choice for a TS is at the saddle point on the PES separating reactants from products, as that *a priori* avoids all trajectories that have insufficient energy to surmount the barrier; most, but not all, practical statistical rate calculations are thus based on the assumption of a TS hyperplane located at this saddle point, which is perpendicular to the minimum energy path connecting reactants and products.

A second important assumption is ergodicity, i.e. the energy in a molecule can be rapidly redistributed across all internal degrees of freedom due to their coupling (subject to conservation of translational and angular momentum), where all states thus possible have equal probability of occurring, and where the molecule will pass through each of these states sooner or later if left unperturbed. Alternatively, these states can be seen as a uniformly distributed superposition of quantum states with energy E and angular momentum J , where each quantum state is described by a unique set of quantum numbers. While notable exceptions exist,¹¹⁰ both experiments and simulations have shown that the intramolecular vibrational energy redistribution (IVR) is generally fulfilled in 0.1 to 10 ps, and is typically much faster than virtually all chemical reactions. Ergodicity implies that a molecule with a certain energy content can be described based on the number of accessible quantum states at that energy, i.e. quantum state occupation is effectively randomized. This justifies the statistical analysis of a molecule, and of a reaction. The core idea behind all statistical rate theories can then be paraphrased as counting the quantum states of the reactants, and the sum of quantum states at the TS; their ratio is

the key property determining the reaction rate coefficient. The activation energy and reaction entropy, which determine this ratio, thus determine the reaction rate.

Some, but not all, statistical rate theories also assume that the energy populations of the molecules are canonical, i.e. a thermal equilibrium distribution. Any chemical reaction disturbs the population, and a canonical population distribution across the new, smaller population is restored by collisional energy transfer between the molecules or by influx of molecules from a reverse reaction. The assumption of canonical populations is thus only valid when energy transfer between reacting species and the bath gas is sufficiently fast, i.e. when there are sufficient collisions; this is called the high-pressure limit. When the chemical reaction is faster than recovery of the canonical populations, the change in energy distribution affects the overall reaction rate; clearly, the discrepancy depends on the number of collisions occurring in a characteristic reaction time, inducing pressure-dependence on the reaction rate. In the low-pressure regime, the number of collisions has become negligible in the reaction time, while intermediate pressures are called the fall-off regime. Examples of pressure dependent reactions include unimolecular reactions, such as dissociation, but such reactions can also occur under the low pressure conditions found at high altitudes, where product molecules formed with excess energy in a chemical reaction undergo subsequent reaction before collisional relaxation can occur. Pressure-dependence is discussed in more detail in section 2.4.3. Statistical rate theories assuming a canonical distribution, e.g. canonical Transition State Theory (TST), yield temperature-dependent results, while energy- and angular-momentum-specific theories, e.g. RRKM, explicitly consider the energy content of the reactants and TS and are thus able to incorporate pressure-dependent energy distributions in a so-called Master Equation analysis (see section 2.4.3).

2.3.1. Molecular Degrees of Freedom

The total energy, translational momentum, and angular momentum of a molecule are all conserved properties of a molecule, if left unperturbed. This energy is present as potential and kinetic energy in the $6n$ phase space degrees of freedom for a molecule with N atoms. The translation of the center of mass is conserved and can be separated out of the kinetic equations, leaving total energy and rotational momentum as constants, with corresponding quantum numbers. The motion of the internal modes is non-separable in general, and the internal modes and the molecular rotation must conserve these quantum numbers E and J . Treating this internal mode coupling explicitly is complex, and strictly speaking is only valid in the harmonic limit – i.e., where there is very little energy in a molecule's constituent modes and the displacements from equilibrium are very small. Nevertheless, it is typically the case that molecular degrees of freedom are approximated as separable, i.e. molecular translation, molecular rotation, and internal degrees of freedom are incorporated as separate ensembles into the rate theory methodology. Where possible, even the internal modes – mostly vibrations and internal rotations – are each treated as separable degrees of freedom. In this section, we describe how the dynamics of the molecular degrees of freedom are included in statistical kinetic methodologies, where one needs the ability to predict the quantized energy levels for each degree of freedom, or each ensemble of coupled modes. For energy-specific rate theories, these are then all convoluted to obtain a quantum state density at a specific energy (a microcanonical approach), while for a thermal reaction at a temperature T , the states are summed across a Boltzmann distribution to obtain partition functions (a canonical approach). Thermodynamic properties, such as energy $U(T)$, enthalpy $H(T)$, entropy $S(T)$, heat capacity $C_v(T)$, Gibbs energy $G(T)$ and Helmholtz energy $A(T)$, etc., can be easily derived from the partition functions and their first and second derivatives with respect to temperature.

For statistical rate theories, the impact of the molecular degrees of freedom on the predicted rate coefficient depends on how the molecular properties change between reactant and transition state, specifically, how the state density changes for the energy content considered. For product energy distributions, one should consider their further change upon transition to the products. This entropic factor combines with the energy factor determined by the reaction barrier height to yield the absolute rate coefficient, and its temperature-dependence. A transition state that has a strongly reduced state density (i.e. widely spaced energy levels), compared to the reactants, is often called a “rigid” or a “tight” TS and typically yields a lower rate coefficient, while one with an increased state density, often called a “loose” TS, nearly always has a higher rate coefficient.

2.3.1.1. Molecular translation and rotation

The effect of molecular translation and rotation on reaction kinetics is relatively well understood for simple systems, though conservation of (angular) momentum¹¹¹ does sometimes complicate *a priori* predictions for some types of reactions due to coupling with the internal modes. Translation and rotation are the molecular degrees of freedom with the smallest energy quanta and highest state density (and therefore often amenable to a classical treatment), and thus can have a strong impact on reaction kinetics, in particular for association and dissociation reactions where spatial degrees of freedom of separated reactants or products correlate with more rigid, large-quanta internal degrees of freedom in the TS. Furthermore, conservation of angular momentum J in molecular rotation can hinder or facilitate reactions, depending on whether the reaction complex contracts or expands during the reaction. To explicitly account for this J -dependence, microcanonical $k(E,J)$ rate coefficients need to be calculated, introducing a two-dimensional computational problem over E , energy, and J , rotational quantum

number. This induces a severe computational cost, such that most scientists choose only a representative J , such as a non-rotating molecule ($J=0$), the thermally averaged J , or the most populated J , though two-dimensional energy-specific kinetics has been applied in numerous cases.^{e.g. 112–115} The rigorous implementation of conservation of angular momentum is further complicated when considering quantum number K , i.e. the projection of the quantized vector \mathbf{J} on a molecular axis, which is not a conserved, "good" quantum number due to coupling with other modes. Again, most applications pragmatically simplify its treatment, either choosing a K -adiabatic approach, where K is a conserved or only slowly changing variable during the time interval for passing through the TS from reactant to product side, or a K -active approach, treating K as an active variable rapidly varying by coupling with other degrees of freedom, and with or without constraints imposed on K by quantum number J . There is no consensus at this time in the literature as to which approach is better in general, or if it is dependent on the reaction,^{116–119} and this state of affairs is exacerbated by the fact that the error incurred by ignoring such effects is often comparable to the error in the calculated stationary point energies. Recent work by Ghaderi *et al.*¹¹⁹ find a better agreement against trajectory calculations for the O_2+O reaction using the K -adiabatic approach, while others¹¹⁷ argue that molecules are not rigid rotors and K is likely to vary significantly for more complex reactions. Finally, there is also coupling between molecular rotation and internal rotations, as they combine to yield the conserved angular momentum \mathbf{J} . We are not aware of any examples where this coupling is rigorously treated in energy-specific rate calculations, i.e. molecular rotation and internal rotation are typically treated as separable modes.

2.3.1.2. Vibrational Modes

Traditionally, most internal degrees of freedom are treated as uncoupled harmonic oscillators,

for which the state density is easily obtained using direct count methods (e.g. the Beyer-Swinehart-Stein-Rabinovitch¹²⁰⁻¹²² convolution algorithm). This treatment, called the rigid-rotor harmonic-oscillator approximation, has proven its worth in a large number of theoretical studies and often provides an acceptable level of accuracy (compared to errors in calculated energies). For non-harmonic oscillators, there are several options available. Third- and higher-order derivatives¹²³ of the potential energy allow for the calculation of anharmonicity constants, which can generally describe the spacing of the oscillator energy levels as higher-order polynomials. Typically, anharmonicity constants are small, changing the lowest vibrational energy levels by a few 10s of cm^{-1} . At higher energies, or for a large number of anharmonic oscillators, the effect becomes larger, but usually cancels out mostly between reactants and TS, which is often the reason for the good performance of the harmonic oscillator model in calculating rate coefficients. For a non-dissociative oscillator whose potential energy curve is steeper than quadratic, e.g. for molecular bending in linear molecules, quartic ($\sim x^4$) or squared tangent ($\sim \tan^2$) functions are often suitable.¹²⁴⁻¹²⁶ An interesting special case is the double-well oscillation, which can be used to describe e.g. puckering in ring systems.^{126,127} Many analytical forms have been described in the literature,^{124,125} involving polynomials such as quadratic-quartic functions, or $\cos \cdot \tan^2$ functions. For anharmonic vibrations that lead to dissociation at higher energies, e.g. for a diatomic molecule, description as a Morse oscillator function allows for analytical solutions of the quantum chemical oscillator Hamiltonian. The Morse oscillator is sometimes found to have difficulties to properly reproduce the higher-energy, large separation part of the PES, and alternative potentials such as the Varshni energy curve or the Murrell-Sorbie curve, among many other, can be used.¹²⁸⁻¹³¹

For the non-harmonic oscillator functions mentioned above, partition functions are available,

though often only in their classical limit, i.e. in the assumption of a continuous state density rather than a quantized set of energy levels. A first-order correction can be performed using the Pitzer-Gwinn approximation,¹³² which transfers the difference between quantized and classical harmonic oscillators to that of the non-harmonic oscillator:

$$Q_{quant}^{non-harm} = Q_{class}^{non-harm} \times \left(\frac{Q_{quant}^{harm}}{Q_{class}^{harm}} \right) \quad (1)$$

Analytical equations to calculate the quantized energy levels are often not available for the non-harmonic oscillators. A technique that has gained wide-spread adoption in the last decades is the use of the Meyer method, the Fourier Grid Hamiltonian, FGH, or similar numerical solutions to the oscillation Schrödinger equation to obtain the energy levels;^{133–135} these methods are easily implemented, and generally applicable to the solution of 1D oscillators on arbitrary potentials. For higher dimensions the computational cost increases exponentially, making this method less practical. A partial solution is to treat the respective dimensions as separable, operating in a mean-field approximation¹³⁶ induced by the other dimensions; for the lowest energy levels, additional correlation treatments are practical.¹³⁶

The treatment of non-separable degrees of freedom, where the coupling between the modes is explicitly included, intrinsically suffers from the large number of states that needs to be calculated, which explodes combinatorially with the number of coupled degrees of freedom. Still, the state of the art moves towards including the coupling between the modes. VPT2 calculations, i.e. 2nd order vibrational perturbation theory,^{123,137} treats the anharmonicity as a perturbation of the harmonic Hessian, using third- and some fourth-order derivatives of the potential energy surface to supplement the description in the 2nd-order derivative in the Hessian. From this, one can obtain the full anharmonicity matrix \mathbf{X} , including the off-diagonal elements X_{ij} that couple the vibrational modes i and

j , but are ignored for separable modes. Using \mathcal{X} and the harmonic vibrational wavenumbers, one can then obtain all of the vibrational energy levels in a first anharmonic approximation, and from these the state density, sum of states, or partition functions. The computational cost of direct count methods are prohibitive for most non-trivial molecules with more than a few atoms, so several methods have been proposed using Monte Carlo sampling or limiting the number of couplings which are simultaneously treated.^{138–143}

2.3.1.3. Treating Internal Rotations

Internal rotations can have a large impact on the prediction of thermodynamic and kinetic properties, often making them the most critical modes for which a non-harmonic-oscillator description is necessary. Their impact becomes even more pronounced in chemical reactions that involve a change in the number and/or properties of the internal rotors, such as cyclisation reaction or H-migrations. An example is the formation of sulphinic acid in Figure 2, where internal rotors of the biradical intermediate are converted to skeletal vibrational modes in the cyclic H-shift transition state.

The impact of internal rotation is twofold. First, the energy level spacing of internal rotation is typically significantly smaller than for a vibrational mode, but the energy levels of an internal rotor depend quadratically on the quantum number for a free separable rotor, whereas energy levels of harmonic modes depend linearly on the number of quanta, leading to different absolute state densities, and a different energy-dependence. Secondly, for hindered internal rotors, multiple conformers exist, corresponding to different orientations of the rotating moieties. For degenerate rotors, this is relatively easy to account for, but in general internal rotors yield non-identical conformers. For example, internal rotation of the $\text{HOCH}_2\text{C}^\bullet\text{O}$ intermediate in Figure 1 leads to both a H-bonded and a non-H-bonded

conformer. Internal rotations are often non-separable from the other degrees of freedom, as different conformers can show different energies, molecular and internal moments of inertia, and vibrational frequencies. Still, for reasons of tractability, internal rotors are often treated as separable in a first approximation. The simplest description is the use of a free internal rotor, for which analytical expressions exist to calculate the partition function and quantum energy levels. It represents one extreme for hindered rotors, and thus is often useful to estimate the maximal impact of internal rotation on a kinetic problem. Most rotors, however, are hindered, i.e. the potential energy of the geometry depends on the angle of rotation.

The reduced moments of inertia for internal rotation are nowadays^{144,145} mostly obtained from the general N-dimensional treatments by Kilpatrick and Pitzer,^{132,146–148} or by Harthcock and Laane.¹⁴⁹ Most other methods available for obtaining moments of inertia involve approximating the internal rotor as symmetric, which is not always the case. Obtaining rectilinear moments of inertia from the Hessian harmonic oscillator mode corresponding to the internal rotor was found to yield poorer results,¹⁵⁰ especially considering that the modes of internal rotation often mix in with other rotational modes, molecular and internal, as well as with low-frequency vibrations. The potential energy profile for an internal rotation can, in the first approximation, be described as a cosine function with a periodicity suitable for the rotor studied. For this case, a relationship can be found between the height of the hindrance potential and the second derivative of the PES at the minima,¹⁵¹ allowing fairly good estimates of the barrier height to rotation from accurate quantum chemical frequency analysis at the minimum energy geometries. For non-degenerate rotations, more complex functions are necessary, and can be constructed by more elaborate trigonometric functions, polynomials, Fourier-transforms of explicitly calculated PES, or other interpolation methods based on a characterization of the PES as a

function of the rotational angle. The quantum chemical characterization of the rotational PES is performed by constrained optimizations where the rotational angle is fixed, but the remaining degrees of freedom are relaxed; the use of rigid internal rotation would yield significant reduction in computational cost, but is found to yield an unrealistically high barrier to internal rotation, owing to an unphysical description of the steric hindrance between the rotating moieties.

To account for internal rotation in the calculation of the partition function, several options are available. A first set of approximations involve replacing a vibrational mode obtained from a quantum chemical frequency analysis with a more appropriate description as a 1-dimensional, separable torsional mode.^{126,144,145,150–166} The most commonly used methods, proposed by Truhlar and coworkers^{150,151,153} approximate the hindered rotor partition function as a harmonic oscillator in the low-temperature limit, a free rotor in the high-temperature limit, and interpolate between these limits using a non-exact, smooth function. Barker and Shovlin¹⁵⁴ likewise propose a smooth switching function between harmonic oscillator and free rotor, based on the earlier work by Troe *et al.*¹⁶⁷ and Knyazev,¹⁵⁶ whereas e.g. McClurg *et al.*^{155,168} represent their results as temperature-dependent correction factors to the harmonic oscillator limit. Gang *et al.*¹⁶⁹ use a Monte-Carlo integration scheme across all rotational degrees of freedom to obtain the partition function, and an analogous geometry sampling technique has been proposed by Magoon and Green¹⁷⁰ for probing the conformational space of ring structures, internal rotors, and other multi-conformational problems. However, directly substituting a harmonic oscillator mode with an internal rotor is rarely straightforward: the internal rotor modes in a quantum chemical Hessian eigenvector analysis couple to molecular rotation and the other internal degrees of freedom, such that isolating the internal rotor mode is ambiguous. Furthermore, the separable 1D rotor approach does not account for the changes in the other degrees of

freedom along the rotation. For these reasons, explicitly accounting for all possible conformers in the calculation of the partition function is becoming more common.^{144,152,159,171,172} Even without further anharmonicity corrections, a rigid rotor harmonic oscillator multi-conformer description incorporating all conformers already accounts^{153,171} for most of the torsional correction at ambient temperatures for many practical applications, though not at elevated temperatures > 500 K. More elaborate methods, e.g. as proposed by Zheng *et al.*,¹⁵³ additionally correct the multi-conformer harmonic oscillator partition function across all internal degrees of freedom for the internal rotation anharmonicity. Also, they propose to project the internal rotor modes out of the Hessian, uncoupling them from the other internal degrees of freedom and obviating the need for selecting and replacing harmonic internal modes as torsions.

For the prediction of the energy levels for hindered internal rotors, fewer options are available. For a free internal rotor, analytical expressions are available. For hindered internal rotors, Troe¹⁶⁷ proposed using harmonic energy levels below, and free rotor energy levels above the hindrance barrier. Barker and Shovlin¹⁵⁴ refined this approach by describing a switching function smoothly connecting these two limiting cases. In its most general form, the energy levels for an arbitrary N-dimensional hinderance potential can also be obtained by numerical solution of the Schrödinger equation.^{133–135,173–175} For 1D torsions with constant reduced moment of inertia, the Fourier Grid Hamiltonian (FGH) method by Marston and Balint-Kurti^{133,134} is in wide-spread use. For high internal energies, the rotation is expected to approach free rotation, which allows good prediction of energy levels to arbitrary energies even for practical sizes of the Hamiltonian matrix. For higher dimensionalities, however, direct solution of the Schrödinger equation suffers from the large number of rotational quantum states that need to be obtained. Alternative methods, e.g. the mean-field approximation proposed by Dutta *et*

*al.*¹³⁶ are perhaps less appropriate for hindered rotations, due to ambiguities in selecting the mean. Higher-correlation treatments¹³⁶ could provide a solution for the critical lower-energy quantum states, but strongly increase the computational cost. Fernández-Ramos¹⁷⁶ has also described a 2D non-separable treatment using a Fourier-expansion of the potential energy surface; they propose the use of sparse-matrix techniques to circumvent solving the eigensystem of an overly large matrix.

The FGH method is applicable only when the inertia factor, i.e. the reduced moment of inertia, is constant. Reinisch *et al.*¹⁷⁷ propose the use of an effective moment of inertia, derived from a thermally weighted average of the reduced moment of inertia along the rotation, to allow application of the FGH methodology. More generally, Mellor *et al.*^{174,175} propose a method incorporating an angle-dependent moment of inertia, which amounts to defining a Fourier-expansion of an effective potential, and uses root-finding instead of an FGH eigenvalue analysis to obtain the torsional energy levels. Likewise, the method by Meyer¹³⁵ uses a Fourier series expansion of angle-dependent energy and moment of inertia on a set of gridpoint to obtain the energy levels from a matrix hamiltonian. Finally, if a state density is required, rather than specific energy levels, it is in general possible to perform an inverse Laplace transform (ILT) from a general partition function expression, including any of those mentioned above. Knyazev¹⁵⁶ has also proposed analytical solutions for the state density, based on an ILT formalism. Partition functions can also be obtained by the sum of the thermally weighted energy levels (torsional eigenvalue summation, TES).

2.3.2. Canonical Transition State Theory

In this section, we treat canonical transition state theory, CTST, i.e. rate theories which are based on the concept of a 'transition state' dividing hypersurface discussed at the start of section 2.3,

and which assumes canonical energy distributions. We also assume reactions have an intrinsic energy barrier (a local maximum on the reaction coordinate energy profile) of sufficient height, which can be used as a good, prescribed TS approximation; variational TST for reactions without intrinsic barriers, or with broad low-energy barriers, is discussed in section 2.3.4. The history, development, and underlying assumptions and prerequisites of TST has been discussed extensively in reviews and books in more detail than we can afford here;^{178–186} we refer the readers to these works for an in-depth overview. CTST, in its most simple incarnation, describes the reaction rate as a ratio of the total partition functions $Q(T)$ of the transition state, excluding the reaction coordinate, over that of the reactants. This ratio, which quantifies the contribution of reactive quantum states over the reactant states, includes contributions from translation, molecular rotation, and all internal degrees of freedom; for the TS, the reaction coordinate is excluded from the partition function (indicated by symbol \neq) and is treated as a translational degree of freedom that takes the system over a barrier of energy E_b , which introduces time via the factor $k_B T/h$, and gives the appropriate units of s^{-1} :

$$k(T) = \frac{k_B T}{h} \frac{Q^\ddagger(T)}{Q_{\text{reactants}}(T)} \exp\left(\frac{-E_b}{k_B T}\right) \quad (2)$$

ZPE corrections of the relative energy are accounted for either by using a ZPE-corrected potential energy surface, or by defining partition functions rooted on the potential energy minimum rather than the ground state energy. Obtaining accurate rate predictions at any temperature then requires obtaining an accurate estimate of the barrier height, and a correct description of the partition functions. Tunneling corrections are introduced by a factor $\kappa(T)$, discussed in more detail in section 2.3.5. For reactions that are not in the high-pressure regime, a fall-off correction factor $I(P,T)$ can be introduced that accounts for a non-canonical energy distribution as well as related recrossing effects; pressure-

effects are discussed in section 2.4. Incorporating these factors leads to the CTST expression often used in theoretical kinetic work.

$$k(T) = \alpha \frac{k_B T}{h} \frac{Q(T)}{Q_{\text{reactants}}(T)} \kappa(T) \exp\left(\frac{-E_b}{k_B T}\right) \Gamma(P, T) \quad (3)$$

If multiple symmetrically equivalent reaction pathways are accessible, this can be accounted for by a symmetry factor α as obtained from the ratio of the internal and external rotational symmetry numbers, σ , of reactants and TS, the number of optical isomers, m , and the electronic state degeneracy g :^{187–189}

$$\alpha = \frac{\sigma_{\text{reactant}} m_{\text{TS}} g_{\text{TS}}}{\sigma_{\text{TS}} m_{\text{reactant}} g_{\text{reactant}}} \quad (4)$$

The symmetry number for molecular rotation is typically already incorporated in the partition function for molecular rotation; if so, then it should not be included in the calculation of α . The accuracy of CTST predictions relative to experimental work has been found to be excellent in general, provided a sufficiently accurate PES is available, and the degrees of freedom of the critical PES points can be appropriately described; both these aspects are discussed *in extenso* in sections 2.2 and 2.3.1. Alternative notations of canonical transition state theory can be based on enthalpies and entropies, or Gibbs energies; these macroscopic properties are directly related^{179,182,190} to the underlying partition functions.

$$k(T) = \sigma \frac{k_B T}{h} \exp\left(\frac{-\Delta G}{k_B T}\right) \quad (5)$$

Like molecular rotation, internal rotations introduce symmetry factors, which historically have been incorporated in the symmetry factor α . While this works for degenerate rotors (e.g. a three-fold symmetric $-\text{CH}_3$ rotation), it has been abused in the case of non-degenerate rotors, where the different

rotamers do not necessarily have the same molecular symmetry, e.g. the trans- and gauche- conformers of butane with symmetry C_s and C_1 respectively, or can even have different energy and rovibrational characteristics. Dealing with such situation in general through a single symmetry factor is not straightforward, even when allowing for non-integer¹⁵⁰ symmetry numbers. There is currently a drive towards explicitly accounting for all conformers generated by internal rotation; while this introduces a (sometimes significant) computational cost towards the quantum chemical characterization, it does allow for the correct lifting of the otherwise incorrectly imposed internal rotor degeneracy. A first approximation is summing the partition functions for all conformers, which emphasizes the properties and energetics of the individual rotamers and is appropriate only at ambient temperatures where the low hindrance barriers to rotation are still large compared to the average energy content per degree of freedom:^{153,171}

$$Q_{total}(T) = \sum Q_{rotamer}(T) \exp\left(\frac{-E_{rotamer}}{k_B T}\right) \quad (6)$$

More elaborate treatments account for coupling between the different conformer energy wells which accommodates the broadening and merging of the individual energy wells where the state density is described as a single non-separable rotational space.¹⁵³ For reactions at atmospheric temperatures, it is found that accounting for all conformers explicitly by summing their individual contributions, even in a simple harmonic-oscillator rigid-rotor approximation, recovers most of the non-harmonicity introduced by the internal rotation, as for these temperatures the molecules reside mostly in the thermally-weighted lower-energy harmonic wells. This approximation breaks down at higher temperatures, e.g. at combustion temperatures above 1000K the molecular moieties are mostly rotating rather than residing within an oscillator energy well, and their coupled rotation needs to be

taken into account.¹⁶⁰

Semi-Classical Transition State Theory, SCTST,^{191–195} is a more detailed version of TST that explicitly accounts for non-separable coupling among all degrees of freedom, including the reaction coordinate. This method has been recently revived, following improvements^{139,140,195} based on a modern state density calculation algorithm that side-steps the difficulty of explicitly calculating the high number of quantum states.

2.3.3. Microcanonical Transition State Theory

For the prediction of energy-specific rate coefficients for unimolecular reactions, the Rice-Rampsberger-Kassel-Marcus theory (RRKM)^{178,182,184,186,196–199} is the most widely used methodology :

$$k(E) = \frac{\alpha W(E)}{h N(E)} \quad (7)$$

For a given internal energy E of the reactant, the quantum state density $N(E)$ which accommodates this internal energy is calculated. At the transition state, part of this energy E is fixed into the reaction coordinate (RC) to surmount the energy barrier E_b , while the remainder $E - E_b$, is randomly distributed across the RC and the remaining degrees of freedom. As the excess energy within the RC thus ranges from 0 (i.e., the zero-point corrected barrier height) to $E - E_b$, this leads to a summation of the state density across all non-RC degrees of freedom, noted as $W(E)$, which corresponds to the number of states which are accessible at total energy E as the system passes through the transition state. As with canonical TST, the RC can be described as a translation, whose state density contribution over all accessible energies combined with the rate of crossing the energy barrier reduces to a factor h^{-1} . Below the energy barrier, $W(E)$ is zero in the absence of tunneling.

Molecular rotation can be accounted for explicitly in the calculation of the rate coefficient, i.e.

for a given molecular rotation quantum number J conserved over the entire reaction, the change in geometry from reactant to TS changes the moments of inertia I , and hence the amount of energy that is retained in molecular rotation. The change in rotational energy is released into, or extracted from, the pool of randomizable internal energy of the reacting molecule, depending on whether the TS has an expanded, or contracted, geometry respectively, thus yielding a $k(E,J)$ -specific rate coefficient. Tunneling corrections (see section 2.3.5) are likewise easily incorporated within the summing of the TS quantum states, where this time the amount E_{RC} of energy in the RC is allowed to be less than the energy barrier E_b , and the remaining energy is distributed over the other degrees of freedom; the energy-specific tunneling probability is then easily accounted for at each E_{RC} . Similar to CTST calculations, symmetry-equivalent pathways can be accounted for by introducing a non-unity reaction symmetry.

The RRKM rate expression can be averaged across a canonical energy distribution. In this summation, the reactant state density yields the reactant partition function, while the TS sum of states becomes $k_B T \times Q^\ddagger(T)$; shifting the zero energy of the partition functions for reactant and TS to a common point then recovers the factor $\exp(-E_b/k_B T)$, showing that RRKM and CTST rate expressions are equivalent in the high-pressure regime or at equilibrium.

Maranzana *et al.*²⁰⁰ have proposed a methodology for obtaining the rate coefficient $k(E,T)$ for bimolecular reactions $A(E) + B(T)$ of a reactant $A(E)$ with a given internal energy E , and a canonical energy distribution at temperature T for reactant B . The methodology has been examined and verified by Green and Robertson.²⁰¹ This method allows for inclusion of bimolecular reactions in energy-specific reactions^{200,202,203} of energized species, of importance for pressure-dependent reaction systems (see section 2.4).

On the assumption that the reactant partition functions are thermalized, and provided the temperature-dependent rate coefficient $k(T)$ is available, then the inverse Laplace transform (ILT) can be exploited to yield a set of energy-specific fluxes for the association process.²⁰⁴ However, in many cases, explicit dynamics calculations (section 2.5) are a more natural fit to this problem, e.g. for molecule-surface reactions, for crossed-beam experiments, or for state-selective reactions.

2.3.4. Variational Calculations

For reactions with a well-defined energy barrier, it stands to reason that the rate-determining step in the transition from reactant to product is to overcome this energy barrier. Passing the barrier at any position other than the lowest saddle-point between the two endpoints of the reaction often introduces an additional energetic disadvantage. The saddle-point is therefore an excellent first guess for where to locate the TS dividing hypersurface, and often the optimal choice for where to intersect the minimum energy path. For reactions without an energy barrier (e.g. the $\text{CH}_2\text{OO} + \text{SO}_2$ reaction shown in Figure 2, or radical-radical recombination reactions), or for reactions with low-lying, broad saddle points, positioning the dividing hypersurface is less obvious. The definition of the TS as the divider between reactant and product phase space in such a way that the number of recrossing trajectories is minimized (or alternatively where the free energy is maximized), allows for a variational approach where the reaction bottleneck is optimized to a position along the RC where the predicted rate coefficient is minimized, i.e. the reaction coordinate location that is most rate-determining.^{180,205,181,206} Such rate calculations are computationally more costly than those for a saddle-point TS, as one needs information at multiple points along the reaction coordinate. The energetic and rovibrational characteristics along the RC are typically obtained by explicit quantum chemical calculations on a set of (equidistant) points along the reaction coordinate, where a smoother description (if desired) is

obtained by interpolation.^{180,207–211} Simplified schemes exist that link reactant and product rovibrational characteristics by a sigmoid curve, where the rate of change along the RC is tuned by a switching variable;¹⁸⁴ such schemes typically need access to experimental data to derive the switching variable, but then allow fairly good extrapolation to other temperatures. A significant problem for some reactions, such as barrierless recombination or dissociation reactions, is that the nature of the degrees of freedom changes significantly, e.g. for a dissociation there are changes whereby internal vibrations are converted into the molecular rotation of a fragment, or to relative translation, or where there is a change in the number of internal rotors, with a concomitantly large change in state density. These modes are called the transitional modes, and are often the key determinants of the rigidity or looseness of the TS in association/dissociation reactions. The seamless description of these modes over the entire RC remains problematic, and is currently best treated by re-examining the hessian or other molecular properties at each point along the RC, and applying the description that is most appropriate at that point.

Canonical variational transition state theory (CVTST) re-optimizes the position of the TS for each temperature.¹⁸⁰ This methodology is already sufficient to explain and quantitatively predict some reactivity trends for barrierless reactions. For the example of a barrierless association reactions (e.g. Figure 2 or a radical-radical recombination), it is seen that one generally recovers a negative temperature dependence of the rate coefficient as a natural result of the minimization procedure. Indeed, at low internal energies, i.e. at low temperatures in canonical terms, the lowest rate coefficients are predicted for the larger fragment separations where the energy profile is at its highest values, thus limiting the amount of internal energy and hence leading to the lowest state density. For higher internal energies / temperatures, the lowest TS partition functions (or accessible number of TS quantum states)

are found at shorter separations, where the newly formed bonds are stronger, with larger energy quanta for these more rigid degrees of freedom; the somewhat higher internal energy afforded by the downward slide of the potential energy curve becomes a less significant factor. Overall, we then see a tightening of the TS from lower energies / temperatures to higher energies / temperatures, leading to a decrease in the activation entropy and hence in the effective rate coefficient. For some reactions, and especially at lower pressures, this negative temperature dependence is further strengthened by increased redissociation of the adduct at higher nascent internal energies.

Further refinement of the variational procedure, for canonical TST (CVTST) and especially for microcanonical TST (μ VTST, RRKM) can be achieved by optimizing the TS for each internal energy E , and even for each J quantum number for molecular rotation. Once the energy-specific optimal TS is known, i.e. when the point along the RC that yields the smallest number of reactive quantum states is found for each energy E , the temperature-dependent rate coefficient can be recovered for each T by averaging over the appropriate Boltzmann distribution. It is clear that every additional dimension that is optimized increases the computational cost, but also improves the quality of the description. Examples include the study of Vereecken *et al.*²¹² on the CH₂OO self-reaction, and the work by Kuwata *et al.*²¹³ on H-migration reactions in peroxy radicals; both find a reduction of ~30 % of the predicted rate coefficient when improved via the variational treatment.

In the above discussion, we have implicitly assumed that the transition state hyperplane lies perpendicular to the reaction coordinate, i.e. one can separate the RC from the other degrees of freedom. Often, one even approximates the reaction coordinate vector as a single bond length, obtaining rovibrational characteristics along the RC by quantum chemical calculations on constrained bond length geometries. The variable reaction coordinate approach, VRC-TST,^{205,214–219} allows for a

more flexible description of the TS dividing surface by allowing the distance between moieties to be described based on pivot points that are additionally optimized to variationally provide an optimal RC representation. This method also includes the anharmonic coupling between the transitional modes by a direct Monte Carlo sampling of the relevant phase space. This allows for an improved description specifically for those modes that change significantly in the reaction, such as the modes that correlate with relative rotation and translation of products. This method has been implemented using on-the-fly, multi-reference quantum chemical calculations (CASPT2 and MRCI) in the sampling of the phase space.

Most radical + radical association reactions and the reverse dissociation reactions occur on potential energy surfaces without an intrinsic barrier; making variational transition state theory calculations essential to an accurate treatment. Because transition states in radical-radical reactions are typically rather early, the accurate calculation of canonical and microcanonical rate coefficients is difficult and requires a high quality potential energy surface (which accounts for the multi-reference character of the wavefunction where necessary) and a detailed treatment of the transitional modes.²¹⁹ The difficulty of such calculations, and the considerable inaccuracies resulting from the use of lower level quantum chemical and kinetic methodologies, present problems in the more routine analysis of barrierless reactions.

Reactions are pressure dependent (see section 2.4) and the high pressure limiting rate coefficient is a key target for theory. It has been recognized for many years that $k_{\infty}(T)$ for dissociation can be obtained by calculating the Laplace transform of $k(E)N(E)$, with $1/k_B T$ as the transform variable. $N(E)$ is the rovibrational density of states of the reactant.^{184,220} This relationship allows $k(E)$ to be calculated from the inverse Laplace transform (ILT) of $k_{\infty}(T)$ (dissociation). If an Arrhenius form is used, the ILT is

very simple. The problem is that accurate experimental determination of the rate coefficient over the required wide range in T is difficult and uncertainties in the calculated $k(E)$ can be substantial. It is much more accurate to use an ILT based on $k_{\infty}(T)$ (association) for the reverse reaction, which is linked to $k_{\infty}(T)$ (dissociation) via the equilibrium constant.²⁰⁴ The association rate coefficient varies weakly with T and can be determined accurately over a sufficiently wide range of temperature to allow the calculation of reliable values for $k(E)$. The approach has been used in fitting to experimental data using a master equation analysis of measurements in the fall-off region (section 2.4.3).^{221,222}

2.3.5. Tunneling

Tunneling is a quantum phenomenon that occurs when the wave function of a particle hitting a potential energy barrier extends beyond the barrier to the other side, allowing the particle to travel through the barrier. Tunneling is important only for the lightest of particles, such as electrons or, in the present context, hydrogen atoms. For heavier particles, the probability for tunneling becomes very small, and tunneling corrections are negligible compared to the uncertainties induced by errors on the barrier height or calculations of state densities. For chemical reactions, the largest effect of tunneling is typically seen upon substitution of H-atoms by D-atoms; the observed isotope effect on the rate coefficient is largely governed by a significant change in tunneling probability; a second effect impacting the rate coefficient upon deuteration is the difference in the change in ZPE between reactant and TS. At atmospheric temperatures, tunneling corrections can be several orders of magnitude for e.g. H-transfer reactions, especially at lower temperatures.

The simplest methodology to describe tunneling is the Wigner theory,²²³ which assumes an inverse parabolic barrier of a width determined by the imaginary wavenumber for the RC saddle point.

This methodology typically does not yield reliable tunneling corrections, even when fitting the parabola to the actual PES energy profile rather than merely relying on the imaginary frequency. The reaction coordinate energy profile can be described more accurately by using an (asymmetric) Eckart energy curve²²⁴ for the energy barrier; its shape is determined by the energy difference between reactant, TS and product, and the width implied by the imaginary frequency for movement along the reaction coordinate. Eckart tunneling corrections²²⁵ are often, though not always, found to yield results in good agreement with more elaborate treatments, and the method remains a cost-effective choice for tunneling corrections. A more elaborate version of one-dimensional tunneling corrections explicitly uses the energy profile of the reaction along the RC, integrating the tunneling probabilities for a particle of effective reduced mass μ_{eff} through the energy barrier cross-section.

$$\kappa(E) = \exp\left(\frac{-4\pi}{h}\right) \int \sqrt{2\mu_{eff}(RC)(E_{RC} - E)} dRC \quad (8)$$

This method is often called WKB tunneling, based on the mathematical treatment by Wentzel, Kramers, and Brillouin needed to describe the quantum chemical problem near the turning points of a square potential, i.e. where the potential energy equals the available energy. The above tunneling methodologies are zero-curvature tunneling^{185,226} (ZCT) corrections, as they include tunneling solely along the 1-dimensional reaction coordinate; the Wigner and Eckart approaches can be seen as special cases of the general ZCT method for which analytical solutions to the integration are available.

For most reactions, the reaction coordinate is not linear, but curved. This allows multidimensional tunneling on the concave side of the curve of the 1-dimensional reaction coordinate, so-called “corner cutting”.^{227,228} The most popular methods incorporating this effect are small-curvature tunneling²²⁹ and large-curvature tunneling.²³⁰ Large-curvature tunneling corrections carry an additional computational cost, as Hessians need to be calculated for geometries outside the minimum energy path.

The small-curvature correction, in contrast, calculates an effective mass for tunneling based solely on the shape of the PES surface as obtained from the first and second-order derivatives (hessian) of the PES along the reaction coordinate, i.e. it provides a correction on the zero-curvature approximation that is only valid when the curvature is small to moderate. The SCTST method intrinsically incorporates multi-dimensional tunneling corrections, though solely using anharmonicity constants at the TS geometry as a measure of the entire energy profile for tunneling is not always sufficiently accurate. The iSCTST method^{231,232} corrects for this, incorporating additional data to ensure the chemically correct reactants and products energies are recovered.

2.3.6. Multi-surface Reactions

The vast majority of the radical reactions which drive atmospheric chemistry mechanisms are ultimately a result of initial photolysis reactions which derive from the interaction of incident solar radiation with a molecule, producing chemical species in electronically excited states. However, the theoretical description of electronically excited states in tropospheric chemistry remains a specialized field of research, with most workers focusing on ground state kinetics and dynamics, except for the specific case of O(¹D). This tendency is a result of two considerations: (1) the atmospheric lifetimes of electronically excited molecules is typically very short at atmospheric temperatures and pressures (especially in the troposphere), and (2) accurate modeling of a molecule's electronically excited states presents a significant computational challenge. A detailed account of non-adiabatic dynamics is beyond the scope of this review, and the reader is referred to a number of other reviews^{102,233,234} on this topic. Suffice it to say that there are a number of chemical events that cannot be explained solely by invoking

the Born-Oppenheimer approximation on a single adiabatic PES. Below we outline some recent efforts^{235–241} aimed at treating the dynamics of atmospheric reactions which involve electronically excited states. In general, molecules are characterized by a range of electronic potential energy surfaces, each of which is associated with a particular electronic and spin symmetry. When the spacing between these states is large, then it is a good approximation to invoke the Born-Oppenheimer approximation and consider only a single electronic state (typically the ground state); otherwise, the Born-Oppenheimer approximation breaks down as a result of the fact that the timescales for nuclear rearrangement are similar to those for electronic rearrangement. In such cases, more sophisticated methods are required to make accurate predictions – in order to characterize the multiple electronic surfaces, and also in order to propagate dynamics or calculate kinetic quantities.

The earliest analytical treatment^{242,243} of non-adiabatic transitions was outlined by Landau and Zener for the case of a simple one-dimensional system composed of a diatomic molecule which exhibits an avoided crossing between two adiabatic curves which result from an intersection between coupled diabatic curves that are approximated as linear. The approach is only strictly applicable to one dimensional systems, similar to tunneling corrections like the Wigner, WKB, and Eckart methods; however, there are a number of cases where the simple 1D Landau-Zener approach provides reasonable results even for multi-dimensional systems. Such applications, for example in the case of spin-hopping,²⁴⁴ require removal of the ‘hopping coordinate’ along which non-adiabatic transition occurs, analogous to the removal of the reaction coordinate in adiabatic transition state theory. In such non-adiabatic rate theories, the minimum energy crossing point (MECP) occupies a role similar to that of the transition state (TS) in conventional ground-state TST. The density of states of the spectator degrees of freedom at the MECP can then be convoluted with the hopping probability to yield an effective

density of states within the crossing seam between the two surfaces, and used in the numerator of an RRKM-like expression to give energy-dependent rate coefficients for spin-hopping. Plane *et al.*²³⁹ recently implemented such an approach within a weak-collision master equation to explain experimental observations of pressure-dependent spin-hopping fluxes for reactions occurring in Earth's ionosphere; however, applications of such methodologies to atmospheric chemistry have not been widespread.

Beyond this statistical approach, another strategy for treating non-adiabatic processes involves explicitly simulating the atomistic dynamics of a molecular system. In many cases, such approaches provide remarkable insight into non-adiabatic dynamical phenomena;^{242,245} however, they often incur significant additional computational cost, insofar as they require either pre-computation or on-the-fly evaluation of multiple potential energy surfaces. Again, a detailed account of the different strategies for non-adiabatic dynamics propagation is beyond the scope of this review. The most rigorous approach for non-adiabatic dynamics propagation is the multiconfigurational time-dependent Hartree (MCTDH) method,²⁴⁶ in which nuclear propagation is treated using multi-dimensional Gaussian wave packets. However, the computational cost of the MCTDH approach is significant, limiting its application to systems with less than approximately twelve degrees of freedom.

In practice, the Ehrenfest mean-field approach, and the surface hopping approach are the most commonly adopted strategies for simulating non-adiabatic dynamics.²⁴² Both of these take a mixed quantum-classical approach to dynamical propagation, where the nuclear motion is treated using classical mechanics, but the forces that govern the classical motion incorporate the influence of non-adiabatic transitions. Within the Ehrenfest approach, the nuclear degrees of freedom evolve on a mean-field potential energy surface which is effectively the average of the relevant adiabatic surfaces. In the

surface-hopping approach, trajectories typically evolve on a single adiabatic PES, with instantaneous hops between surfaces determined by the evolving quantum mechanical state amplitudes. For atmospherically relevant molecular systems, there are a handful of recent studies which have utilized the surface hopping approach to investigate non-adiabatic dynamics.^{235–238,240,241} However, particularly in the case of conjugated hydrocarbon oxidation (e.g., toluene and isoprene),^{5,247,248} there is an increasing recognition that strictly ground state approaches struggle to adequately explain experimental observations, opening up fertile territory for applications of non-adiabatic dynamics to understand atmospheric oxidation mechanisms.

2.4. Pressure-dependent Reactions.

2.4.1. Interaction of Reaction and Collisional Energy Transfer.

Many reactions involve the interaction between collisional energy transfer and chemical transformation. The processes involved are schematized for a model reaction shown in Figure 4.

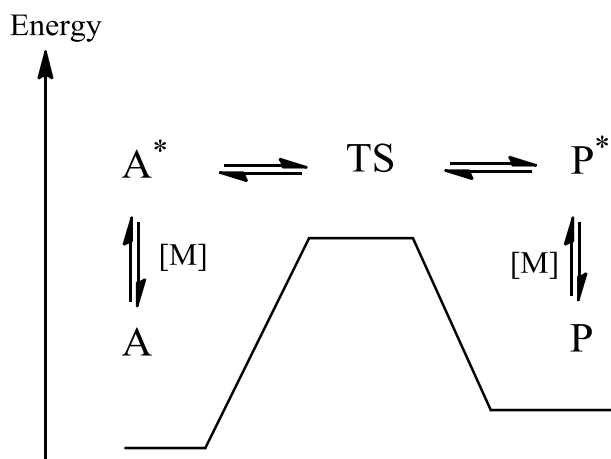


Figure 4. The interaction of a chemical reaction, and the collisional energy transfer between

reactant A and product P with bath gas M.

On the reactant side, low-energy reactants, A, have insufficient energy to cross the barrier, while energized reactants A^* have enough energy to cross the barrier. This causes a depletion of the high-energy tail of the Boltzmann energy distribution for A. At the high pressure limit, collisions with the bath gas, M, are plentiful and energy transfer reshapes the energy distribution of A and restores the Boltzmann distribution. At zero-pressure, the reaction continues until A^* is exhausted, while A remains as unspent reactants, with energies confined to those below the barrier. At intermediate pressures, the rate of energy transfer co-determines the effective rate of reaction. On the product side, a similar effect exists: the products are initially formed with a high-energy content P^* , equal to that of A^* , allowing them to revert to reactants across the barrier; they can be thermalized to products P by energy loss in collisions. At zero pressure, there will be no net formation of stabilized product P, with P^* reverting back to and in a steady-state with A^* . In the high pressure limit, the product P will attain a Boltzmann distribution. Intermediate pressures induce results between these extremes. All energy transfer models describe both collisional energy gain and energy loss, either explicitly or implicitly through microscopic reversibility, that leads to the formation of a Boltzmann distribution at high pressure.

2.4.2. Modelling Collisional Energy Transfer

The modeling of energy transfer events consists of two components: a) how often a collision occurs, and b) when a collision *does* occur, what is the probability $P(E \rightarrow E')$ that a molecule with initial energy E has an energy E' (above, below or equal to E) after the collision? Describing collisional energy transfer has received significant attention in the study of reaction dynamics and current theories still build²⁴⁹ on the seminal work by Landau and Teller published in 1936.

The calculation of the collision number has been described by Lennard-Jones²⁵⁰ as a collision integral governed by the temperature, the reduced mass and pair-wise collision diameter of the molecules, and the well-depth of the mutual attraction potential between the molecules. The pair-wise parameters for collision between two different molecules are derived from the parameters for collision between identical molecules,^{167,250} obviating the need for separate parameters for each collision pair. The exact collision parameters are not known for most molecules, and while mass and diameter can be estimated from geometric information, estimating the well depth ε is not straightforward without explicit quantum chemical calculations. Most authors therefore estimate the collision parameters based on similar molecules for which information is tabulated,^{e.g. 250} though they can also be obtained from dynamics calculations.²⁵¹ It is found that the number of collisions per unit time is similar for most molecules. The uncertainty on the collision number is therefore usually overwhelmed by uncertainties on the energy transfer probability. Notable exceptions to this are collisions between molecules that have strongly attractive potentials at long range, such as charged or strongly polar molecules, e.g. H₂O, or even the attractive interaction between two radicals, e.g. ³O₂ in air chemically interacting with free radicals. Such strongly interacting collisions also tend to transfer more energy per collision compared to the purely physical interaction in collisions with e.g. a noble gas atom.

Experimental data on the collisional relaxation of highly excited molecules show that the probability for energy loss depends exponentially on the amount of energy transferred, i.e. transfers of small amounts of energy are much more likely to occur than large exchanges in energy.²⁵²⁻²⁵⁵ The exponential-down energy transfer model has thus become the most widely used model in theoretical kinetic work. For $E > E'$, the probability for an energy transfer $E \rightarrow E'$ is

$$P(E \rightarrow E') = A(E) \exp(-(E - E') / \alpha) \quad (9)$$

where A is a normalization constant and α is the average energy transferred in a downward direction. α is typically not constant, but depends on the energy of the system.^{255,256} The upward transition probabilities, where the molecule studied gains energy in a collision, are obtained from detailed balance considerations, ensuring that a Boltzmann population is retrieved for equilibrium systems. The upward probability function is also fairly well approximated by an exponential curve, which has led to the use of a bi-exponential energy transfer model proposed by Troe *et al.*²⁵⁷ Recently, Barker and Weston¹¹⁵ examined the E - and J -specific energy transfer by extensive quasi-classical molecular dynamics trajectory calculations of the collision process. They found that the change in the rotational J quantum number is likewise nearly exponential, where the small changes in J in a collision carry the highest probability. This result invalidates some earlier E, J -specific energy transfer models where it was assumed that the J after collision was randomized^{258,259} and thus independent of the pre-collision J value. Barker and Weston¹¹⁵ proposed a two-parameter analytical model that reproduces the trajectory calculations well; this is expected to strongly simplify the inclusion of this model in 2-dimensional (E, J -specific) Master Equations. The exponential models above are fair representations of the energy transfer process, but recent advances^{255,260–266} show that significant improvements are possible by the use of energy- and temperature dependent model parameters, double or stretched exponential functions, and other extensions. The use of dynamics calculations to probe the energy transfer combined with improved experimental methods^{115,267–272} has increased the detail of the data available, and has become a critical tool in the qualitative and quantitative advancement of our understanding. Dynamics calculations are actively used to derive theoretical models for energy transfer, such as the Partially Ergodic Collision Model (PECT).^{273–276} Jasper and Miller^{277,278} examined the validity of the exponential down model, equation 9, for highly vibrationally excited CH_4 , with a temperature-

dependent α using direct dynamics trajectory calculations with a range of methods for calculating the interaction potential between CH₄ and the collider. For He, they found that α varies almost linearly with T, with a value at 300 K close to 100 cm⁻¹. More recently they used the same method to investigate energy transfer between a wide range of hydrocarbons, including radicals, and atomic and bimolecular colliders.²⁷¹ They found that their results were more accurately incorporated in a master equation if a 2-dimensional (E, J) analysis were used.²⁵⁹ The use of trajectory-calculations for obtaining energy transfer parameters has recently²⁷² also been included in the theoretical study of pressure dependent reactions, allowing for a full *a priori* analysis.

2.4.3. Modelling Pressure Dependent Reactions

The simplest example of a pressure dependent reaction is a dissociation, e.g. of PAN, CH₃C(O)O₂NO₂, to form acetyl peroxy (CH₃C(O)O₂) and NO₂. The interaction between energy transfer and reaction leads to a pressure dependence in the rate coefficient that historically was treated using Lindemann theory.^{279,280} For the dissociation reaction, AB → A + B, the steps are described schematically as:



where AB* is a collisionally energized species and M is a bath gas. The overall rate coefficient, k , to form A + B is obtained by applying the steady state approximation to AB*, giving

$$k = \frac{k_1 k_2 [M]}{k_{-1} [M] + k_2} \quad (12)$$

As $[M] \rightarrow \infty$, i.e. at high pressure, $k \rightarrow k_\infty = k_1 k_2 / k_{-1}$ and as $[M] \rightarrow 0$, in the low pressure limit, k

→ $k_0 = k_1[M]$, making it linearly dependent on pressure. At intermediate pressures, k assumes intermediate values between k_∞ and k_0 , leading to a "fall-off curve" for $k(M)$ of which we show explicit examples below. A similar model and rate coefficient structure can be obtained for an association reaction, such as $\text{OH} + \text{C}_2\text{H}_2$, which is discussed below.

The Lindemann model has fundamental deficiencies related to the assumptions that: (a) the rate coefficient for dissociation of AB^* is independent of its energy whereas in reality a molecule dissociates more rapidly as its energy increases, and (b) collisional excitation and de-excitation are essentially single step processes, while in reality energy is added and removed in many smaller steps, as discussed above.

Troe^{167,257} showed that these effects broaden the fall-off curve, i.e. $k(M)$ approaches its high and low pressure limits more slowly than the Lindemann model predicts. He accommodated this broadening by multiplying the Lindemann form for $k(M)$ by a factor F , which he expressed in parametric form as a function of temperature and pressure. Compilations of evaluated rate data, for example by the JPL and IUPAC groups^{1,2} express pressure dependent rate coefficients in terms of $k_\infty(T)$, $k_0(T)$, and a parameter $F_c(T)$, related to F . The parameterisations are usually based on fitting experimental data to the Troe (modified Lindemann) expression.

More fundamentally based methods are increasingly used to describe pressure-dependent reactions. Most approaches use an energy grained master equation (EGME), which allows explicit description of the energy content of an intermediate. The EGME involves the calculation of energy resolved rate coefficients using microcanonical transition state theory coupled with a description of collisional energy transfer. Several methods are available to solve the resulting ME. Some approaches,

discussed below, are based on a stochastic description of the random walk reaction process, while deterministic approaches, described first, express the chemistry in terms of differential concentration changes. The deterministic model generates differential rate equations for bundles of energy states, or grains, in AB, based on the microscopic rates of dissociation (the energy dependent form of k_2 in Figure 5) and energy transfer ($k_1[M]$, $k_{-1}[M]$) and solves these rate equations using matrix methods. Typical grain sizes are a few tens of cm^{-1} ($\sim 0.5 \text{ kJ mol}^{-1}$). Microcanonical transition state/RRKM theory, discussed above, is employed to calculate the rate coefficients for dissociation. Typically, an exponential down model is used for collisional energy transfer (see section 2.4.2). The energy grains and reaction and energy transfer processes are shown schematically in Figure 5.

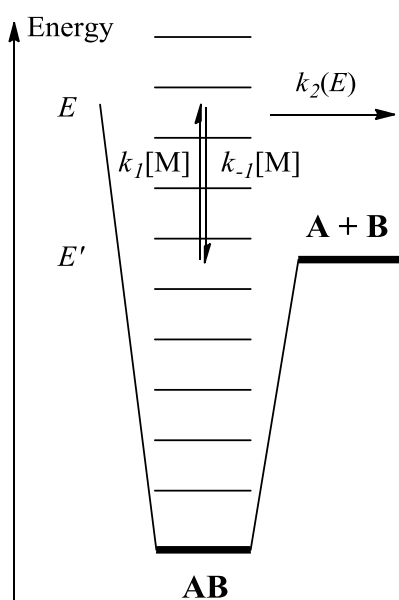


Figure 5. Schematic representation of the set up of a master equation model for dissociation.

The bold horizontal lines represent the ground state energies of the reactant, AB and the products, A +

B. The fine horizontal lines represent the edges of the energy grains. Microcanonical first order rate constants are shown for dissociation from the grain at energy E and for energy transfer between the grains at energy E and E' .

The whole set of coupled differential equations, describing the evolution of the populations in the grains of AB, is then expressed in matrix form:

$$\frac{d}{dt} \mathbf{n} = \mathbf{M} \mathbf{n} \quad (13)$$

where \mathbf{n} is a vector containing the populations of the grains and \mathbf{M} is a matrix that describes collisional energy transfer, and reactive loss by dissociation. Diagonalization of \mathbf{M} yields a set of eigenvalues and eigenvectors, from which the time-dependence of the fractional populations of each of the grains can be calculated. The total number of eigenvalues (and eigenvectors) is equal to the number of grains and the eigenvalues are all negative. The modulus of the eigenvalue of smallest magnitude corresponds to the rate coefficient for dissociation, i.e. $k = |\lambda_1|$ describes the overall loss of reactant to product. The other eigenvalues are termed the internal energy relaxation eigenvalues (IERE), and describe the collisional re-equilibration rates between the energy grains. We can understand the processes involved by considering air containing PAN descending rapidly from low temperature conditions at high altitude to higher T conditions at lower altitude, for example from 5 km and a temperature of 273 K to the surface and $T = 298$ K. At the lower temperature, the lifetime of PAN with respect to dissociation is ~ 3 days and it can be transported over large distances. As the air descends, collisions promote PAN to higher energies from which dissociation takes place more rapidly and the IEREs describe the reciprocal timescales on which this evolution occurs, which are much shorter than those for reaction. When the

relaxation process is complete a new steady state energy distribution is established appropriate to the higher ambient temperature with an enhanced population at higher energies. At 298 K, the dissociative lifetime of PAN has decreased to ~ 45 minutes, which is equal to $|\lambda_1|^{-1}$. For PAN, the steady state distribution is close to the Boltzmann distribution: collisions occur on a faster timescale than reaction and the reaction kinetics follow the high pressure rate coefficient, k_∞ . The microcanonical dissociation rate constant, at a specific energy above the dissociation energy, is much larger for smaller molecules than for larger molecules (because of the relative magnitudes of $W(E)$ and $N(E)$, equation 7). For example, for thermal dissociation of HONO near the Earth's surface, collisions are unable to maintain the Boltzmann distribution, the higher-energy tail of the population is depleted and the rate constant is consequently well below the high pressure limit.

Association reactions ($A + B \rightarrow AB$) are treated similarly, with the rate of association into a specific grain of AB calculated from $k_2(E)$ by detailed balance. Pseudo first order conditions are generally employed (e.g. $[B] \gg [A]$) so that the first order nature of the ME is retained, but the results are applicable for all concentrations $[A]$ and $[B]$. It is still possible to use a master equation approach when $[A] = [B]$ and the macroscopic decay is no longer first order, through a local linearization of the decay, which yields an identical relationship between the smallest magnitude eigenvalue and association rate coefficient. The problem has been discussed in detail by Davis and Klippenstein²¹⁷ for the reaction $A + A \rightarrow A_2$ (specifically for $CH_3 + CH_3$) who delineate conditions where the approach breaks down. When treating association reactions, an additional grain is added to \mathbf{n} to describe the evolution of A, which is assumed to have a Boltzmann distribution of energy (i.e. the pressure is assumed to be sufficiently high to ensure that collisional relaxation of A is faster than reaction). In addition to predictive modelling of dissociation, association and more complex reactions (see below),

master equation methods can be used to fit to experimental data.²²¹ The calculations generate pressure and temperature dependent rate coefficients, $k([M], T)$ which can, for example, be used to generate parameterisations in the Troe format^{167,257} for use in atmospheric models.

Figure 6 shows experimental data for OH + C₂H₂ with He as the bath gas,²⁸¹ and demonstrates the fall-off in the rate coefficient with pressure at all temperatures studied. The data were fitted using a master equation approach and the best-fit rate coefficients were then fitted to a Troe format, which is shown as continuous curves in Figure 6.

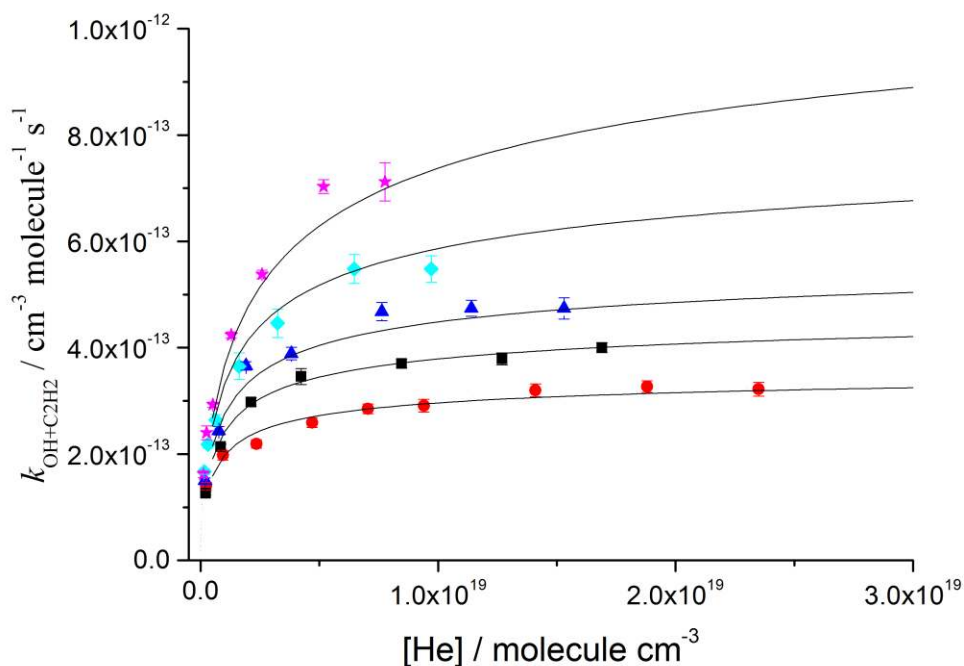


Figure 6. Bimolecular rate constants, $k(T)$, for OH + C₂H₂ at 210 K (circle), 233 K (square), 253 K (triangle), 298 K (diamond) and 373 K (star) in He. Also included as full lines are the Troe format rate coefficients obtained by fitting to a master equation fit to the experimental data. Based with permission on McKee *et al.*²⁸¹ Copyright 2007 American Chemical Society.

More complex examples involve a range of coupled processes, association, dissociation and isomerization, linking bimolecular reactants and products with intermediates consisting of a number of coupled isomers. Figure 2 shows a simplified PES for the $\text{CH}_2\text{OO} + \text{SO}_2$ reaction. The reactants form a cyclic compound with a ground state energy of -159 kJ mol^{-1} relative to the reactants, which can isomerise to a non-cyclic biradical (energy = -113 kJ mol^{-1}) or dissociate back to the reactants. The biradical can dissociate via two transition states to two sets of products. Each of the isomers can be collisionally stabilised. Such systems necessarily involve, in at least some range of pressures and temperatures, timescales for collisional thermalisation and reaction that are comparable, resulting in transient non-equilibrium distributions of molecules across energy states. The language and machinery of equilibrium thermodynamics is consequently inappropriate and alternative methods are needed. The ultimate aim is to derive macroscopic or so-called phenomenological rate coefficients that describe the kinetic behaviour of the reactants and isomeric intermediates and that arise from competition between reaction and thermalization of nonequilibrium ensembles. It is these temperature- and pressure-dependent phenomenological rate coefficients that are used in atmospheric chemistry models.

The same EGME approach discussed above for dissociation can be used for these more complex reactions.^{221,282,283} We consider the schematic reaction shown in Figure 7 where AB is formed from $\text{A} + \text{B}$ and isomerises to AB' , which can dissociate to $\text{C} + \text{D}$

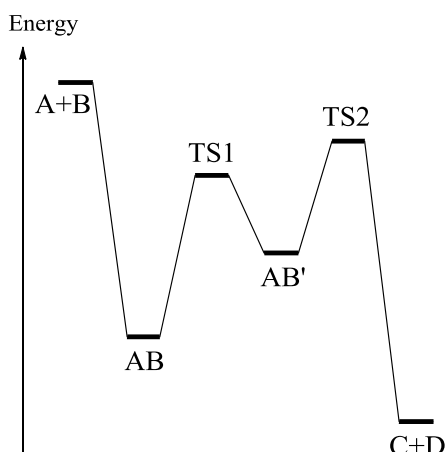


Figure 7. Schematic reaction for formation of AB from A+B, isomerisation to AB', and disassociation to fragments C+D.

As before, the rovibrational energy levels in each different isomer on the potential energy surface are lumped into energy grains, and the time dependent population in each grain for isomer i , $n_i(E)$, is described by a set of coupled differential equations that account for collisional energy transfer affecting each isomer as well as formation from the reactants (A + B), isomerization and dissociation back to the reactants and on to products, C+D. The model assumes that the reactants, A + B, are thermalized via bath gas collisions and conform to a Boltzmann distribution, with one reactant (say B) in excess so that pseudo-first order kinetics apply. Microcanonical rate coefficients for the unimolecular reactions that occur in each energy grain, $k_i(E)$, are calculated from electronic structure data on the isomers and transition states, TS1 and TS2 via RRKM theory. Note that the reactive processes conserve energy and link isoenergetic grains on either side of a transition state. In the case shown in Figure 7 these microcanonical rate constants link A + B with AB, AB with AB' and AB' with C + D. Forward and reverse rate constants are linked via detailed balance, so that, for example

$$\frac{k_f(E)}{k_r(E)} = \frac{N_{AB'}(E)}{N_{AB}(E)} \quad (14)$$

where f and r refer to the forward (from AB to AB') and reverse rate constants. Collisional energy transfer is incorporated using the methods discussed above, based on the collision frequency and the energy transfer probability, $P(E \rightarrow E')$.

In the case where reaction includes a pseudo-first order bimolecular source term to describe the fractional rates of population of the grains in the entrance well by the reactants, then the final element of \mathbf{n} corresponds to the time dependent population of the reactant that is not in excess. Thus the vector \mathbf{n} contains the populations of the energy grains in the isomers AB and AB' and the population of reactant A. The matrix \mathbf{M} contains the microcanonical rate constants for reaction (association, dissociation, isomerisation) and for collisional energy transfer.

Solution yields a set of eigenvalues and eigenvectors. As before, the total number of eigenpairs is equal to the total number of grains. The eigenvalues can be divided into the faster internal energy relaxation eigenvalues (IEREs), and the slower chemically significant eigenvalues (CSEs). The number of CSEs is equal to the number of chemical species. If we treat C + D as a *sink* (i.e. we assume that the final step is irreversible and the products cannot return to the reacting system), then there are three species, A (+B), AB and AB' and three CSEs. All the eigenvalues are negative and, generally speaking, the CSEs are numerically smaller than the IEREs so that the timescales (the reciprocals of the moduli of the eigenvalues) for the chemical evolution of the system are longer than the timescales for energy relaxation. If C (+D) are allowed to re-react, so that the final step becomes reversible, then there are four CSEs, the smallest of which is zero, reflecting the ultimate establishment of equilibrium in the system.

It is important to understand the description and behaviour of a reaction system at both the microcanonical and macroscopic or phenomenological levels. The microcanonical description provides connections, based on our knowledge of the form of the potential energy surface, between the different intermediates, products and reactants. Isomerisation and dissociation occur isoenergetically, across a transition state linking the two microcanonical grains involved. The energy of the system is changed within isomers on collision with the bath gas. The phenomenological description refers to the reactions between the component species where an isomer concentration is given by the sum of the grain populations for that specific isomer. The concentration of the minority reactants (A if $[B] \gg [A]$) is given by the final element in the vector \mathbf{n} . Our aim is to determine the component rate coefficients of the macroscopic system, which are related to the chemically significant eigenvalues. These component rate coefficients are the parameters that are needed for inclusion in atmospheric models.

The phenomenological reactions differ from their microcanonical counterparts in that species that are not directly connected via a transition state can be linked in a phenomenological reaction. For example, despite the fact that $A + B$ must go through intermediates AB and AB' in order to make $C + D$, it is possible for the lifetime within the intermediates AB and AB' to be so short that the most appropriate *phenomenological* description is one where A and B can react directly to form $C + D$ (Figure 7). This occurs at low pressures, where the reactions from AB to AB' and from AB' to $C + D$ occur so rapidly that collisional stabilisation in the isomers cannot compete and the system moves through the energised states and out to the products. The process is termed *well-skipping*. As the pressure is increased there is competition between reaction and stabilisation, well-skipping is suppressed and eventually reaction only connects directly linked species.

The evolution of the macroscopic system is described by a matrix equation comparable to

equation (13):

$$\frac{d}{dt} \mathbf{c} = \mathbf{K} \mathbf{c} \quad (15)$$

where \mathbf{c} is a vector of concentrations ($[A]$, $[AB]$, $[AB']$) and \mathbf{K} is a matrix of first order phenomenological rate constants. The eigenvalues of \mathbf{K} are identical to the CSEs determined from solution of the master equation. The individual rate coefficients can be determined from the eigenpairs. This relationship was first discussed by Bartis and Widom²⁸⁴ and has been further developed by Miller and Klippenstein,²⁸⁵ who have provided two methods for determining the phenomenological rate constants, while a third has been discussed by Robertson *et al.*²⁸⁶ It is important to emphasise that the approach only works if the CSEs and IEREs are well separated in magnitude, i.e. if the timescales for collisional relaxation are significantly shorter (more than a factor of 10) than are those for chemical reaction. If this is not the case, then it is necessary to use the time dependent species concentrations, obtained from the ME, and to fit these to a phenomenological model and extract rate coefficients. These rate coefficients may be compromised by the overlap between the processes of chemical reaction and energy relaxation, and they may not be applicable at conditions of temperature and pressure removed from those covered by the solution of the ME. In many cases where eigenvalue overlap occurs, and especially at higher temperatures, the temporal evolution of the species cannot be described by a phenomenological model. The rate coefficients simply do not exist and it is only possible to derive an expression that reproduces the time dependence for the specified initial set of conditions. In some cases, even this procedure can fail, as discussed by Robertson *et al.*²⁸⁶ for isomerisation and dissociation of 1- and 2-pentyl radicals. In this case the radicals isomerise and dissociate to a significant extent while the collisional relaxation is occurring – the processes of reaction and energy relaxation cannot be temporally separated. Miller and Klippenstein²⁸⁷ have developed methods to

overcome this problem by reducing the number of species involved by invoking local equilibration on short timescales.

As an alternative to describing reaction kinetics as a deterministic change in concentrations governed by a set of differential equations, one can describe the kinetic flow of chemical reactions as a stochastic process,²⁸⁸ implementing the molecular changes as a sequence of discrete, randomly occurring reaction events. Pioneered by the work of Gillespie²⁸⁹ who described the Exact Stochastic Method (ESM), now called the *stochastic simulation algorithm* (SSA), the explicit simulation of chemical kinetics by Monte Carlo simulation is a powerful and versatile technique which adheres closely to the true underlying chemical process. Gillespie showed that it is equivalent to the deterministic approach in the limit of a large number of trials, and Monte Carlo techniques have been applied successfully to the solution of ME for almost 40 years.^{290,291} For a given chemical system, i.e. knowing the number of reactant molecules for each reaction, and the rate coefficients, the time of the next reaction event can be chosen randomly, based on the summed reaction rate across all reactions; the specific reaction event is then again random, where the probability of an individual reaction occurring is directly dependent on its reaction rate relative to the total reaction rate. A step-by-step simulation of this sequence of reaction events then accurately describes the stochastic time-evolution of the chemical process, providing all information needed to reduce the result back to traditional kinetic descriptors such as rate coefficients, product distributions, etc. Monte-Carlo simulations have significant advantages over the deterministic matrix methodologies: their implementation is straightforward and easily parallelizable, the memory requirements are lower, and they are less susceptible to numerical errors. Contrary to matrix-based methods, one can include e.g. delayed events, or reactions that are not

first-order,²⁸⁸ though this is typically less critical for Master Equation analyses. A drawback of Monte Carlo methods for the solution of the ME is that a fitting procedure is needed to derive the phenomenological rate coefficients, as one recovers only the time-dependent concentrations from the simulation. Another drawback is reproducibility, insofar as the underlying Monte-Carlo procedure relies on a random number generator. Thus, the statistical accuracy of the predictions depends on the number of reaction trials simulated. As the computing time depends linearly on the number of trials, Monte Carlo calculations can be rather costly, especially for predicting very-low probability channels. While these channels can also be problematic for deterministic methods due to numerical accuracy, such methods generally provide a more reliable determination of phenomenological rate constants for these minor channels on complex potential energy surfaces with several wells. Still, Monte-Carlo simulations could alleviate some practical problems when moving e.g. toward finer energy grids and two-dimensional E,J-specific Master Equations. Several methods have been proposed to speed up the simulations; an important technique is based on tau-leap methods²⁸⁸ which simulate multiple reaction events simultaneously at accuracies nearly as good as the exact per-reaction methodology.

Matrix-based methodologies for the solution of ME, building upon a stochastic description of the chemical process have been described;²⁹² e.g. the CSSPI method, which calculates the probabilities for finding an intermediate in a particular species energy well and grain, or the DCPD method which directly predicts the product distribution originating from any given starting grain. These methods describe the overall cumulative probabilities over the entire reaction process without requiring steady-state assumptions, but also apply to steady-state conditions. The stochastic matrix-based methods currently available are not as versatile as either Monte-Carlo simulations or the solution of the full deterministic Master Equation, but provide a very cost-effective alternative for some of the most

commonly used results of a ME analysis, e.g. product distributions, for incorporation in general chemical kinetic models.

2.5. Dynamics

The statistical theories outlined so far in this paper play an indispensable role in rationalizing the microscopic mechanisms that drive atmospheric chemistry, and also in our ability to make quantitative predictions. There are a few key requirements that determine the accuracy of statistical theories for a particular system: (a) that it may be adequately described with reference to its constituent stationary points – namely minima and transition states, (b) that robust procedures are in place for mapping the relevant stationary points, and (c) that intramolecular vibrational energy redistribution (IVR) occurs fast enough such that the ergodicity hypotheses holds – i.e., both bond-breaking and bond-forming involve the concentration of substantial energy in a particular subset of normal modes, and ergodicity guarantees that the timescale for intramolecular vibrational energy redistribution (IVR) within the pool of the available vibrational modes is extremely rapid compared to subsequent reaction steps.

As a complement to statistical theories, and also in order to tackle questions which are beyond the scope of statistical approaches, molecular dynamics (MD) simulations have several important roles to play in atmospheric chemistry. An exhaustive account of MD methodologies and applications in atmospheric chemistry is beyond the scope of this review. Consequently, our discussion herein is limited to outlining the most common methodologies along with a few key examples wherein MD has been effectively applied to gain microscopic insight into atmospheric chemistry problems.

In general, ‘MD simulations’ refer to any of a large class of methods wherein one numerically

integrates an equation of motion for the time dependent nuclear dynamics of a particular molecular system, usually within the Born-Oppenheimer approximation. For very small systems, it is possible to explicitly solve the time-dependent Schrodinger equation within a suitably chosen basis set;²⁴⁶ however, in the vast majority of cases where MD is applied to atmospheric chemistry, one propagates a classical equation of motion for the n nuclei of the system, i.e.:

$$-\frac{dV(\mathbf{q})}{d\mathbf{q}} = \mathbf{m} \frac{d\mathbf{v}}{dt} \quad (16)$$

where V is the system potential energy, and \mathbf{q} and \mathbf{v} are $3n$ dimensional vectors comprised of each atom's respective atomic coordinates and velocities at a particular time point. Within the classical Born-Oppenheimer approach, each atom is treated as a point particle, and the forces that it feels depend on the instantaneous electron configuration at a particular geometry. The classical propagation strategy can provide reasonable accuracy so long as quantum effects related to zero-point energy and tunneling are not too important (in general, such effects are most important for light atoms at low temperatures). Furthermore, the classical treatment of nuclei as point particles means that only $3n$ force evaluations are required per timestep. This is a key point given that force evaluations are the most costly component of any dynamics propagation algorithm. It is for this reason that quantum dynamical propagation strategies incur a much larger computational overhead: the nuclei are delocalized, requiring the force to be evaluated as an integral rather than at a specific point.

The ability to accurately predict experimental observables using MD propagation strategies depends very sensitively on the method used to compute the forces. MD simulation studies therefore require one to carefully consider computational cost vs. accuracy in selecting a force evaluation method. There are two primary strategies: (a) “on-the-fly” calls to an *ab initio* force evaluation method at each dynamical propagation step, and (b) calls to efficient parameterized functional forms (which are

usually fit to reproduce *ab initio* or experimental data). Owing to the number of force evaluations typically required within an MD simulation, on-the-fly approaches are generally limited to DFT, semi-empirical methods, MP2 theory, or molecular mechanics (MM) force fields. The latter are formulated in terms of efficient parameterized functions that describe characteristic structural features like bond-stretches, angle bends, torsional rotations, and non-bonded interactions (van der Waals and electrostatic).²⁹³ MM force fields are probably the most common means for running MD simulations, and recent work has shown that the results generated using MM force fields can be considerably improved via the inclusion of terms allowing some treatment of polarization of the electron densities.²⁹⁴

However, even with such improvements, MM force fields do not permit bond breaking and forming, confining their use to understanding phenomena which do not involve such processes – e.g., structural transformations, diffusion timescales, uptake coefficients, etc. One of the simplest ways to transform MM force fields into reactive force fields involves the use of the so-called EVB (empirical valence bond) method, which is a sort of multi-reference MM approach wherein an MD simulation can move smoothly between different MM basis states, and thereby undergo chemical reactions.²⁹⁵ The EVB method is extremely efficient, but it relies on accurately fitting off-diagonal elements of a Hamiltonian matrix which couple together the various MM diabatic basis states. With the appropriate functional forms, recent work has shown that EVB potentials are able to reproduce PESs generated from high-level CCSD(T)-F12 methods.²⁹⁶ Another approach which is commonly used to carry out reactive dynamics simulations involves the so-called QM/MM approach, which invokes a system/bath type division, where the system is treated using *ab initio* methods (and thereby able to undergo reactions), with the unreactive bath treated using MM methods.²⁹⁷ In recent years, there have been fitting strategies developed which utilize other basis sets altogether. For example, Braams and

Bowman²⁹⁸ have recently applied a permutationally invariant PES fitting methodology, in which thousands of basis function parameters are fit to reproduce high level CCSD(T) calculations over large regions of the molecular configuration space. Such methods allow one to efficiently carry out MD simulations on PESs which approximately reproduce many of the topological features of more expensive methods, and have provided significant insight into phenomena like roaming (discussed below); however, owing to the exponential scaling of basis functions with respect to system dimensionality, their use is generally confined to relatively small systems – e.g., ten atoms or less.

Below, we describe a number of areas in which MD simulations have proven useful in an atmospheric chemistry context. Our first example concerns characterizing regimes in which the statistical assumption of ergodicity is valid, and those in which it breaks down. In general, bond-breaking, bond-forming, and infrared excitation involve the concentration of substantial energy in a particular subset of normal modes on short timescales. In some cases, this energy localization can couple to the dynamics of subsequent elementary steps, producing results which are at odds with the predictions of statistical theories.^{299–301} For example, recent MD simulations following OH vibrational overtone excitations in HONO and HONO₂ have revealed fast ‘chattering’ mechanisms that involve rapid H transfer.²⁹⁹ MD simulations following OH vibrational overtone excitation in H₂SO₄ show similar chattering mechanisms which occur on fast timescales, and which are linked to rapid dissociation to SO₃ + H₂O,³⁰⁰ an observation which has helped to resolve well-known discrepancies between measured and modeled stratospheric [SO₂].³⁰²

A second area where MD has contributed is in the discovery of reaction mechanisms that might otherwise be difficult to guess. In this respect, the so-called ‘roaming’ mechanism has attracted a great deal of recent attention.^{303–306} Roaming was first observed to occur in formaldehyde (H₂CO),³⁰⁷ and is a

unimolecular dissociation (and photolysis) mechanism characterized by a nascent co-product which contains a high degree of vibrational excitation. In the case of H_2CO , roaming arises from a pseudo-dissociation wherein H can undergo a ‘roaming’ orbit with respect to its HCO co-fragment, and subsequently abstract the other H atom to give vibrationally hot $\text{H}_2 + \text{CO}$.³⁰⁸ It has since been shown that roaming type mechanisms occur in a range of other systems, including acetaldehyde,³⁰⁹ acetone,³¹⁰ methyl nitrate,³¹¹ and addition-elimination mechanisms in Cl + alkenes.³¹² Whether or not roaming can be treated in a statistical framework is the subject of debate,^{313,314} less controversial is the fact that a “roaming” explanation for the original experimental observations would have been difficult to discover by any sort of method apart from MD simulations.

Finally, MD helps in calculating quantities which are difficult to obtain in a purely statistical framework. As discussed previously in this article, the accurate application of statistical theories requires a treatment of anharmonicity and tunneling coefficients, which impact experimental observables like infrared spectra and rate coefficients. For small, relatively rigid molecules, a statistical framework based on stationary point analysis can be very accurate. However, for larger and less rigid molecules, which sometimes involve weakly non-bonding interactions, MD simulations often provide a more natural framework for treating the effects of anharmonicity, tunneling, and their corresponding impact on vibrational spectra and rate coefficients.^{315,316}

For molecules that include more than ~20 atoms, it becomes a difficult task to map all the stationary points for a given molecular system. In systems with hundreds or even thousands of atoms, there is a large host of thermally accessible minima, and small-molecule concepts like that of a stationary point are of limited use; one must sample a statistically meaningful portion of the relevant phase space. In this context, molecular dynamics (MD) simulations offer a useful sampling strategy,

particularly for understanding chemical mechanisms that occur within condensed phase systems and at gas-liquid interfaces, where there tends to be a large array of local minima. For example, MD simulations have been the theoretical tool of choice for a range of studies aimed at understanding the microphysics of adsorption of halogen-containing species at liquid-air interfaces.^{317,318} The atmospheric context for many of these simulations is the so-called ‘halogen explosion’, an observed spike in halogen radicals (particularly bromine) which occurs during the polar spring and results in tropospheric O₃ depletion. The onset of the halogen explosion has been postulated to occur as a result of heterogeneous chemistry at the seawater-air interface which leads to a build-up in species like Br₂ during the polar winter.^{319,320} A number of MD simulations have been undertaken to understand the corresponding ionic microsolvation dynamics.^{321–323} In general, these MD studies have shown that the propensity of halide ions to accumulate either within the bulk or at the surface varies considerably as a function of the ion polarizability, ion size, ionic concentration, and the precise constituents of multi-component ionic mixtures. For multi-component ionic mixtures at high concentrations, the heavier and more polarizable the ion (i.e., I⁻ > Br⁻ > Cl⁻), the more it will preferentially localize in the interfacial region.

In addition to being used to study ionic behavior at aqueous interfaces, there have also been a host of studies aimed at understanding the kinetics related to the uptake of both organic and inorganic molecules into bulk liquids,^{324–328} as well as associated nucleation phenomena.^{329,330} A detailed understanding of these sorts of kinetic processes is important for understanding the catalytic effects of surfaces,³³¹ as well as the kinetics of aerosol formation and depletion, a physical process which represents a major uncertainty in the radiative forcing of climate models.

2.6. Product Energy Distributions

For decomposition reactions, the energy available in the TS will be distributed over the two fragment moieties, and their relative translation and rotation, subject to overall conservation of inertia and angular momentum. Even when assuming the energy contained in the TS is statistically distributed owing to ergodic energy redistribution, the fragment energy distribution is intrinsically non-statistical. The decomposition dynamics, especially when large geometric changes occur on the product side of the TS, introduce a repulsive interaction between the separating fragments that depends on the separation and the reaction-unique rearrangement of chemical bonds beyond the TS, often placing large quantities of energy in translation motion, far from what one would predict within a statistical framework.^{e.g. 10,296,332,333}

Within an atmospheric chemistry context, product energy distributions are important insofar as they can influence subsequent kinetic processes. For example, a highly excited product molecule will likely undergo subsequent unimolecular processes at a faster rate than one with a low level of nascent excitation, an observation which has been made for the atmospheric oxidation of methylglyoxal.³³⁴ In such cases, dynamics calculations are particularly well-suited to obtain product energy distributions, because they do not invoke the ergodicity assumption, opting instead for an explicit treatment of the sorts of ballistic motions that determine product energy partitioning. Nevertheless, Statistical theories, e.g. Phase Space Theory (PST)^{335,336} or the Statistical Adiabatic Channel Model (SACM),^{337,338} can provide useful qualitative insight into product energy distributions, although the results are often inaccurate compared to experimental data, or costly to apply without major simplifications. For some reactions, such as those proceeding without a barrier on the product side, the re-arrangements past the kinetic bottleneck are fairly minor, and a near-statistical distribution of the energy can be assumed.

Similarly, in cases where there is a strong post-reaction complex (i.e., a complex which has a significant lifetime) on the product side of the barrier, this can serve to increase the probability of energy exchange between the constituent degrees of freedom, improving the statistical requirement of ergodicity. However, in many cases, the timescale for fragment separation is simply too fast to maintain a statistical energy distribution. For this reason, the Statistical Separate Ensembles theory by Wittig *et al.*³³⁹ partitions a dissociating molecular system into three distinct ensembles, each of which corresponds to a distinct collection of degrees of freedom – i.e., two which correspond to the internal degrees of freedom of the fragments, and one for their relative motion. This theory has also been applied for reactions with a product-side barrier, e.g. in the decomposition of primary ozonides to a Criegee intermediate and a carbonyl atom. It was found^{340,341} that the best agreement with the experimental observations was obtained when about 50-60% of the potential energy released on the product side was going to kinematic separation of these fragments, with the remainder distributed across the product fragments as internal energy.

2.7 State of the Art

The rapid increase in computational power available to theoreticians has made the advanced approaches of a decade ago accessible for everyday use. This computational power also allowed specialists to push the boundaries of what is feasible, setting a new baseline for what is expected from contemporary theoretical work in atmospheric chemistry.

For quantum chemical characterizations of potential energy surfaces, CCSD(T) and CCSD(T)-F12 energy calculations based on DFT or QCI geometries have become some of the most widely methodologies, often used with extrapolations to infinite basis set size, and have become the reference

level of theory for compounds up to 7-8 non-hydrogen (so-called "heavy") atoms. For slightly larger molecules, composite methods yield the energy calculations at the required accuracy, while only for the largest of molecules, with ~15 or more heavy atoms, are the use of pure DFT or MP2 PES considered appropriate. For small systems with only a handful of heavy atoms, methodologies that were once considered benchmark-quality are becoming common, e.g. coupled-cluster geometries, energies and wavenumbers. Benchmark results are based on the applications of "sub-chemical accuracy" methodologies, such as HEAT, Focal point analysis, and Wx methodologies (see e.g. section 3). For multi-reference systems, CASPT2 appears to be the most popular method.

The calculation of rate coefficients, and the related product distributions, currently puts a strong emphasis on including "anharmonicity", i.e. effects that are not described by a simple rigid-rotor harmonic oscillator model of the lowest energy geometry of reactant and TS. Whereas separable models for the degrees of freedom are still widely used, the most advanced methods include coupling between the modes, e.g. based on VPT2 calculations obtaining the vibrational anharmonicities. The treatment of internal rotors has progressed tremendously, where current baseline work builds upon the harmonic framework by examining the full conformational space of reactant and TS, and where advanced calculations include the rotations explicitly, including the coupling between the rotations modes. For specific internal modes, such as certain non-harmonic vibrations, fluxional molecules, and internal rotations, the energy profiles along these modes are calculated explicitly and used to obtain quantum state energy levels by solving the pertaining Schrödinger equations. Tunneling corrections likewise use explicit energy profiles, with small-curvature tunneling corrections becoming commonplace. For pressure-dependent reactions, Master Equation analysis are performed incorporating all of the advanced rovibrational methodologies mentioned.

A truly exciting development is the increasing importance of dynamic calculations. For the study of collisional energy transfer, this is rapidly transforming how we are parametrizing our collision models. Likewise, dynamics calculations finally allow for probing non-statistical effects, which are key in e.g. product energy distributions, but also for the many systems that have eluded theory-based quantification by TST and RRKM theory. It appears that, in time, dynamics calculations will also be a natural methodology to further improve our description of the reaction entropy as determined by the coupled anharmonic internal modes, and the coupling to molecular rotation.

3. Thermodynamics.

Electronic structure calculations are widely used to determine enthalpies of formation of radicals to what is widely known as ‘chemical accuracy’, which is generally used to mean to 1 kcal mol⁻¹ (~4 kJ mol⁻¹). Recently a number of higher level methods have been developed to generate enthalpies of formation at 0 K to 1 kJ mol⁻¹; these include W3,⁹⁰ W4⁹¹ and the focal-point⁹⁶ methods and the HEAT protocol.⁹³ HEAT is an acronym for “high accuracy extrapolated *ab initio* thermochemistry” and was developed by an international consortium. The method includes treatment of electron correlation up to the full coupled-cluster singles, doubles, triples and quadruples, calculation of anharmonic zero-point vibrational energies, a scalar relativistic correction, first-order spin–orbit coupling, and the diagonal Born–Oppenheimer correction. Early approaches to the determination of enthalpies of formation depended on the calculation of atomization energies, in which the molecule in question was fully dissociated to its component atoms. A more accurate approach is to determine the enthalpy change of reaction in which the enthalpies of formation of all the component species, other than that under investigation, are known. The enthalpy of reaction should be close to zero to ensure the

highest accuracy (ideally it should be an isodesmic reaction in which the bonds broken in the reactants are of the same type as those formed in the products).

The first HEAT paper determined total energies of 31 species (atoms and molecules) containing a maximum of two non-hydrogen atoms (and up to three hydrogens) that, in combination, allowed enthalpies of formation at 0 K to be determined. A comparison with experimental values (based on the Active Thermochemical Tables (ATcT),³⁴² see below) gave an average error over the 31 species of only 0.3 kJ mol^{-1} and a maximum error of 0.8 kJ mol^{-1} , despite many of the reactions used in the calculations being far from isodesmic. For example the calculations gave $\Delta_f H^\circ$ -values at 0K for OH and HO₂ of 37.07 ± 0.04 and $15.0 \pm 0.6 \text{ kJ mol}^{-1}$ respectively, where the errors are the differences from the ATcT values.

The Active Thermochemical Tables,^{342,343} developed by Ruscic and co-workers, utilise a thermochemical network(TN) which contains all available experimental and theoretical determinations of quantities that thermochemically interconnect the species in the network. Examples include reaction enthalpies, equilibrium constants and atomization energies. Each of these has an associated uncertainty that is used for weighting in the subsequent statistical analysis. This analysis uses all of the available thermochemical cycles in the TN and checks for mutual consistency; the uncertainties in inconsistent determinations are increased until consistency is obtained. Once the TN is internally consistent, ATcT obtains the final results by solving the cycles simultaneously for all included chemical species. The large number of species, cycles and interconnections, coupled with the consistency procedure leads to much lower uncertainties than those associated with traditional sequential, single species analyses.

An example of the approach is provided in an analysis of diatomic molecules.³⁴⁴ The dissociation energies of homonuclear diatomics, such as H₂, N₂, O₂, F₂ define the enthalpies of

formation of the component atoms, which are important in determining many reaction enthalpies and equilibrium constants for atmospheric reactions. They are also essential in evaluating and utilising theoretical calculations based on atomisation energies. The dissociation energy reported for O₂, for example, is $D_0(\text{O}_2) = 493.687_8 \pm 0.004_2 \text{ kJ mol}^{-1}$. The use of comparisons with ATcT in providing improved benchmark theoretical atomization energies has been discussed by Feller *et al.*³⁴⁵

ATcT also provides information on the provenance of its latest enthalpies of formation. The measure used is the relative contribution of a given determination to the final value of the variance of the thermochemical quantity in question. For O₂, 90% of the provenance derives from only four experimental determinations, while 99.9% derives from 106 determinations. The dissociation energy of F₂ is much less accurate than that of O₂: $D_0(\text{F}_2) 154.57_5 \pm 0.10_8 \text{ kJ mol}^{-1}$ and the provenance is much more widely distributed with 78 determinations contributing to the top 90% of the provenance and 99.9% deriving from 1197 determinations. Both experimental and theoretical determinations make prominent contributions to the provenance, and a large number of species and related determinations, in addition to those directly connecting F and F₂, are involved in the overall dissociation energy and its uncertainty, emphasising the utility of the network optimisation approach.

The approach used in ATcT has provided a step change in the determination of enthalpies of formation and their associated uncertainties. From an atmospheric chemistry perspective, the improvement in the data for radicals is particularly significant; both experimental and theoretical determinations contribute significantly to the ATcT values.

4. Reactions of OH Radicals

OH reacts by H-abstraction and by addition to C=C double bonds, major contributors to the initiation of the oxidation of an organic compound emitted to the atmosphere. The rate coefficients have been extensively studied using experimental methods and these measurements generally form the main basis of recommendations in rate data evaluations.^{1,2} Theory, as applied to OH kinetics, is primarily used to rationalise and understand observed behaviour, to determine (or help to determine) product branching ratios, and to identify new and perhaps unrecognised reaction channels. The rate coefficients are usually determined using canonical transition state theory. The transition states are usually well defined, although variational techniques are required in some cases. We provide a brief review of a few selected reactions to illustrate the role that theory plays.

4.1. OH + H₂, CH₄

There are a number of challenges facing the calculation of a rate coefficient, which were discussed in section 2. Calculations of the energy of the TS typically have an uncertainty of ~ 4 kJ mol⁻¹, which translates to an uncertainty in a rate coefficient of a factor of 5 at 300 K. Higher levels of theory are needed for greater accuracy, but are generally only feasible for small molecules. Anharmonicity is usually neglected, assuming that the consequent errors in the densities of states in the reactants and transition state approximately cancel. Internal rotation is often difficult to model and the separability of degrees of freedom, as generally assumed in TST, is not always appropriate. In this section we discuss two examples where high accuracy, as assessed by comparison with experiment, has been achieved.

OH + CH₄ is one of the key reactions in the background troposphere. It has been extensively studied experimentally, mainly by pulsed photolysis. Both the IUPAC¹ and JPL² evaluations recommend an uncertainty in $k(298\text{ K})$ of ~10%. The Arrhenius plot is curved over the wide

temperature range studied (195 – 2000 K), but a linear representation is accurate over the tropospheric range, 200 – 300 K, where the uncertainty in the activation energy is given as $\pm 0.8 \text{ kJ mol}^{-1}$. So the experimental determination is quite secure.

Theoretical values have been calculated by Ellingson *et al.*¹⁴⁴ They used multilevel electronic structure methods that combine several calculations to extrapolate to an accurate result. Their main method was an MCG3/3 extrapolation which includes a QCISD(T) calculation with the 6-31G(d) basis set and an MP2 calculation with the MG3S basis set. The rate coefficients were calculated using canonical variational TST, with small curvature tunnelling. The main complication was the internal rotor in the transition state in which OH rotates with respect to CH₃ about the transferring H atom. They compared their calculations with evaluation recommendations³⁴⁶, finding that they underestimated the rate coefficient by a factor of 1.4 at 250 K and of 1.04 at 700 K, comparable with the uncertainties in the evaluated experimental data.

Nguyen *et al.*³⁴⁷ used Semi-Classical TST (SCTST), discussed in Section 2.3.2, to calculate rate coefficients for OH + H₂ over the temperature range 200 to 2500 K. The use of SCTST intrinsically included multidimensional tunneling and also allowed them to include anharmonicities of the fully coupled vibrational modes. Anharmonicity was of greatest importance at high *T* and tunneling at low *T*. They used the HEAT method (see section 2.2.6 and section 3) to calculate energies, with an uncertainty of better than 0.2 kJ mol^{-1} for the reaction enthalpy change and of 0.8 kJ mol^{-1} for the barrier height. The resulting rate coefficients agreed with experiment within 10% over the whole experimental range.

4.2. OH + CO

OH + CO, like OH + CH₄, is an important reaction in the background troposphere, especially in the northern hemisphere. It has a zero pressure, temperature independent rate coefficient of 1.4×10^{-13}

$\text{cm}^3 \text{ molecule}^{-1} \text{ s}^{-1}$, which increases linearly with pressure to a value $\sim 60\%$ higher at 1 atm.¹ The reaction proceeds through an adduct, HOCO, to form $\text{H} + \text{CO}_2$.

The reaction has been modelled using SCTST coupled with a master equation analysis of the pressure dependence, using the HEAT method to generate the stationary points on the potential energy surface.^{348,349} The surface is comparable to Figure 7 with AB and AB' representing *trans*- and *cis*-HOCO with energies 103.8 and 97.5 kJ mol^{-1} below the reactant energy. There is a small barrier of 3.6 kJ mol^{-1} between the reactants and *trans*-HOCO (TS0). TS2 is 8.2 kJ mol^{-1} above the energy of the reactants. TS1 is the barrier to *trans*-*cis* isomerisation and lies only $\sim 34 \text{ kJ mol}^{-1}$ above the energy of the *trans* isomer. There is, in addition, a small van der Waals well, with a depth of 5.8 kJ mol^{-1} , before TS0, although it does not play a significant role in the reaction under the conditions investigated (75 – 2500 K, $[\text{He}] = 0 - 10^{23} \text{ cm}^{-3}$). Tunnelling through TS2 to form the products is significant below 1000K, enhancing the rate by a factor of 6.5 at 300 K. The pressure dependence arises because the reverse dissociation of HOCO* to form reactants competes with the forward reaction to form the products. Collisional stabilisation of HOCO* favours both formation of HOCO and forward reaction by tunnelling, compared with reverse dissociation. The high pressure limiting rate coefficient is determined by reaction to form HOCO over TS0. The agreement between theory and experiment is excellent, without any tuning of the calculated parameters other than the energy transfer parameter, α (equation 9).

4.3. OH + C₂H₄

As discussed in section 2.3.4, the transition state can be defined canonically as the maximum in the Gibbs energy of activation or microcanonically as the minimum in the sum of states along the

minimum energy path. The interplay between longer range attractive forces and shorter range chemical forces can lead to important kinetic effects of relevance to reactions of OH with polarisable molecules, where there is a relatively strong long range interaction. This can form a van der Waals well which lies at greater intermolecular separations than the energy barrier caused by the chemical interaction. There are now two transition states. The outer transition state lies at the minimum in the sum of states as the reactants approach and experience the decreasing potential energy in the van der Waals well. This transition state is comparable to those discussed in section 2.3.4 and requires a variational treatment. The inner transition state lies at or close to the energy barrier caused by the rearrangement of the electrons in the formation of the new chemical bond.

A good example is provided by the reaction



The non-bonding interaction between OH and the double bond in ethene gives rise to a van der Waals well of $\sim -5 \text{ kJ mol}^{-1}$ and there is an inner transition state, at a shorter distance, that lies below the energy of the separate reactants: it is *submerged*. The inner transition state is much tighter than the outer one, so that its energy levels are more widely spaced. In canonical terms, its entropy is higher than that of the outer TS. While the well depth is comparable to that for OH + CO, it is now kinetically significant because of the low energy of the inner TS.

The reaction has been discussed in detail by Greenwald *et al.*¹¹² The sum of states in Eq. (7) needs to be treated in a unified way including both TS,^{350,351} and is therefore replaced by an effective sum of states $W_{\text{eff}}(E,J)$, where

$$\frac{1}{W_{\text{eff}}(E,J)} = \frac{1}{W_{\text{outer}}(E,J)} + \frac{1}{W_{\text{inner}}(E,J)} \quad (18)$$

At low energies, just above the long range asymptote, there is much more energy available for redistribution among the vibrations at the inner TS, so that the sum of states at the inner TS is much greater than that at the outer TS, the rate coefficient is mainly determined by $W_{\text{outer}}(E,J)$ and the TS lies at long distances. As the energy increases, however, the lower state density at the inner TS becomes a more significant bottleneck and both transition states make a contribution to the effective sum of states, until, at still higher energies, the inner transition state is the main determinant of k . This behaviour is termed transition state switching or channel switching, and can be governed both by internal energy content and by angular momentum conservation.^{112,352,353} Greenwald *et al.* found that the E,J -resolved rate coefficient predictions can be over a factor of 10 below less refined CTST calculations; for atmospheric temperatures, this effect imparts a 30% slowdown¹¹² on the critical OH+C₂H₄ reaction.

OH + C₂H₄ is pressure dependent and the main focus of the calculations of Greenwald *et al.*¹¹² was the high pressure limit. The energy of the inner TS (calculated using roQCISD(T) with the Dunning-style, triple- ζ , and quadruple- ζ (cc-pVQZ) basis sets) was decreased by 4 kJ mol⁻¹ to -4.6 kJ mol⁻¹ to improve agreement with experiment. At 300 K, the calculated rate coefficient, as determined by the inner TS alone, is $\sim 1 \times 10^{-11}$ cm³ molecule⁻¹ s⁻¹ and increases as the temperature is reduced. The outer TS gives a T -independent value of 3.6×10^{-10} cm³ molecule⁻¹ s⁻¹, corresponding to the capture rate coefficient. The two estimates cross at $T = 130$ K, but the outer TS still makes a significant (~30%) contribution at room temperature. They expressed their best estimate of the high pressure limit as a sum of two modified Arrhenius terms: $k_{\infty} = 4.93 \times 10^{-12} (T/298 \text{ K})^{-2.488} \exp(-54.3 \text{ K}/T) + 3.33 \times 10^{-12} (T/298 \text{ K})^{0.451} \exp(59.2 \text{ K}/T)$ cm³ molecule⁻¹ s⁻¹ from 10 – 600 K. For comparison, the IUPAC recommendation¹ is $k_{\infty} = 9 \times 10^{-12} (T/300 \text{ K})^{-0.85}$ cm³ molecule⁻¹ s⁻¹ over the range 100 – 500 K, with an uncertainty of a factor of two.

4.4. OH + (CH₃)₂CO, CH₃OH

The rate coefficient for OH + acetone, which involves H-abstraction to form acetyl + H₂O,^{354,355} shows a complex T dependence, increasing with T above 250 K, but then increasing with decreasing temperature below this value. The reaction has been extensively studied, especially by pulsed photolysis and the IUPAC evaluation gives an uncertainty of $\pm 20\%$ over the range 195 – 440 K in its recommended rate coefficient expression which is a sum of two Arrhenius terms, one with a positive the other with a negative activation energy.

The reaction has been modelled by Caralp *et al.*³⁵⁶ based on electronic structure calculations of Henon *et al.*³⁵⁵ (CCSD(T)/6-311G**//MP2/6-31G**). The reaction involves van der Waals pre-reaction complexes with well depths of 8 – 18 kJ mol⁻¹ and energy barriers of $\sim +8$ kJ mol⁻¹. Caralp *et al.* used a master equation analysis, to allow for collisional relaxation in the van der Waals well, although they could find no pressure dependence. Tunnelling is important at all temperatures investigated (200 – 700 K), and especially at low T .

OH + CH₃OH provides an even more striking example of the role of the van der Waals complex and of tunnelling. The reaction has two channels forming (a) CH₂OH + H₂O and (b) CH₃O + H₂O, corresponding to abstraction of H from the methyl or OH groups respectively. The Arrhenius plot is curved but the IUPAC group recommended a simple Arrhenius expression with an effective activation energy of 2.9 kJ mol⁻¹ over the temperature range 210 – 300 K.¹ They recommended a 15% yield of channel (b) at 298 K, based on kinetic studies of the effects of isotopic substitution, as expected given the greater O-H bond strength.

Shannon *et al.*³⁵⁷ studied the reaction by pulsed photolysis in a pulsed Laval nozzle at 63 and 82

K. They found that the rate coefficient *increased* substantially as the temperature was reduced with values of $\sim 5 \times 10^{-11} \text{ cm}^3 \text{ molecule}^{-1} \text{ s}^{-1}$, an enhancement of a factor of 70 compared with the recommended value at 210 K. They modelled the reaction using a master equation analysis, based on the electronic structure calculations of Xu and Lin³⁵⁸ (CCSD(T)/6-311/G(3df,2p)//MP2/6-311/G(3df,2p)), who found a van der Waals well depth of 20.5 kJ mol^{-1} and energy barriers for channels (a) and (b) of 4.2 and 15.0 kJ mol^{-1} . Shannon *et al.*³⁵⁷ found that pressure had no effect, i.e. there is no collisional relaxation in the van der Waals well. They explained their kinetic observations through an analysis of the energy dependence of the relative rates of reverse dissociation from the well to form the reactants ($k_r(E)$) and tunnelling to form the products ($k_t(E)$). The tunnelling rate increases slowly as the energy is increased above the zero point energy of the reactants, while k_r increases very sharply but is asymptotically zero at that energy. At 300 K the thermal distribution is such that $k_r(E) \gg k_t(E)$ at all significantly populated energies. At 70 K, however, a significant fraction of the distribution has $k_r(E) < k_t(E)$: the lifetime of the complex, with respect to dissociation, at low T is sufficiently long that reaction to form the products by tunnelling is competitive. At still lower temperatures, tunnelling will dominate and the reaction rate will become controlled by the flux over the outer transition state and the rate coefficient will approach the capture value.

The tunnelling calculations of Shannon *et al.* showed that CH_3O is the more probable product at low T , because the imaginary wavenumber for channel (b) ($2958i \text{ cm}^{-1}$) is much larger than that of channel (a) ($1420i \text{ cm}^{-1}$); their calculations gave a yield of CH_3O of 0.36 at 300 K, somewhat higher than the experimental value, but >0.99 below 250 K. They confirmed this interesting result experimentally by observing the formation of CH_3O at 82 K with a first order formation rate constant equal to that for the decay of OH.

The low T behaviour observed for $\text{OH} + \text{CH}_3\text{OH}$ is of no direct importance in tropospheric chemistry; the rate coefficient over the temperature range of interest is well-described by the IUPAC recommendations, although the yield of methoxy at low T should probably be revised. The results are significant, though, in modelling reactions in the interstellar medium, where temperatures can be as low as 10 K. The reaction would be assumed inoperative on the basis of the higher temperature behaviour and the height of the energy barriers. The van der Waals well, coupled with tunnelling through the reaction barrier, introduces a massive change in low temperature reactivity.

In both of these examples, theory plays a secondary role to experiment, one of explaining interesting behaviour rather than providing quantitative *a priori* predictions. The importance of that role, in applications such as atmospheric chemistry, should not be underestimated. Models provide a means of extrapolating experimental data beyond the range of conditions under which measurements were made. The yield of channel (b), for example, is almost certainly underestimated in current models of the upper troposphere, a conclusion that would not be reached on the basis of available experimental data alone. The quality of the low temperature experimental data encourages a more detailed theoretical analysis. Important issues include a variational treatment of the outer transition state using an accurate long-range radial and angular potential, an improved analysis of tunnelling, more accurate transition state energies and a detailed examination of internal rotation in the van der Waals complexes and the transition states.

4.5. OH + Terpenoids

The OH addition and H-abstraction reactions with hydrocarbons have been well-studied, and summarized in extensive libraries with rate coefficients and product channels,^{1,2,359} as well as condensed into structure-activity relationships (SARs, see section 7) that allow prediction of site-

specific rate coefficients even for large hydrocarbons, such as the ubiquitous terpenoids, for which no direct, or no site-specific data are available. For some compounds, however, it was found that their observed rate coefficients were incompatible³⁶⁰ with the SARs and the experimental rate data underlying them; direct product measurements³⁶⁰ found a larger than expected contribution of H-abstraction reactions. Theoretical work correlating the C–H bond strengths in hydrocarbons with their H-abstraction rate coefficient by OH radicals showed^{361,362} that many terpenoids have weakly bonded H-atoms, in particular H-atoms whose abstraction leads to allyl- or superallyl-resonance stabilized alkyl product radicals. At the same time, other H-atoms were found to be deactivated³⁶² towards H-abstraction due to unexpected lack of stabilisation of the product radical. A particularly important example for bicyclic terpenes are the H-atoms on the bridgeheads connecting two fused ring systems where geometric constraints prevent rehybridization from an sp^3 to an sp^2 orbital arrangement in the product radical. The correlations observed between the bond strength and H-abstraction rate then led to the development of predictive correlations, dependent on the type of H-atom abstracted, that allow facile prediction of the abstraction rate, and improve the agreement between SARs and experiment for specific compounds.³⁶² These SARs have since been used extensively in the construction of complete degradation schemes for terpenoids, such as α -pinene,^{363–367} β -pinene³⁶⁸ or pinonaldehyde,³⁶⁹ with often excellent agreement with available environmental chamber data.

5. Peroxy Radical Chemistry

5.1. Peroxy Radicals in Atmospheric Chemistry and Combustion

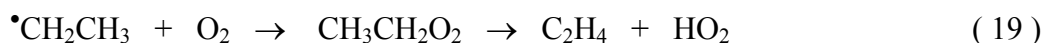
Peroxy radicals play a central role in the oxidation of organic compounds in the troposphere.

Carbon centered radicals, R^\bullet , formed by H-abstraction by OH or OH addition to a double bond, react

rapidly with O₂ to form peroxy radicals. Other formation routes, e.g. via NO₃ addition or H-abstraction by Cl are also important. The high [O₂] in the atmosphere means that the timescale of the R + O₂ reaction is short, typically < 1 μs. Under high [NO_x] conditions, peroxy radicals react with NO to form oxy radicals and nitrates. Under low [NO_x] conditions they react with other peroxy radicals including HO₂.

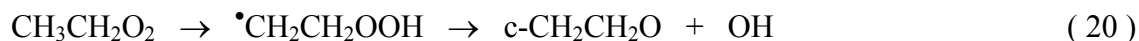
Other reaction routes have been proposed in recent years to explain the observed deficiencies in this mechanistic description. The most discussed example is that of isoprene oxidation, where new mechanisms have been developed in response to higher than anticipated field observations of [OH] in forested regions with low [NO_x].^{370–372} The proposed mechanism, supported by electronic structure calculations^{5,373–376} and later by experiment,³⁷⁷ involves isomerization of the peroxy radical by internal hydrogen atom transfer to form a hydroperoxy radical. Subsequent reactions of one of the hydroperoxy radicals leads to OH formation, and may help to explain the field observations. This topic is discussed in more detail below.

Peroxy → hydroperoxy radical isomerizations play a key role in low temperature autoignition chemistry and have been the subject of numerous investigations.⁶ It is instructive to examine briefly the behaviour observed in such systems and recent insights obtained from both theory and experiment. The ethyl radical provides a well-studied example.^{378,379} Ethyl reacts with O₂ to form a peroxy radical; under tropospheric conditions this is the sole reaction channel. As the pressure is lowered, a new reaction channel occurs, leading to formation of ethene and HO₂.



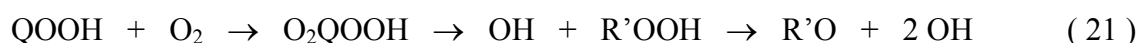
This reaction involves a concerted mechanism and occurs at low pressures by a well-skipping reaction as discussed in section 2.4.3: the system skips over the peroxy radical well at low pressures but is

stabilised into it as the pressure increases. A low yield of OH is also observed at high temperatures, a result of isomerisation to form a hydroperoxy radical which dissociates to OH and oxirane.



The hydroperoxy radical is usually referred to as QOOH. The isomerisation occurs through a cyclic transition state and has a high barrier in this example, because the 1,4-H-shift involves a 5 membered ring structure. Lower barriers, looser TSs and therefore higher rates of QOOH formation are found for 1,5- and especially 1,6-H-shifts. How facile the H-shift is, and the associated rate of the formation of QOOH, thus depend on the structure of the radical, R[•]. Further reaction competes with the reverse isomerisation to RO₂, and the relative energies of RO₂ and QOOH (AB and AB' in Figure 7) are important determinants of the rate, together with the barrier height.

QOOH is central to the autoignition mechanism because it leads to a branching step, following reaction with O₂,



where R'OOH is an oxygenated hydroperoxide. The potential energy surface outlined in Figure 7 provides the basis of the formation of QOOH and its dissociation for a reaction system with lower barriers and more facile formation of QOOH than is the case for the ethyl peroxy radical. It is based on reaction of CH₃OCH₂, formed from dimethyl ether by H abstraction, with O₂, with AB = RO₂ (= CH₃OCH₂O₂), AB' = QOOH (= CH₂OCH₂OOH), C = OH and D = 2HCHO. The phenomenological reactions (section 2.4.3) are shown in Figure 8.

The energies of RO₂ and QOOH relative to R + O₂ are -145 and -100 kJ mol⁻¹ respectively, while TS1 and TS2 have respective energies -57 and -35 kJ mol⁻¹. Thus both transition states have energies below that of the reactants. The reaction system has been examined by Eskola *et al.*,²²² both

experimentally and theoretically. The transition state energies given above were obtained by tuning potential energies from electronic structure calculations to obtain agreement the experimental results, using a master equation model.

At 300 K and at low pressures, OH is formed efficiently by well-skipping over RO₂ (CH₃OCH₂O₂) and QOOH (CH₂OCH₂OOH). As the pressure increases, the OH yield is reduced and RO₂ is the main product. The OH yield, at a given pressure, increases with *T* as the internal energies in RO₂^{*} and QOOH^{*} increase, their lifetimes decrease and stabilisation becomes more difficult. There are three chemically significant eigenvalues (CSEs), λ₁, λ₂ and λ₃, in order of increasing magnitude, which are related in a complex way to the nine phenomenological rate constants (c.f. Figure 7). To a good approximation, though, the moduli of these eigenvalues are close to the reciprocal lifetimes of RO₂, R (+O₂) and QOOH.

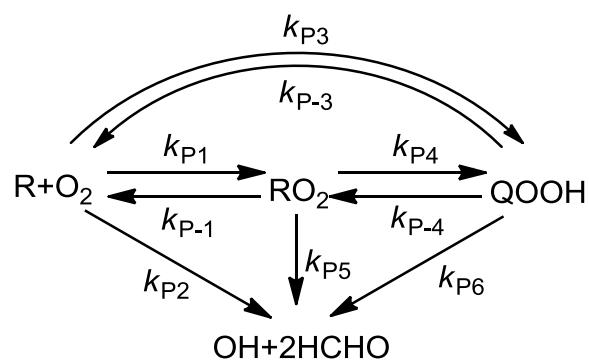


Figure 8. Phenomenological reactions and rate coefficients for methoxymethyl + O₂, as an example of a typical R + O₂ reaction.

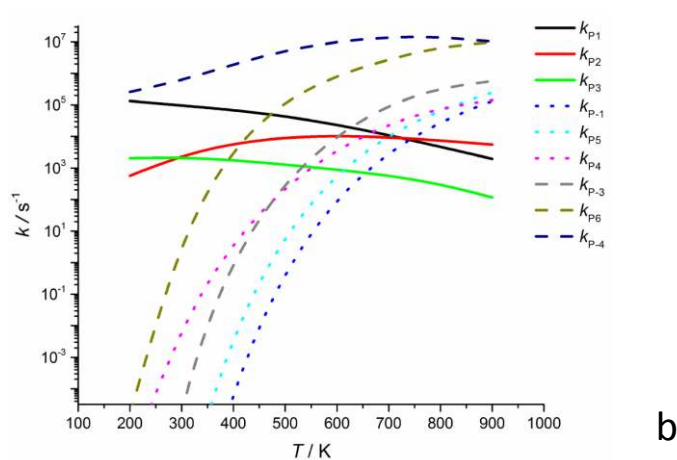
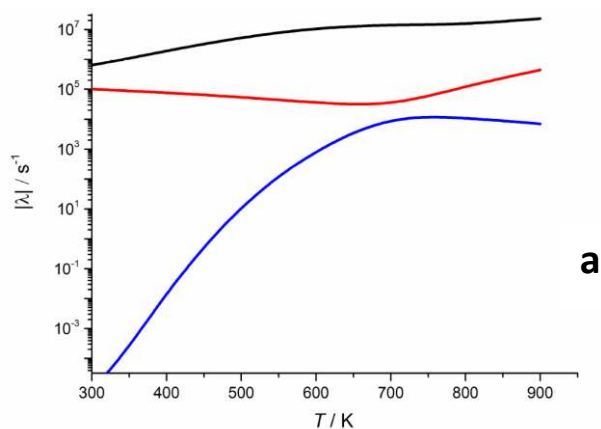


Figure 9. (a) Chemically significant eigenvalues (CSEs) for the methoxymethyl + O₂ reaction system: λ_1 , blue; λ_2 , red; λ_3 , black. **(b)** Phenomenological rate constants for the system as shown in Figure 8. Reaction for R (+ O₂) are shown as full lines, for RO₂ as short dashed lines and for QOOH as long dashed lines. For both figures [O₂] = 1×10^{16} molecule cm⁻³ and the nitrogen pressure is 500 Torr. Reprinted with permission from Eskola *et al.*²²² Copyright 2014, American Chemical Society

The moduli of the CSEs are shown in Figure 9a as a function of temperature at a total pressure

of 500 Torr and with $[O_2] = 5 \times 10^{16}$ molecule cm^{-3} . An eigenvalue-eigenvector decomposition allows the phenomenological rate constants to be determined and these are shown in Figure 9b for the same conditions. At 300 K the lifetime of QOOH is primarily determined by (P-4), isomerisation to RO_2 , but dissociation to $OH + 2 HCHO$ (P6) becomes more significant at higher T as the higher population of the more energised states leads to a higher rate of dissociation. $R + O_2$ leads mainly to RO_2 (P1), although formation of OH (P3) becomes more important at higher T for similar reasons. The main reaction channels for RO_2 at 300 K are formation of QOOH (P4), with well-skipping over QOOH to form OH (P5) next in importance, and dissociation back to $R + O_2$ (P-1) of least importance. The rates of all three channels increase with T and coalesce at the highest temperatures shown in Figure 9. Note that, under these concentration and pressure conditions, λ_1 and λ_2 approach one another at ~ 700 K; the two eigenpairs become mixed and the simple identification of λ_1 with RO_2 and λ_2 with $R^\bullet (+O_2)$ becomes invalid, although the phenomenological rate constants can still be extracted. Figure 9 shows that at higher T the rate constants for RO_2 become higher than those for $R^\bullet (+O_2)$ and are clearly now associated more closely with the higher eigenvalue, λ_2 . Note also that the rate coefficients depend on pressure and that the distributions in the RO_2 and QOOH isomers do not conform to a Boltzmann distribution, even at pressures as high as 10 bar.

The experiments and master equation analysis did not examine the reaction of QOOH with O_2 , which is the key step in autoignition. The lifetime of QOOH is short ($\leq 1 \mu s$) and the radical does not react with O_2 under the conditions studied. Conditions in practical combustion devices, though, involve high pressures (~ 10 bar) and high O_2 mixing ratios (0.2), so that reaction (21) is effective. The potential importance of $QOOH + O_2$ in atmospheric reactions, and the dependence of the lifetime and fate of QOOH on structural factors, are discussed in Section 5.6.

While the above analysis was primarily aimed at the interpretation of experimental results and combustion applications, the ideas developed are relevant to atmospheric chemistry. Key issues determining the behavior of the system and the products formed are the relative ground state energies of RO_2 and QOOH , which influence the relative magnitudes of the forward and reverse isomerisation rates, and the energies of the transition states relative to the energy of $\text{R} + \text{O}_2$, which influence the accessibility of QOOH and of the dissociation products at a particular temperature. We now use the ideas to consider examples from tropospheric oxidation chemistry.

5.2. Oxidation of Acetylene

Acetylene reacts with OH to form the β -hydroxyvinyl radical, HOC_2H_2 , with OH *cis* or *trans* to the radical orbital. Chamber studies have shown that the adduct reacts with O_2 to form glyoxal (+ OH) and formic acid (+HCO); the product yields were unaffected by addition of NO, demonstrating that their formation occurs directly from the peroxy radical, which is short-lived. The yield of glyoxal was 0.7 ± 0.3 and that of formic acid 0.3 ± 0.1 .³⁸⁰ Bohn *et al.*^{381,382} used flash photolysis to generate OH in the presence of $\text{C}_2\text{H}_2 + \text{O}_2$; they showed that OH is regenerated in the reaction sequence, and confirmed Hatakeyama's yield³⁸⁰ of 0.7 for the OH + glyoxal channel.

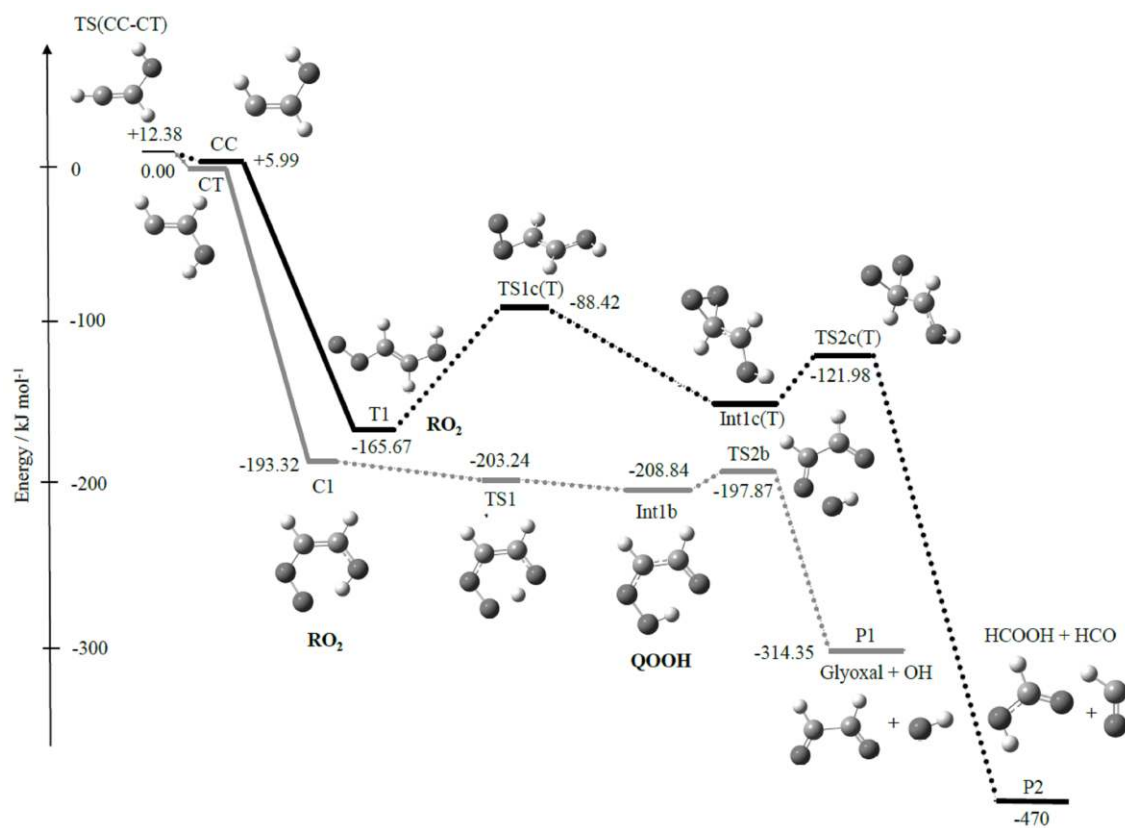


Figure 10. Stationary points on the potential energy surface for $\text{HO-C}_2\text{H}_2 + \text{O}_2$, obtained using B3LYP/6-311+G(3df,2p) geometry optimizations and subsequent G3X single-point energy calculations. CT is the *trans* β -hydroxyvinyl radical and CC is the *cis* radical. Reprinted with permission from Glowacki and Pilling.³⁸³ Copyright 2010 Wiley.

Figure 10 shows the stationary points on the potential energy surface obtained for $\text{HO-C}_2\text{H}_2 + \text{O}_2$. In the *cis* configuration, the peroxy radical (C1, formed from CT) is strongly bound, relative to the reactants, but the transition state for QOOH formation lies even lower in energy and that for QOOH dissociation to form glyoxal and OH also lies below the ground state energy of RO_2 , nearly 200 kJ mol^{-1} below the energy of the reactants. As a result addition of O_2 to the OH adduct CT leads to

unhindered dissociation to glyoxal + OH. There are higher barriers on the reaction route from the *trans* peroxy radical (T1 formed from CC), which occurs via a three membered ring rather than a QOOH species, but these barriers again lie well below the reactant energies, so that the forward rate constants are large and collisional stabilisation ineffective – rapid well-skipping reactions occur to form the products, formic acid + HO₂. The reaction system has been studied in some detail by Maranzana *et al.*^{384,385} using master equation calculations, confirming these conclusions quantitatively .

Bohn *et al.*³⁸¹ observed experimentally that the yield of OH (and therefore of glyoxal) is sensitive to the fraction $f(\text{O}_2)$ of O₂ in a mixture of N₂ and O₂. This was confirmed in a series of experiments by Glowacki *et al.*³⁸⁶, in which $f(\text{O}_2)$ was varied systematically as a function of temperature and total pressure. The yield of OH fell from 0.75 at low $f(\text{O}_2)$ to ~ 0.55 at $f(\text{O}_2) = 0.9$ at $T = 300$ K. The yield was independent of pressure but decreased as the temperature was increased. They rationalised this behaviour on the basis of incomplete vibrational relaxation in the β -hydroxyvinyl radical, following its formation from OH + C₂H₂, before reaction with O₂. The barrier for CT to CC isomerisation is ~17 kJ mol⁻¹, with the CT isomer ~ 6 kJ mol⁻¹ more stable than CC. The OH + HCCH association barrier is ~5.3 kJ mol⁻¹, so that, at 298 K, the average internal energy for the nascent *trans* (CT^{**}) and *cis* (CC^{**}) β -hydroxyvinyl isomers is ~146.6 kJ mol⁻¹ (relative to the ground state energy of the *trans* isomer). At these energies, Figure 11 shows that the state densities of the two isomers are comparable, giving a CT^{**}:CC^{**} population ratio of ~50:50. Because the ground state energy of the *trans* isomer is lower, this ratio falls on collisional stabilisation to ~78:22 for thermal equilibrium at 298 K, also indicated qualitatively in Figure 11. Thus the ratio of the product channel yields depends on the degree of collisional stabilisation of the β -hydroxyvinyl radical when it reacts with O₂, as observed experimentally. The temperature dependence also agrees with this interpretation, with the highest OH

yields being observed at low T , for low $f(\text{O}_2)$.

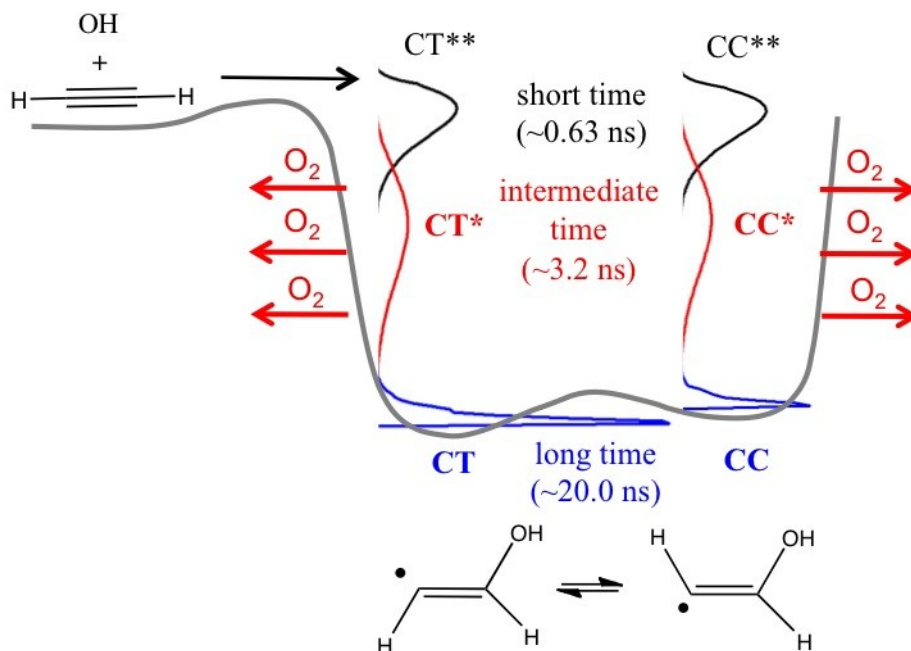


Figure 11. The reaction of acetylene with OH , followed by reaction with O_2 prior to thermalization. Reprinted with permission from Glowacki *et al.*³⁸⁶ Copyright 2012, American Association for the Advancement of Science.

Glowacki *et al.*³⁸⁶ investigated this explanation quantitatively using a master equation method. They had to modify the approach described in Section 2.4, where it is assumed that the reactants in a bimolecular association reaction are fully thermalised. Instead, they initialised the reaction at the $\text{OH} + \text{C}_2\text{H}_2$ stage. The two energised radical isomers so formed could then undergo collisional energy transfer, dissociate back to the reactants and isomerise, as usual, but, in addition, they could react with O_2 as shown in Figure 11. Such a model allows reaction with O_2 at any stage of the thermalisation

process, as required. The peroxy radicals can isomerise and dissociate to form the appropriate products, depending on which isomer was under consideration, and also undergo collisional stabilisation.

Following addition of O₂ to a given CT or CC isomer, collisional stabilisation was unable to compete with the rate of reaction, given the large amount of excess energy compared with the transition state energies, so that well skipping to the products of dissociation was the predominant reaction for both isomers. Glowacki *et al.* identified three distinct collisional relaxation timescales, all shown in Fig 10. At short times (i.e., CC & CT lifetimes less than 0.63 ns prior to O₂ “interception”) collisional stabilization is not sufficient to perturb the CT:CC yield much from 50:50. At long times (i.e., CC & CT lifetimes greater than ~20.0 ns prior to O₂ “interception”) collisional stabilization is complete and the product goes to the equilibrium limit of 78:22. For intermediate times (CC and CT lifetimes between 0.63 – 20.0 ns), the product ratios fall in between these two limits.

Glowacki *et al.*³⁸⁶ also examined the generality of reaction prior to complete thermalisation for peroxy radicals formed under atmospheric conditions. They calculated the fraction of radicals formed in an abstraction or addition reaction that react with O₂ before collisional vibrational relaxation. They carried out the calculations as a function of the R + O₂ rate coefficient, over the range 10⁻¹² – 10⁻¹¹ cm³ molecule⁻¹ s⁻¹, corresponding to timescales at the Earth’s surface of 2 – 20 ns. They also varied the energy of the initial radical from 60 – 180 kJ mol⁻¹ showing that the residual vibrational energy carried forward into the nascent peroxy radical can be substantial. The effects of this residual energy will depend on the reactions available to the peroxy radical. The acetylene case sensitively probes such a process, with product yields that provide a clear demonstration of non-thermalisation. Commenting on the paper of Glowacki *et al.*, Tyndall³⁸⁷ cited the work of Dibble *et al.*³⁸⁸ on *cis trans* isomerisation of the 1-methallyl radical, formed by H-abstraction from *trans*-2-butene, and the potential for subsequent

reaction with O₂ prior to thermalisation of the radical to form the predominantly *trans* species. Tyndall pointed out that 1-methallyl can be considered a prototype for isoprene, which can also exist as *cis* and *trans* allylic radicals, as discussed below.

5.3. Residual Energy in Reactions of Peroxy Radicals with NO

There have been several investigations of the importance of residual energy in oxy radicals formed from the reaction of small peroxy radicals with NO.^{389–393} Small oxy radicals can either dissociate or react with O₂. Orlando *et al.*³⁹⁰ investigated the OH initiated oxidation of ethene in a chamber and over a range of temperatures. They also carried out a theoretical study of the reaction of HOCH₂CH₂O₂ with NO and the dissociation of the oxy radical product. The latter required an analysis of the internal energy retained by the oxy radical in its formation, which was assumed statistical, and a master equation analysis of the competition between dissociation to CH₂OH + HCHO and collisional stabilisation. The results show that the yields of oxy radical dissociation products compared with those from reaction of the oxy radical with O₂ (glycolaldehyde + HO₂) depend sensitively on the prevailing conditions of temperature and pressure.

These analyses emphasise the importance of understanding reaction systems in some detail and not taking experimental results at face value. Not all laboratory experiments are conducted under atmospheric conditions, which themselves vary with altitude. Pulsed photolysis and especially discharge flow experiments are often conducted at reduced pressures and at oxygen concentrations much lower than atmospheric. Variation of the experimental conditions and, wherever possible, the coupling of experiment with theory facilitates a fuller understanding of the reactions system and confidence in the parameters inferred for use in atmospheric models.

5.4. Peroxy Radicals from Aromatics

Detailed mechanisms for the tropospheric oxidation of aromatics are provided by the master chemical mechanism (MCM v 3.2)³⁹⁴ and SAPRC-07/11³⁹⁵. Their mechanisms for benzene, for example, differ in detail but their overall structures are similar and are largely based on chamber and direct rate coefficient measurements and a good deal of conjecture. Experiments show that the initially formed peroxy radical cannot be intercepted by NO under atmospheric conditions and that the main stable products are phenol and, in the presence of NO, glyoxal+butenedial. The mechanism involves initial addition of OH and the phenol product is ascribed to subsequent direct H abstraction by O₂, although a concerted HO₂ elimination from the *trans* equatorial peroxy radical has also been proposed.³⁹⁶ The glyoxal and butenedial derive from a bridged bicyclic peroxy radical via ring opening and dissociation, although their unequal yields found experimentally are accommodated in the MCM by proposing that there is a channel forming 2(3H)-furanone as a co-product of glyoxal, in addition to that leading to butenedial, although 2(3H)-furanone has not been observed experimentally. A minor yield of 2,3-epoxy muconaldehyde is also proposed in the MCM. This compound has been observed but its yield has not been quantified.

The current aromatic mechanisms in the MCM (v3.2) were derived following a substantial analysis and revision based on chamber experiments performed by Bloss *et al.*³⁹⁴ There remained, however, a number of deficiencies, where the mechanisms were unable to reproduce the observed behaviour, including an underestimation of OH, an overestimation of O₃ and a poor representation of the time dependence of NO_x. Chamber experiments suffer from wall reactions, which are not always easy to quantify and such reactions may have contributed to the mechanistic deficiencies, but it is clear that the tropospheric oxidation of these important compounds is imperfectly understood. Experimental

investigations have been extensive but the complexity of the mechanisms presents many problems. Theory has a substantial role to play, especially as a means of directing experiment by identifying reaction channels.

Early investigations of benzene oxidation used B3LYP or semi-empirical methods and mapped out the initial stages of the mechanism,^{397–400} although the accuracy of the resulting energetics was strongly criticised.⁴⁰¹ Raoult *et al.*⁴⁰², in a combined experimental and theoretical investigation, used a CCSD(T)/6-31G(d,p)//B3LYP/6-31G(d) model chemistry for stable species and their own intrinsic method (IM) for transition states. Glowacki *et al.*³⁹⁶ used results from G3X(MP2), G3X(MP2)-RAD, CASSCF, and CASPT2 electronic structure theory to model the behaviour of the system in the early stages of reaction. They found substantial multireference character, whilst identifying a number of potential sources of error in their calculations. Accordingly, they tested the results against the flash photolysis experiments of Raoult *et al.*⁴⁰² using master equation calculations.

The potential energy surface is complex. O₂ adds to the HO-benzene adduct, **I1** (Figure 12), in ortho and para positions with *cis* and *trans* isomers for each, and direct abstraction by O₂ to form phenol + HO₂ also occurs. Glowacki *et al.* made a number of strategic simplifications in constructing their master equation model, based on an initial assessment of transition state energies and timescales of reaction. The *cis* and *trans* para peroxy radicals (**I2-c-p**, **I2-t-p**) have no reactive channels and simply act as a peroxy radical pool, dissociating back to form the HO-benzene adduct + O₂. The ortho species exist as axial and equatorial isomers, which equilibrate rapidly under atmospheric conditions, in 10⁻¹⁰s (for RO₂ trans), with >95% as the equatorial configuration (**I2-t-eq**) and in 10⁻⁸ s for RO₂(cis), with 90% as the axial configuration (**I2-c-ax**). The ortho species provide reactive isomerisation channels, in addition to direct abstraction, leading to formation of a bridged bicyclic peroxy radical, as

shown in Figure 12 for the *cis* case (**I3-c-2,6**). Accordingly, the ME analysis included just the four peroxy radicals, **I2-c-p**, **I2-t-p**, **I2-t-eq**, **I2-c-ax**) In addition, the HO-adduct was included as the minority bimolecular reactant, with O₂ as the majority reactant. There were, in consequence, five chemically significant eigenvalues (CSEs).

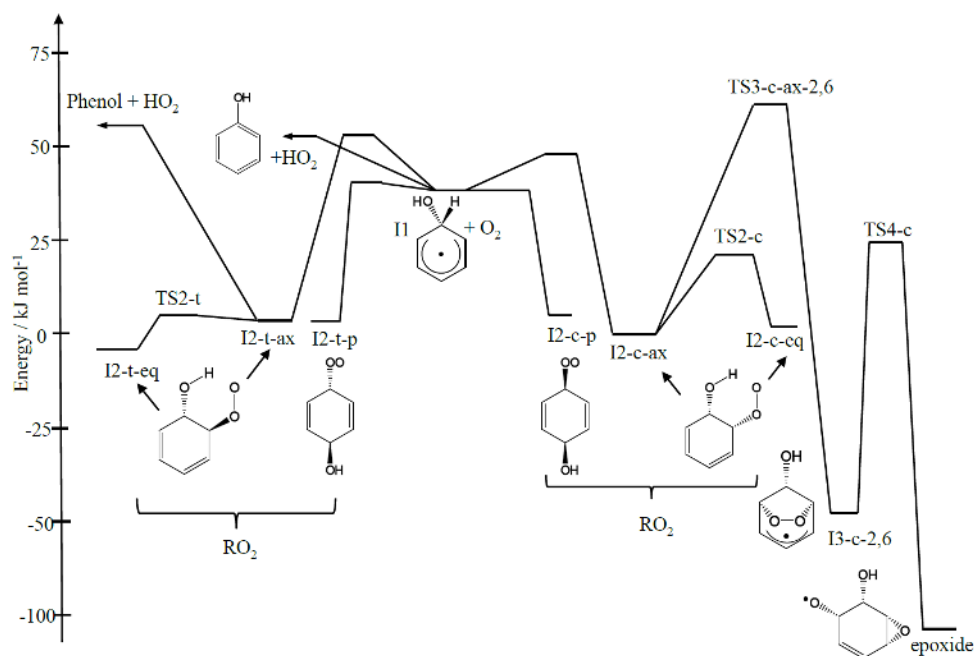


Figure 12. Main stationary points on the potential energy surface for reaction of the OH_{benzene} adduct with O₂. Energies in kJ mol⁻¹. Reprinted with permission from Glowacki *et al.*³⁹⁶ Copyright 2009 Wiley.

The experiments of Raoult *et al.*⁴⁰² monitored the time-dependence of the HO-benzene adduct, **II**, at O₂ pressures of 8 and 150 Torr which they analysed as biexponential decays. The ME analysis of Glowacki *et al.*³⁹⁶ showed that three of the five eigenvalues correspond to reaction timescales much shorter than the experimental values. From a consideration of the uncertainties in the electronic

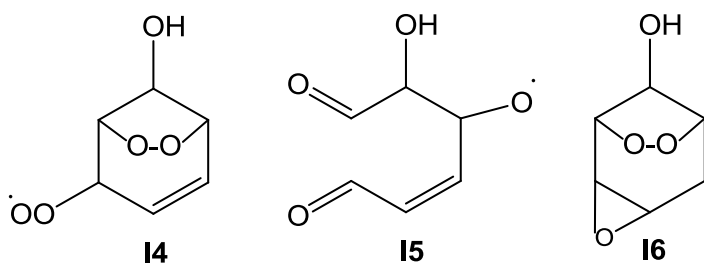
structure calculations, they fitted the biexponential profiles, by minimising χ^2 in a comparison of experimental and theoretical relative **I1** concentrations, using four variable parameters corresponding to the energy of **I1** + O₂, the energies of the transition states from **I1** + O₂ and from **I2-t-ax** (the minority species in the equilibrium with **I2-t-eq**) to phenol + HO₂ and the energy of the transition state from **I1** + O₂ to **I2-c-ax**. They constrained these energies within recognised limits. Other kinetically significant energies were fixed at their calculated values.

The shortest timescales related to the equilibration of **I1** (+O₂) with the two para RO₂ species which occurred in ~1 μs or less, while equilibration with **I2-c-ax** occurred in ~10 μs, all faster than the experimental timescale. The slowest two timescales related to equilibration with **I2-t-eq**, and reaction from the equilibrated system (**I1**(+O₂) and the four peroxy radicals) to form phenol and HO₂, and the bridged bicyclic peroxy radical, **I3-c-2,6**. A Bartis-Widom analysis of the five eigenpairs allowed the rate constants for 11 component phenomenological reactions to be determined. The analysis showed that, even under atmospheric conditions, the system was not quite at the high pressure limit.

They obtained a yield for phenol of 0.66, with the majority deriving from direct abstraction with 0.05 of that yield deriving from **I2-t-ax**. This result is in quite good agreement with the MCM v3.2 (yield 0.53) which is based on experimental values, although there is a good deal of scatter in the latter. The rest of the calculated reaction leads to formation of the bridged bicyclic peroxy radical, **I3-c-2,6**. The most precisely determined tuned energy (i.e. that with the best defined minimum in χ^2) was the energy of **I1** (+O₂), from which the enthalpy of formation of the HO-benzene adduct can be obtained; this agreed very closely with the experimental value obtained by Raoult *et al.*⁴⁰²

Glowacki *et al.*³⁹⁶ also investigated the fate of the bridged bicyclic peroxy radical, and showed that it may isomerise to form an epoxide radical at the experimental pressures; however, this channel

shuts off at atmospheric pressure, because of collisional stabilisation of **I3**. Instead **I3** reacts with O₂ to form the peroxy radical, **I4**. Recent measurements by Birdsall and Elrod,⁴⁰³ in which **I4** was detected directly by chemical ionization mass spectrometry and the dependence of its relative concentration on [O₂] and [NO] determined, could provide the basis for further refinement of the model parameters and the resulting kinetics.



Wang *et al.*⁴⁰⁴ investigated reactions of the oxy radical formed from **I4** at the BH&HLYP/6-311++G(2df,2p) level, refining the optimized structures with single-point energy calculation using the restricted open-shell complete basis set model chemistry (ROCBS-QB3). They used Gibbs energy calculations, arguing that any intermediates are fully collisionally relaxed on experimental timescales. They found that the oxy radical undergoes reaction via two channels: (i) rapid ring opening to form the radical **I5**, which dissociates to form butenedial + the radical CH(O)CH(OH), which in turn reacts with O₂ to form primarily glyoxal + HO₂; (ii) formation of the tricyclic radical, **I6**, which reacts with O₂ and then NO to form glyoxal, 2,3-epoxybutandial and HO₂. The two channels are predicted to occur in the ratio 1:2. 2,3-epoxybutandial has not been observed experimentally, but the calculated butenedial:glyoxal ratio is consistent with experiment.

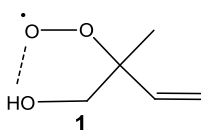
Wu *et al.*⁴⁰⁵ investigated the mechanism of toluene oxidation from the addition of OH to the formation of first generation products, using electronic structure calculations coupled with transition

state theory and master equation calculations. They proposed an oxidation scheme that generates a lower yield of glyoxal and higher yield of butenedial than existing mechanisms. 2,3-epoxybutandial and 2-methyl-2,3-epoxybutandial are products in the mechanism and are proposed as new experimental targets.

5.5. Isoprene

A number of recent field measurements in the Amazon,³⁷⁰ Pearl River Delta³⁷¹ and Borneo,³⁷² found much higher concentrations of OH than conventional mechanisms predict. The conditions under which the measurements were made (high concentrations of isoprene, moderate to low concentrations of NO_x) led to a focus on the chemistry of isoprene. Peeters *et al.*^{373–375} and da Silva³⁷⁶ proposed modifications to the conventional mechanism based on RO₂ \rightleftharpoons QOOH chemistry. The original calculations were at the B3LYP level but a revised analysis has recently been made at the CCSD(T)/aug-ccpVTZ//QCISD/6-311G(d,p) level of theory, and using multiconformer partition functions obtained at the M06-2X/6-311++G(3df,2p) level.⁵

Over 90% of the addition of OH to isoprene (2-methyl-1,3-butadiene) occurs at the 1- and 4-positions (labelled cases I and II by Peeters *et al.*⁵); both give *cis* and *trans* OH adducts. These adducts are resonance stabilised allyl radicals and the peroxy radicals formed following O₂ addition are relatively weakly bound, because the allylic character is lost, with bond energies of only ~80 kJ mol⁻¹, compared with the more usual 120 – 140 kJ mol⁻¹. Three peroxy radicals can be formed for each of cases I and II with similar rate coefficients; crucially, the most stable of these peroxy radicals (**1**)



can be formed from both *cis* and *trans* OH adducts. As a result of the low bond energy, the reverse dissociative loss of O₂ regenerating the OH adduct is relatively fast and the peroxy radicals can interconvert by dissociation followed by reformation of one of the peroxy radicals and a pool of linked peroxy radicals is formed for each of the cases I and II.

Peeters *et al.*⁵ adopted a canonical model, arguing that all of the intermediates are fully thermalised. Pfeifle and Olzmann²⁰³ used a master equation analysis in which the various stages of reaction were coupled. They found that the peroxy radicals were not chemically activated, but rather that fast formation and reformation of the RO₂ intermediates maintained the rate coefficients at their high-pressure limits and prevented steady-state population depletion of the high energy tail, which would lead to fall-off. Peeters *et al.*⁵ criticised their analysis, arguing that the rate coefficients they had adopted for the peroxy formation and dissociation reactions were too high by up to a factor of 100 and that if more accurate values had been used in the calculations, any deviations observed from thermal energy distributions would have been negligible.

We examine the reaction mechanism for case I (OH addition at the 1-position); that for case II is similar. The main reaction channel for **(2)** in Figure 13 is a 1,6-H atom shift to form the QOOH species **(3)**, which is stabilised by both the allylic resonance energy and by H-bonding. This behaviour contrasts with the rate of QOOH formation from alkyl peroxy radicals, discussed above, where the peroxy radical is more stable and QOOH is less strongly bound.

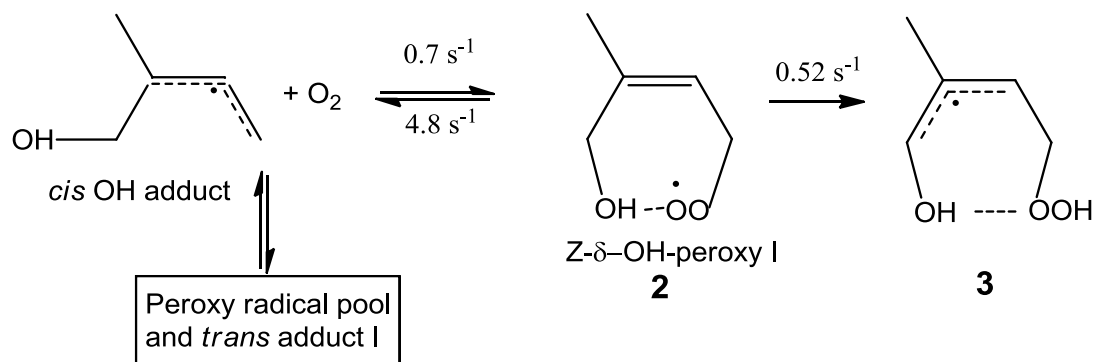


Figure 13. Formation of the hydroperoxy allyl radical **3** via O₂ addition on the allylic OH adduct followed by a 1,6-H-migration.

Peroxy radical (**1**) can form a non-resonance stabilised QOOH species by a 1,5-H shift but the rate coefficient is much smaller ($6.5 \times 10^{-4} \text{ s}^{-1}$ at 298 K) and it reacts instead in the conventional manner with NO or with peroxy radicals, as does the other peroxy radical formed from the *trans* adduct.

QOOH (**3**) reacts with O₂ to form a peroxy hydroperoxy radical which rapidly eliminates HO₂ to form a conjugated aldehyde, O=CHC(CH₃)=CHCH₂OOH, termed HPALD I. In the proposed mechanism, HPALD I is rapidly photolyzed, breaking the weak O-O bond to form OH and an oxy radical, and thus providing a means of regenerating OH from isoprene, in accordance with the field measurements. There is good experimental evidence for this photolysis channel, based on chamber investigations of a molecule whose structure is similar to HPALD.²⁴⁷ The yield of HPALD, and thus OH, is limited, however, by the reversible reactions linking (**2**) to the peroxy radical pool, to which it contributes a steady state fraction of only ~1%, thus substantially decreasing the effective reaction flux to OH. The resulting effective rate coefficient, k_{bulk} , defined as the rate of the 1,6-H shift divided by the total concentration of reactively coupled peroxy radicals, is in agreement, within a factor of two,⁵ with

measurements of the rate of HPALD formation by Crouse *et al.*³⁷⁷

At 298 K, reaction via the isomerization mechanism, with an effective pseudo-first-order rate constant, k_{bulk} , competes with traditional reaction of peroxy radicals (reaction with NO and peroxy radicals) when the pseudo first order rate constant for the latter, k_{tr} , is less than $\sim 0.1 \text{ s}^{-1}$. Interestingly k_{bulk} increases as k_{tr} gets larger, because the steady state fraction of (2) in the pool increases as the lifetimes of the other peroxy radicals decrease – reactions with NO and other peroxy radicals have a greater effect on their lifetimes because they are comparatively long.

Earlier papers from the Leuven group,^{373–375} at a lower level of theory, resulted in larger values for k_{bulk} that were not compatible with the experiments of Crouse *et al.* The new calculations crucially took account of the effects of dispersion forces in the important H-bonding, reduced the uncertainty in the barrier heights for H transfer and improved the treatment of the interconversions in the OH-adduct, peroxy radical pool. Other potential pathways for OH formation were also identified, including a parallel route to that leading to HPALD; the subsequent reactions of these species have not yet been investigated but do have the potential to generate further OH. While the effects of the QOOH chemistry in the Leuven mechanism are smaller than those obtained earlier with lower levels of theory, there is clearly now good agreement between laboratory experiment and theory and clear demonstrations of the importance of the chemistry resulting from the 1,6-H shift. For example, Peeters *et al.*⁵ carried out global modelling with the revised mechanism and found that 28% of the emitted isoprene reacts via the 1,6-H shift isomerisation route.

5.6. Formation of Secondary Organic Aerosol

Jimenez *et al.*⁴⁰⁶ discussed the importance of secondary organic aerosol (SOA) in the total

atmospheric aerosol burden. They argued that the formation of SOA depends on reactions in the atmospheric oxidation of an emitted organic compound that lead to increased functionalization and hence to an increase in the O:C ratio and a decrease in the evolving compound's volatility. This process competes with oxidative degradation which leads eventually to carbon dioxide and water and involves fragmentation and the formation of compounds of higher volatility. More recently, Riccobono *et al.*⁴⁰⁷ obtained experimental evidence that highly oxidized compounds derived from biogenic emissions play an important role, in conjunction with sulphuric acid, in the formation of new particles in the boundary layer, requiring a mechanism in which the increased functionality occurs rapidly.

The mechanism whereby substantial increases in the O:C ratio can compete with oxidative fragmentation is far from clear. Crouse *et al.*⁹ recently obtained evidence that sequential RO₂ → QOOH reactions can play a role in this process. They studied the OH initiated oxidation of 3-pentanone in a chamber under atmospheric conditions, which involves H-abstraction primarily at the 2-position. The peroxy radical, formed from addition of O₂, underwent relatively slow 1,5-H-transfer with a rate constant $\leq 0.002 \text{ s}^{-1}$ to form a hydroperoxy alkyl radical. Following further addition of O₂, a much more rapid 1,5-H transfer ($k > 0.1 \text{ s}^{-1}$) occurred, accompanied by dissociation to give OH and a hydroperoxy diketone (see Figure 14).

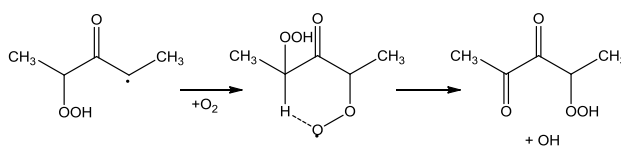


Figure 14. OH formation from QOOH radicals after O₂ addition and 1,5-H-migration.

They deduced the magnitude of the rate constants from the observation of the yields of products from this reaction sequence and from competing reactions with NO and HO₂, for which the total rate constant, under the experimental conditions, was $\sim 0.01 \text{ s}^{-1}$.

Crouse *et al.*⁹ also examined the implications of their experimental finding using electronic structure calculations (B3LYP / 6-31+G(d,p) refining the geometries for the RO₂ 1,5-H-shift reactions with B3LYP/aug-cc-pVTZ). In particular, they examined the energy barriers for the forward and reverse isomerizations for the 1,5-H shift, using a C₅ backbone, with different degrees of functionalisation with carbonyl, hydroxy and hydroperoxy groups. This allowed them to calculate the relative rates of the forward and reverse isomerizations. The different groups essentially change the relative energies of the RO₂ (AB) and QOOH (AB') species in Figure 7, as well as the energy of the transition state. They compared these rates with a pseudo first order rate constant for reaction with NO of 0.02 s^{-1} , corresponding to a NO mixing ratio of ~ 100 pptv. With a hydroxyl group in the 4 position, for example, the yield of QOOH approaches unity. For an alkane, the fractional isomerisation yield was ~ 0.0015 . They concluded that “as organic compounds gain oxygen-containing moieties (and thus partition more strongly to the condensed phase), the rate of autoxidation accelerates. Thus, autoxidation becomes more competitive with other peroxy radical chemistry as the carbon pool becomes more oxidized, leading to formation of carbonyl-rich compounds.” Furthermore, a substantial increase in the oxygen content can occur in a single generation, because of the preservation of the radical centre in repeated $\text{R} + \text{O}_2 \rightarrow \text{RO}_2 \rightarrow \text{QOOH}$ sequences.

Clearly peroxy radical isomerization, so central to low temperature combustion but rarely invoked in atmospheric chemistry until recently, plays an important role in a number of important tropospheric processes.

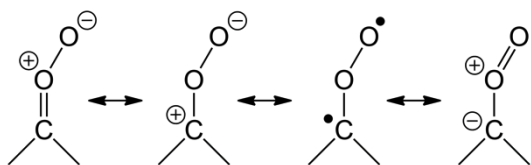
6. Criegee Intermediates

Carbonyl oxides were described for the first time by Rudolf Criegee^{408,409} as early as 1949 as intermediates in the ozonolysis of alkenes, and are typically referred to as Criegee intermediates (CI, not to be confused with Configuration Interaction as discussed in section 2.2). Despite their importance in the ozonolysis reaction, their direct experimental detection did not occur until 2008 by Taatjes *et al.*,⁷ and only in 2012 was a practical source of CI demonstrated by Welz *et al.*⁸ in the reaction of α -iodo-substituted alkyl radicals with O₂.⁴¹⁰ Until that time, most information on CI came from indirect experimental evidence, or from theoretical work. Even with the plethora of measurements recently available, theory remains the most effective means to propose and investigate critical new reactions for Criegee intermediates, and for interpretation and reliable extrapolation of the experimental data. In this section, we give an overview of the breadth and depth of theoretical work available on Criegee intermediates, most of which was obtained without direct experimental data available for comparison.

6.1. Carbonyl Oxide Wavefunction

The wave function of carbonyl oxides has been investigated extensively, as it is key to understanding its reactivity. Criegee⁴⁰⁸ originally described the intermediates as zwitterionic species, yet later it became more common to describe them as biradicals. Earlier theoretical work led to the postulate^{411,412} that carbonyl oxides were best viewed as polar diradicals, with zwitterionic states at higher energies. More advanced theoretical work, however, found that these earlier calculations were lacking as they did not account for the multi-reference character of the CI wavefunction, and

concluded⁴¹³⁻⁴¹⁹ that CI have more zwitterionic character than biradical character, with 4 electrons in the π -system. Spectroscopic studies⁴²⁰⁻⁴²⁹ of CI found also that the spectra agree best with a mostly zwitterionic nature. The transition states for reaction often show significant biradical contributions^{e.g. 419} indicating that the CI moiety rearranges its electronic wavefunction based on its reaction partner. Some of the contributing wavefunctions are shown below as Lewis structures, where we recommend the first structure for chemical diagrams as it shows most of the typical CI characteristics, i.e. a planar zwitterionic structure with a high barrier for *syn/anti* isomerisation of the $>\text{C}=\text{O}-\text{O}$ moiety. Note that the central oxygen does not actually carry a positive charge; it is merely less negatively charged than typical oxygen atoms in oxygenated hydrocarbons.



The predominance of the zwitterionic components in the wavefunction also allows for the approximation of CI as a closed-shell species, i.e. where all electrons are paired and can be described by a single-reference RHF, DFT, and higher-correlation methodologies. Unrestricted SCF calculations, allowing for the spatial separation of the unpaired electron, collapse to a symmetric closed-shell solution in a single-reference calculation, again indicative that the zwitterionic structure is more favorable than the biradical structure, and good agreement with the available experimental data is found for theoretical kinetic predictions (see sections 6.4 and 6.5) based on single-reference closed shell descriptions of the CI.

6.2. Sources of CI

6.2.1. Ozonolysis

The dominant source of CI in the atmosphere is the ozonolysis of alkenes, in particular the monoterpenes and sesquiterpenes. A representation of the ozonolysis reaction is shown in Figure 15, starting by a 1,3-dipolar cycloaddition forming a primary ozonide (POZ, 1,2,3-trioxolane), which falls apart by O–O bond scission, forming a Criegee intermediate and a carbonyl compound. A theoretical description of the ozonolysis process is complex, as the wavefunctions for ozone, the pre-reactive complex, and the addition TS show multi-reference character,^{430–432} requiring the selection of an appropriate level of theory. Similar considerations apply to the decomposition of the POZ forming CI. The POZ five-membered ring exists in two conformers, each with the central oxygen pointing to another side of the plane of the ring, and four decomposition channels are accessible, depending on which side of the alkene receives the CI functionality, and whether the carbonyl oxide is the *syn*- or *anti*-conformer; note that for non-symmetric alkenes, these different channels do not contribute in equal ratios.

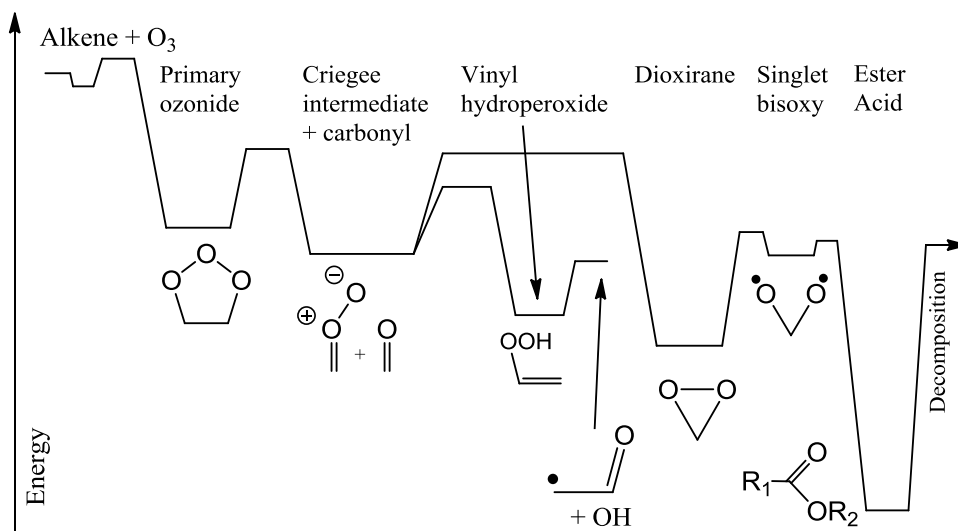


Figure 15. Reaction scheme for the ozonolysis of alkenes and subsequent reactions of the Criegee intermediates. Product yields of fragments and thermalized intermediates depends strongly on the competition between collisional energy transfer and chemically activated reactions.

The Criegee intermediates formed in the ozonolysis reaction have a very broad energy distribution. The high-energy tail in this distribution is determined by the exothermicity of the ozonolysis addition reaction and the POZ decomposition, leading to chemically activated CI which react promptly. However, the formation of CI with a thermal energy content is likewise possible provided the carbonyl fragment receives a significant fraction of the internal energy. Compounds with endocyclic double bonds are interesting in this respect, as the final carbonyl-carbonyloxy product retains all the internal energy present in the POZ, leading to hot CI with a fairly narrow energy distribution. The amount of energy in the CI thus depends on the reaction exothermicity, any collisional energy loss in the POZ, the energy distribution over the product moieties and their relative motion in the POZ decomposition, and any collisional energy loss in the CI; prediction of the CI energy content thus requires RRKM-Master Equation analyses, which typically gives good results even if the POZ decomposition shows some dynamic effects.³³² The energy distribution over the CI and carbonyl fragments also has a non-statistical component; good agreement with experiment was found when about 40-50% of the post-barrier potential energy release is distributed statistically as internal energy in the fragment,^{340,341} with the remainder going to relative translation and rotation.

The fate of the CI depends strongly on the energy content, where chemically activated CI will near-exclusively undergo unimolecular reactions, while thermal CI have a sufficiently long life-time to also undergo bimolecular reactions. As such, we will distinguish CI as either chemically activated or

thermalized in the remainder of this review.

6.2.2. Other Sources of CI

Several other sources of CI were identified; in the atmosphere most of these have a negligible flux compared to the ozonolysis, though some might contribute in specific regions. The photolysis of di-iodo compounds, $I_2C(R_1)R_2$, is currently the most widely used source of CI in laboratory studies of CI. The photofragment, $IC^*(R_1)R_2$, reacts with O_2 , leading to an adduct $IC(R_1)(R_2)OO^*$ that readily decomposes to I-atoms and a $R_1(R_2)COO$ carbonyl oxide.^{410,433–435} This process might contribute to the CI in the remote maritime boundary layer owing to the emission of iodine compounds from e.g. algae, but no in-depth theoretical work is available on these compounds at this time. McCarthy *et al.*⁴³⁶ propose the formation of H_2COO from atmospheric lightning, suggesting H-abstraction by hot O_2 molecules from CH_3O_2 peroxy radicals as the source mechanism in their methane spark discharge. More recent work by Nguyen *et al.*⁴³⁷ propose H-abstraction from CH_3OO peroxy radicals by O_2 as the source in these systems, with a reaction barrier of $\sim 40 \text{ kcal mol}^{-1}$. While currently no theoretical work is published, other H-abstraction agents such as OH or halogen-atoms might be considered as suitable co-reactants.⁴³⁸ The formation of CI from the oxidation of dimethyl sulfoxide (DMSO) was studied theoretically by Asatryan and Bozzelli,⁴³⁹ and is of possible atmospheric relevance given the role DMSO plays in H_2SO_4 and aerosol formation. The mechanism involves facile decomposition of the $CH_3S(O)CH_2OO^*$ peroxy radical intermediate. This reaction was used for the first direct experimental observation⁷ of CI, almost 60 years after their postulation.⁴⁰⁸ Andersen and Carter^{440,441} proposed 1,4- and a 1,6-H-migrations in hydroperoxymethylformate, $HOOCH_2OCHO$, as a potential source of CH_2OO Criegee intermediates with formic acid, $HCOOH$, as a co-product. We conclude that these last

three source channels suggest that some peroxy R_3COO^\bullet radicals might act as a source of Criegee intermediates, either by decomposition or abstraction for suitable combinations of substituents R on the terminal carbon; stabilization effects by oxygenated or unsaturated substituents formed in the atmospheric oxidation of terpenoids might lead to sufficiently low reaction barriers. As an example in organic synthesis,⁴¹² RO_2 decompositions of $ArN_2C(R_1)(R_2)OO^\bullet$ have been proposed as a possible source of CI. Other reactions have been suggested as sources of carbonyl oxides, including the reaction of $^3CH_2 + ^3O_2$,^{415,418} but these bear little relevance for atmospheric conditions and are not discussed here.

6.3. Criegee Intermediate Spectra

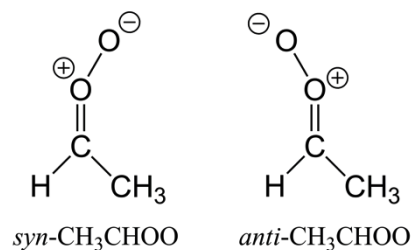
Theoretical work has contributed significantly to the identification of Criegee intermediates in the gas phase. The first experimental observations at the Advanced Light Source used time-resolved tunable photoionization with multiplex mass spectra for H_2COO and CH_3CHOO . The CI of known mass were identified by their characteristic photoionization spectrum^{7,8,442} predicted in theoretical work, at the same time excluding other isomers. Even *syn*- and *anti*- CH_3CHOO could be resolved and identified based on these theoretical spectra,⁴⁴² allowing conformer-specific kinetic observations. The infrared and Raman spectra for CI have been predicted at high levels of theory over 20 years ago,^{e.g. 417} aiding in the detection and analysis of the UV and IR spectrum of H_2COO , *syn/anti*- CH_3CHOO , $(CH_3)_2COO$, C_2H_5CHOO and β -pinene-derived Criegee intermediates,^{420-425,428,429,443,444} as well as geometric analysis by microwave spectroscopy.^{426,427} Further advances in the prediction of the rovibrational spectra of CI by full-dimensional quantum calculation of the PES allow^{445,446} for improved assignment of spectroscopic features. The IR absorption by CI was shown to induce

unimolecular reactions, as confirmed by theoretical work.^{447,448}

6.4. Criegee Intermediate Unimolecular Reactions

6.4.1. *Syn/Anti* Isomerisation

The zwitterionic wavefunction of carbonyl oxides comprises a 4-electron π -system which induces a partial but fairly strong double bond character to the $>C=OO$ moiety, hindering internal rotation. Theoretical calculations^{340,413,414,449-451} indicate barriers above 80 kJ mol^{-1} , and typically between $100\text{-}150 \text{ kJ mol}^{-1}$ for *syn/anti* isomerisation in carbonyl oxides (see Table 1). At atmospheric temperatures, this indicates that CI with different internal orientation of the terminal oxygen will interconvert very slowly and act as separate chemical species:



As detailed below, the *syn* and *anti* conformers can have significantly different chemistry, and rate predictions vary as much as 5 orders of magnitude⁴⁵² between the different conformers, making it critical that chemical kinetic models speciate their CI pool appropriately. Chemically activated CI can in principle have enough energy to interconvert, but in all cases other unimolecular reactions have a significantly lower energy barrier (see sections 6.4.2 through 6.4.4) and *syn/anti* isomerisation will remain negligible, except possibly⁴¹³ for H₂COO where it is nugatory.

The energies of the *syn*- and *anti*-conformers are not equal. The *anti*-CH₃CHOO conformer, for example, is $\sim 14.6 \text{ kJ mol}^{-1}$ less stable than the *syn*-conformer.^{212,449,452} At the same time, this absolute

energy difference is not present in all reaction transition states, such that the barrier height relative to the CI reactant is often lower for the higher-energy *anti*-conformer than the more stable *syn*-conformer, leading to faster reactions. Examples include the reaction with H₂O or alkenes,^{212,449,453,454} but also in unimolecular reactions.

The *syn* or *anti* terminology is often used to indicate whether the outer CI oxygen is pointing towards an alkyl group, rather than as an indication for geometric conformism, e.g. (CH₃)₂COO would be labeled a "*syn*" CI. While geometrically not meaningful, this practice does allow for classifying CI into those that have access to low-lying H-migration channels (vinylhydroperoxide, VHP) discussed below, compared to CI that undergo cyclisation to a dioxirane (acid/ester).

Table 1. Barrier heights for unimolecular processes of stabilized Criegee intermediates. The alkyl substituent studied is a methyl group unless the number of carbons in the substituent is indicated, where prefix "c" indicates a cyclic substituent. Vereecken and Francisco⁴⁵² review a larger set of substituents studied in the literature.

R ₁	R ₂	Process	Barrier (kJ mol ⁻¹)	Reference
H	H	O-loss ester channel	136	Anglada <i>et al.</i> , 1996 ⁴¹³
			74	Gutbrod <i>et al.</i> , 1996 ⁴⁵⁵
			100	Anglada <i>et al.</i> , 1996 ⁴¹³
			76	Olzmann <i>et al.</i> , 1997 ⁴⁵⁶
			83	Aplincourt and Ruiz-López, 2000 ⁴¹⁶
			87	Kroll <i>et al.</i> , 2001 ⁴⁵⁷
			86	Selçuki and Aviyente, 2001 ⁴⁵⁸
		1,3-H-shift	83	Zhang and Zhang, 2002 ⁴⁵⁹
			79	Li <i>et al.</i> , 2014 ⁴⁴⁵
			129	Gutbrod <i>et al.</i> , 1996 ⁴⁵⁵
			129	Olzmann <i>et al.</i> , 1997 ⁴⁵⁶
			134	Zhang and Zhang, 2002 ⁴⁵⁹
			108	Anglada <i>et al.</i> , 1996 ⁴¹³
Alkyl	H	O-loss ester channel	143	Anglada <i>et al.</i> , 1996 ⁴¹³
			99.6	Gutbrod <i>et al.</i> , 1997 ⁴⁶⁰
		119	Anglada <i>et al.</i> , 1996 ⁴¹³	
		100	Selçuki and Aviyente, 2001 ⁴⁵⁸	
		101	Kuwata <i>et al.</i> , 2010 ⁴⁴⁹	

			99	Kuwata <i>et al.</i> , 2011 ⁴⁵⁰
			89 (C2) ^a	Kuwata <i>et al.</i> , 2011 ⁴⁵⁰
			100 (C14)	Nguyen <i>et al.</i> , 2009 ⁴⁵¹
			87	Nguyen <i>et al.</i> , 2009 ⁴⁵¹
			52 (C1) ^b	Leonardo <i>et al.</i> , 2011 ⁴⁶¹
			79 (C4)	Leonardo <i>et al.</i> , 2011 ⁴⁶¹
		hydroperoxide	62	Gutbrod <i>et al.</i> , 1997 ⁴⁶⁰
			89	Anglada <i>et al.</i> , 1996 ⁴¹³
			80 (C5)	Chuong <i>et al.</i> , 2004 ⁴⁶²
			70	Kroll <i>et al.</i> , 2001 ⁴⁵⁷
			75	Kuwata <i>et al.</i> , 2010 ⁴⁴⁹
			53 (C2) ^a	Kuwata <i>et al.</i> , 2011 ⁴⁵⁰
			71	Kuwata <i>et al.</i> , 2003 ⁴⁶³
			78 (C14)	Nguyen <i>et al.</i> , 2009 ⁴⁵¹
			66	Nguyen <i>et al.</i> , 2009 ⁴⁵¹
			82	Zhang and Zhang, 2005 ⁴⁶⁴
			48 (C1) ^b	Leonardo <i>et al.</i> , 2011 ⁴⁶¹
			69 (C6)	Leonardo <i>et al.</i> , 2011 ⁴⁶¹
		syn-anti isom	59 (C4)	Leonardo <i>et al.</i> , 2011 ⁴⁶¹
			128	Anglada <i>et al.</i> , 1996 ⁴¹³
			159	Kuwata <i>et al.</i> , 2010 ⁴⁴⁹
			141	Kuwata <i>et al.</i> , 2011 ⁴⁵⁰
			136	Nguyen <i>et al.</i> , 2009 ⁴⁵¹
H	Alkyl	O-loss	132	Anglada <i>et al.</i> , 1996 ⁴¹³
		ester channel	86	Anglada <i>et al.</i> , 1996 ⁴¹³
			56 (C5)	Chuong <i>et al.</i> , 2004 ⁴⁶²
			71	Kroll <i>et al.</i> , 2001 ⁴⁵⁷
			72	Selçuki and Aviyente, 2001 ⁴⁵⁸
			64	Kuwata <i>et al.</i> , 2010 ⁴⁴⁹
			69	Kuwata <i>et al.</i> , 2011 ⁴⁵⁰
			63 (C2) ^a	Kuwata <i>et al.</i> , 2011 ⁴⁵⁰
			67 (C14)	Nguyen <i>et al.</i> , 2009 ⁴⁵¹
			65	Nguyen <i>et al.</i> , 2009 ⁴⁵¹
			115 (C9)	Zhang and Zhang, 2005 ⁴⁶⁴
			79 (C6)	Leonardo <i>et al.</i> , 2011 ⁴⁶¹
		acyl + OH	126	Kuwata <i>et al.</i> , 2010 ⁴⁴⁹
		(1,3-H-shift)	122	Kuwata <i>et al.</i> , 2011 ⁴⁵⁰
			125	Kuwata <i>et al.</i> , 2011 ⁴⁵⁰
			115 (C14)	Nguyen <i>et al.</i> , 2009 ⁴⁵¹
			136	Zhang and Zhang, 2005 ⁴⁶⁴
			117 (C1) ^b	Leonardo <i>et al.</i> , 2011 ⁴⁶¹
		syn-anti isom	118	Anglada <i>et al.</i> , 1996 ⁴¹³
			144	Kuwata <i>et al.</i> , 2010 ⁴⁴⁹
			126	Kuwata <i>et al.</i> , 2011 ⁴⁵⁰
			121	Nguyen <i>et al.</i> , 2009 ⁴⁵¹
Alkyl	Alkyl	ester channel	78	Gutbrod <i>et al.</i> , 1996 ⁴⁵⁵
			91	Kroll <i>et al.</i> , 2001 ⁴⁵⁷
			90	Selçuki and Aviyente, 2001 ⁴⁵⁸
			65 (C13,C1)	Nguyen <i>et al.</i> , 2009 ⁴⁵¹
			88 (C1,C13)	Nguyen <i>et al.</i> , 2009 ⁴⁵¹
			118 (cC8,C1)	Zhang and Zhang, 2005 ⁴⁶⁴
			87 (C1,C6)	Leonardo <i>et al.</i> , 2011 ⁴⁶¹
			92	Leonardo <i>et al.</i> , 2011 ⁴⁶¹
			84 (C3,C1)	Leonardo <i>et al.</i> , 2011 ⁴⁶¹
		hydroperoxide	57	Gutbrod <i>et al.</i> , 1996 ⁴⁵⁵
			67 ^c	Kroll <i>et al.</i> , 2001 ⁴⁵⁷
			78 (C14,C1)	Nguyen <i>et al.</i> , 2009 ⁴⁵¹
			69 (C1,C14)	Nguyen <i>et al.</i> , 2009 ⁴⁵¹
			43 (C1,C8)	Sun <i>et al.</i> , 2011 ⁴⁶⁵
			78 (cC8,C1)	Zhang and Zhang, 2005 ⁴⁶⁴
			82 (C1,C6)	Leonardo <i>et al.</i> , 2011 ⁴⁶¹
			55	Leonardo <i>et al.</i> , 2011 ⁴⁶¹
			62 (C1,C3)	Leonardo <i>et al.</i> , 2011 ⁴⁶¹

^a alkyl substituent is -CH₂-CHO ^b alkyl substituent is -CH₂OH ^c experimental data

6.4.2. Acid/Ester Channel

As shown in Figure 15, all CI can undergo a cyclisation reaction, forming a dioxirane, which in turn can break the ring structure to form a singlet bis(oxy) diradical that readily rearranges to an acid or ester, depending on the presence of H-atom substituents. The acid/ester is formed with a very high internal energy content obtained by the exothermicity of the re-arrangement process but possibly also from the nascent energy in the CI formed in the ozonolysis. Especially for small acids/esters, these internal energies are sufficient to rapidly decompose the acid/ester to CO₂, alkyl radicals and other products; larger acids/esters in contrast are sufficiently long-lived to undergo collisional energy loss and thermalization. There remains a large uncertainty on the rate coefficient for the CI cyclisation, with no direct experimental measurements and theoretical predictions of the barrier height that differs strongly dependent on the level of theory employed (see Table 1) Furthermore, the absolute barrier height depends significantly on the substituents and the CI conformer examined. For CH₃CHOO,^{340,449,450,458} it is found that the *syn*-conformer has cyclisation barriers in excess of 96 kJ mol⁻¹, while the predictions for the *anti*-conformer lie^{340,449,450,458} between 63 and 71 kJ mol⁻¹. The acid/ester channel is thus more accessible for the *anti*-conformers, and is expected to have rate coefficients (Table 2) comparable to the faster channels available to *syn*-conformers.

Table 2. Rate coefficients for unimolecular decomposition of Criegee intermediates

CI	Channel	k (s ⁻¹)	Reference
CH ₂ OO	Ester /Acid	0.3	Olzmann <i>et al.</i> 1997 ⁴⁵⁶

<i>syn</i> -CH ₃ CHOO	Ester /Acid	≤ 8.6 ^{a,b}	Berndt <i>et al.</i> 2014 ⁴⁶⁶
	VHP	24	Kuwata <i>et al.</i> 2010 ⁴⁴⁹
	VHP	76 ^a	Fenske <i>et al.</i> 2000 ⁴⁶⁷
	VHP	3 ^a	Berndt <i>et al.</i> 2012 ⁴⁶⁸
	VHP	2.9 ^a	Horie <i>et al.</i> 1999 ⁴⁶⁹
	VHP	2.5 ^a	Horie <i>et al.</i> 1997 ⁴⁷⁰
	VHP	< 250 ^a	Taatjes <i>et al.</i> 2013 ⁴⁴²
	VHP	10-30 ^a	Novelli <i>et al.</i> 2014 ⁴⁷¹
anti-CH ₃ CHOO (CH ₃) ₂ COO	Total	47 ^{a,b}	Newland <i>et al.</i> 2015 ⁴⁷²
	Ester /Acid	64	Kuwata <i>et al.</i> 2010 ⁴⁴⁹
	VHP	6.4 ^a	Kroll <i>et al.</i> 2001 ⁴⁵⁷
Isoprene CI ^c	Total	230 ^{a,b}	Newland <i>et al.</i> 2015 ⁴⁷²
	VHP	146	Kuwata <i>et al.</i> 2010 ⁴⁴⁹
β-pinene CI ^c	VHP	15	Kuwata <i>et al.</i> 2010 ⁴⁴⁹
	Ester /Acid	1	Nguyen <i>et al.</i> 2009 ³⁴⁰
Limonene CI	VHP	50	Nguyen <i>et al.</i> 2009 ³⁴⁰
	VHP	26	Sun <i>et al.</i> 2011 ⁴⁶⁵
β-caryophellene CI ^c	VHP	1.6	Nguyen <i>et al.</i> 2009 ⁴⁵¹
	Ester /Acid	5.3	Nguyen <i>et al.</i> 2009 ⁴⁵¹
	VHP	0.6	Nguyen <i>et al.</i> 2009 ⁴⁵¹
	VHP	42	Nguyen <i>et al.</i> 2009 ⁴⁵¹

^a Experimental data ^b Measurement relative to the reaction with SO₂, interpreted assuming $k(\text{SO}_2) = 3.6 \times 10^{-11} \text{ cm}^3 \text{ molecule}^{-1} \text{ s}^{-1}$ ^c Diverse CI structures

6.4.3. Vinylhydroperoxide Channel

When the outer oxygen of the CI points towards an alkyl group, a 1,4-H-migration can occur, yielding a vinylhydroperoxide C=C-OOH (VHP) functionality. For *syn*-CI, this is typically the fastest unimolecular route available, and the rate of H-migration can be strongly enhanced if the migrating H-atom is more weakly bonded, e.g. in some CI formed from isoprene (see Table 1). The VHP has a weak O–O bond, and is assumed to rapidly decompose to an OH radical with a vinoxyl radical co-product (see Figure 15); this is the main OH formation channel in the alkene ozonolysis, and is thought to contribute to atmospheric OH formation during the night time, when the photolytic channels for OH formation or regeneration are unavailable. Recent experimental and multi-reference quantum chemical

calculations suggests that a small barrier to decomposition exists,^{341,473} which could allow for temporary stabilization of the VHP, complicating the temperature, pressure and time-dependence of OH formation. VHP decomposition can also lead to a recombination of the two radical fragments, leading to a 2-OH-carbonyl compound,^{340,461,464} these products have been observed as a product in the ozonolysis but their formation pathway has not been confirmed and could also arise from secondary peroxy radical chemistry.

Despite its importance in atmospheric chemistry, the rate coefficient for the 1,4-H-migration remains highly uncertain, with experimental determinations ranging over a wide range, and a strong dependence on the level of theory used for *a priori* predictions (see Table 2). The temperature dependence has not been measured, but is expected to be strong owing to the high barrier of the reaction.

6.4.4. Other Unimolecular Reactions

Theoretical work has identified a number of non-traditional unimolecular reaction channels available to some CI (Figure 16), though few of them can compete with the typical acid/ester or VHP channels. A first channel is a 1,3-H-migration in *anti*-CI, where no alkyl group is accessible by the outer CI oxygen. These reactions lead to formation of an unstable α -OOH singlet biradical that decomposes spontaneously⁴⁷⁴ to an acyl radical + OH. This reaction has typically a rather high barrier (see Table 1) but it is the main OH formation channel from chemically activated H₂COO. Unsaturated CI can also undergo a cyclisation reaction,^{414,450} forming cyclic peroxides. A CI with a cyclic substituent can also undergo ring opening,³⁴⁰ forming an alkyl-alkylperoxy diradical, which in turn might cyclise by recombination of the two radical sites, leading to a cyclic peroxide. Neither of these

latter channels has been confirmed experimentally.

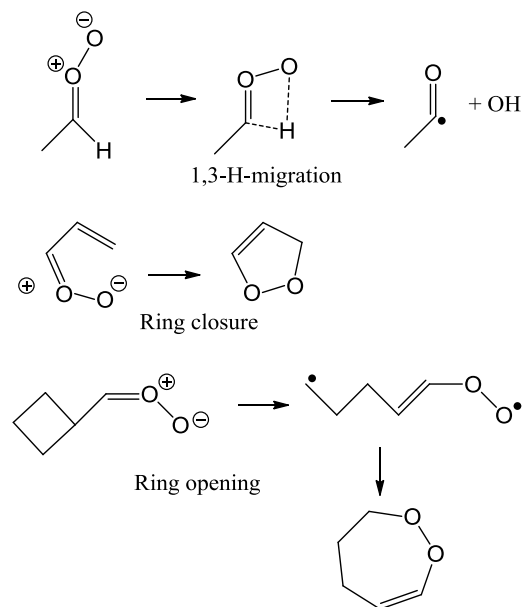


Figure 16. Non-traditional reactions of Criegee intermediates

The ozonolysis of endocyclic alkenes leads to a molecule carrying a CI functionality on one end, and a carbonyl functionality on the other. These ends can react, forming an internal, bicyclic secondary ozonide (SOZ, 1,2,4-trioxalene), provided the backbone chain is sufficiently long to allow for both ends to meet;^{450,451,462,475} a minimum of 6 carbons seems necessary. For many endocyclic alkenes, this process has a significantly lower barrier than either the acid/ester channel or the VHP channel and is a major loss process for thermalized CI. However, for chemically activated CI, the entropic disadvantage of this cyclisation process, in which many degrees of freedom of internal rotations are converted to rigid ring bending modes, is so large that it typically cannot compete with the entropically much more favorable ester or VHP channels. As such, *a priori* prediction of the

importance of this channel depends on extensive RRKM-Master equation analysis to quantify the energy-dependent impact of the different reaction channels.

6.5. Criegee Intermediate Bimolecular Reactions

Theoretical work on the bimolecular reactions of stabilized CI has been recently reviewed by Vereecken and Francisco;⁴⁵² in this section, we will list more recent theoretical work, but we focus mostly on comparing the newly available experimental results against the body of theoretical work. This provides an opportunity to illustrate the usefulness of theory when no experimental data were available, as well as assess the accuracy of the theoretical predictions. In this comparison, it must be borne in mind that the computational capabilities increase exponentially each year, and that older theoretical work did not necessarily have access to the highly accurate levels of theory that are used at present.

6.5.1. The Reaction with SO₂

The first direct experimental measurements⁸ of rate coefficients with CH₂OO included the reaction with SO₂, which was found to be significantly faster than the rates used in kinetic models. Subsequent experiments found that all CI examined react fast with SO₂, though the experimental data can be separated into one set of data^{8,442,443,476,477} indicating rate coefficients of the order of 2.4 to $22 \times 10^{-11} \text{ cm}^3 \text{ molecule}^{-1} \text{ s}^{-1}$, and others⁴⁶⁸ finding values of 0.9 to $7.7 \times 10^{-13} \text{ cm}^3 \text{ molecule}^{-1} \text{ s}^{-1}$. With these rate coefficients, and assuming a sufficiently high concentration of CI in the atmosphere, this could indicate an SO₂ oxidation route^{420,478-483} hitherto unaccounted for in the models, that could influence the gas phase atmospheric formation of H₂SO₄,⁴⁸⁴⁻⁴⁸⁹ and hence aerosol nucleation and

growth. Theoretical work on the CI + SO₂ reaction confirms^{14,483,490–492} that oxidation of SO₂ to SO₃ is the lowest-energy route, following formation of a initial cyclic secondary oxide. The most refined calculations¹⁴ indicate the reaction to proceed first by breaking the cyclic SOZ to a linear singlet biradical prior to fragmentation (see Figure 2). All theoretical work finds the initial SOZ formation to be a barrierless reaction, which implies fast rate coefficients nearing the collision limit but tempered by the entropic disadvantage of forming a rigid cyclic adduct; the experimental data suggesting rate coefficients of the order of $\sim 5 \times 10^{-11} \text{ cm}^3 \text{ molecule}^{-1} \text{ s}^{-1}$ are in full agreement with this view. Vereecken *et al.*¹⁴ argued, based on RRKM Master equation analyses, that the initial SOZ could be collisionally stabilized especially for larger CI at atmospheric pressures, thus delaying the formation of SO₃ or, in the case of competing loss processes for the SOZ, even reducing the SO₃ yield and hence the H₂SO₄ formation potential, rationalizing the experimental data⁴⁶⁸ finding a H₂SO₄ formation rate coefficient of about $\sim 5 \times 10^{-13} \text{ cm}^3 \text{ molecule}^{-1} \text{ s}^{-1}$. However, no competing loss processes for the SOZ have been identified, nor has the SOZ been observed in experiments, such that the SOZ stabilization hypothesis remains as yet unconfirmed.

6.5.2. The Reaction with H₂O and (H₂O)₂

The reaction with water in the atmosphere was long thought to be the dominant, if not sole fate of Criegee intermediates. The available theoretical work all agrees^{449,453,454} that the rate coefficients are low, and strongly dependent on the degree of substitution and on the conformer, but the predictions span about two to three orders of magnitude even for the smallest CI (see Table 3).^{449,453,454} Recently, experimental work has become available directly measuring the rate coefficient (see Table 3), though in many cases only an upper limit could be measured.^{8,442,476,493} The only experimentally quantified^{442,443}

rate coefficient is for *anti*-CH₃CHOO + H₂O where $k(298\text{K}) = (1.0\text{-}2.4)\times 10^{-14} \text{ cm}^3 \text{ molecule}^{-1} \text{ s}^{-1}$, is in the middle of the theoretically predicted values, and less than a factor of 10 below the most recent theoretical predictions by Anglada *et al.*⁴⁵⁴ High levels of theory appear necessary to provide reliable estimates for CI for which no experimental data is available. A pragmatic approach that makes best use of the current available data^{14,212,471} scales the theoretical predictions to match the single experimental value.

The products of the reaction of CI + water are predicted to mostly form hydroxy-alkylhydroperoxides, >C(OH)OOH,^{449,453,454,483} which have been observed in ozonolysis experiments.^{e.g. 494} These hydroxy-hydroperoxides can be involved in SOA formation, but can also decompose to form OH radicals. Recent theoretical work by Jiang *et al.*⁴⁸³ on limonene-derived CI confirmed earlier work⁴⁵⁴ that the water molecule can also catalyze the formation of a VHP by H-migration, leading to more direct formation of an OH radical.

A large uncertainty with regards to the fate of CI in the atmosphere is the role of the water dimers, (H₂O)₂. Theoretical work by Ryzhkov *et al.*^{453,495,496} shows that the rate coefficients can be as much as 6 orders of magnitude faster (see Table 3) than the monomer reactions; analysis of the fate of CI based on literature data^{14,212,471} then concludes near-exclusive reaction with water for H₂COO and *anti*-CH₃CHOO. Again, higher-level calculations and experimental work are needed to confirm these predictions. Recent experimental work by Berndt *et al.*⁴⁶⁶ measured the reaction rate for H₂COO, relative to the reaction with SO₂, confirming the fast reaction rates. (see Table 3). Chao *et al.*⁴⁹³ recently measured this rate coefficient directly, finding a fast rate coefficient of $6.5\times 10^{-12} \text{ cm}^3 \text{ molecule}^{-1} \text{ s}^{-1}$, while Lewis *et al.*⁴⁹⁷ found $4.0\times 10^{-12} \text{ cm}^3 \text{ molecule}^{-1} \text{ s}^{-1}$; both are within a factor of 3 of the theoretical work by Ryzhkov and Ariya.⁴⁵³

Table 3. Rate coefficients ($\text{cm}^3 \text{ molecule}^{-1} \text{ s}^{-1}$) for the reaction of small Criegee intermediates with H_2O and $(\text{H}_2\text{O})_2$, including experimental data (exp.). For more extensive results, see refs. ^{449,452–454}

CI	Co-reactant	Rate coefficient	Reference
CH ₂ OO	H ₂ O	5.8×10^{-18}	Ryzhkov and Ariya 2004 ⁴⁵³
		$1.7\text{-}5.6 \times 10^{-15}$	Anglada <i>et al.</i> 2011 ⁴⁵⁴
		$\leq 9 \times 10^{-17}$ (exp.)	Stone <i>et al.</i> 2014 ⁴⁷⁶
		$\leq 4 \times 10^{-15}$ (exp.)	Welz <i>et al.</i> 2012 ⁸
		1.2×10^{-15} (exp.)	Newland <i>et al.</i> 2015 ⁴⁷²
	(H ₂ O) ₂	2.0×10^{-12}	Ryzhkov and Ariya 2004 ⁴⁵³
		1.0×10^{-11} (exp.) ^a	Berndt <i>et al.</i> 2014 ⁴⁶⁶
		6.5×10^{-12} (exp.) ^a	Chao <i>et al.</i> 2015 ⁴⁹³
		5.0×10^{-13} (exp.) ^a	Newland <i>et al.</i> 2015 ⁴⁷²
		4.0×10^{-12} (exp.)	Lewis <i>et al.</i> 2015 ⁴⁹⁷
<i>syn</i> -CH ₃ CHOO	H ₂ O	7.3×10^{-21}	Ryzhkov and Ariya 2004 ⁴⁵³
		7.2×10^{-21}	Kuwata <i>et al.</i> 2010 ⁴⁴⁹
		$2.4\text{-}3.2 \times 10^{-18}$	Anglada <i>et al.</i> 2011 ⁴⁵⁴
	(H ₂ O) ₂	$\leq 4 \times 10^{-15}$ (exp.)	Taatjes <i>et al.</i> 2013 ⁴⁴²
		$\leq 2 \times 10^{-16}$ (exp.)	Sheps <i>et al.</i> 2014 ⁴⁴³
<i>anti</i> -CH ₃ CHOO	(H ₂ O) ₂	1.2×10^{-15}	Ryzhkov and Ariya 2004 ⁴⁵³
		4.0×10^{-16}	Ryzhkov and Ariya 2004 ⁴⁵³
	H ₂ O	2.9×10^{-16}	Kuwata <i>et al.</i> 2010 ⁴⁴⁹
		$1.7\text{-}2.0 \times 10^{-13}$	Anglada <i>et al.</i> 2011 ⁴⁵⁴
		1.0×10^{-14} (exp.)	Taatjes <i>et al.</i> 2013 ⁴⁴²
(CH ₃) ₂ COO	(H ₂ O) ₂	2.4×10^{-14} (exp.)	Sheps <i>et al.</i> 2014 ⁴⁴³
		2.0×10^{-12}	Ryzhkov and Ariya 2004 ⁴⁵³
	H ₂ O	1.4×10^{-19}	Ryzhkov and Ariya 2004 ⁴⁵³
		3.9×10^{-17}	Anglada <i>et al.</i> 2011 ⁴⁵⁴
		3.1×10^{-15} (exp.)	Newland <i>et al.</i> 2015 ⁴⁷²
(H ₂ O) ₂	5.8×10^{-17}	Ryzhkov and Ariya 2004 ⁴⁵³	

^a Measurement relative to the reaction with SO₂, interpreted assuming $k(\text{SO}_2) = 3.6 \times 10^{-11} \text{ cm}^3 \text{ molecule}^{-1} \text{ s}^{-1}$.

6.5.3. The Reaction with Organic Acids and Carbonyl Compounds

Recent experimental work by Welz *et al.*⁴⁹⁸ measured the rate coefficient of CH₂OO and

CH₃CHOO with formic and acetic acid, obtaining rate coefficients ranging from 1.1 to 2.4×10⁻¹⁰ cm³ molecules⁻¹ s⁻¹, significantly faster than earlier experimental data^{499,500} that suggests values ≤ 10⁻¹⁴ cm³ molecules⁻¹ s⁻¹. Sipila *et al.*⁵⁰¹ found similar values in a relative rate study, where here we assume a rate coefficient with SO₂ of 3.6×10⁻¹¹ cm³ molecule⁻¹ s⁻¹. Theoretical work by Aplincourt *et al.*⁴⁹⁰ and Long *et al.*⁵⁰² found that the CH₂OO + formic acid reaction proceeds without a barrier, either via strongly bonded pre-reactive complexes or by direct barrierless pathways. The energetically most favorable routes were predicted to involve insertion into the acidic O–H bond, leading to hydroperoxyformate, HOOCH₂OC(=O)H; similar insertion reactions are expected to govern all the other CI + carboxylic acid reactions. The absence of an energetic barrier in both the direct reaction channel and the formation of H-bonded complexes typically lead to very fast reaction rates, nearing the collision limit.

Furthermore, the insertion reaction leading to a linear reaction product is expected to be entropically more favorable than an alternative pathway leading to a cycloadduct of the CI across the C=O carbonyl double bond. This will favor the insertion reaction over the cycloaddition, and allow for faster reaction rates. As such, the recent experimental work confirms the theoretical potential energy surface, whereas the older experimental work is fundamentally incompatible with the *a priori* predicted barrierless channels. Theoretical work by Kumar *et al.*⁵⁰³ also showed that acids can catalyse the isomerisation of CI to VHP, making it a reaction without protruding energy barriers.

Compared to the reaction of CI with carboxylic acid, their reactions with carbonyl compounds such as aldehydes and ketones have many similar features, including the barrierless formation of pre-reactive complexes that are nearly as strong as for acids, and an overall reaction without protruding barriers. Extensive theoretical work by Jalan *et al.*⁵⁰⁴ on the reaction of CH₂OO with formaldehyde, acetaldehyde and acetone characterized the formation of the secondary ozonides, SOZ, and found the

reactions to be sufficiently exothermic for the SOZ to undergo chemically activated re-arrangements to esters and decomposition to acids. Recent experimental work by Taatjes *et al.*,⁵⁰⁵ Stone *et al.*⁴⁷⁶ and Liu *et al.*⁴⁷⁷ improve upon earlier experimental work,^{467,469,470,500} and determine the rate coefficient for $\text{H}_2\text{COO} + \text{CH}_3\text{CHO}$ to be 0.9 to $1.7 \times 10^{-12} \text{ cm}^3 \text{ molecules}^{-1} \text{ s}^{-1}$ depending on pressure;^{476,505} for the reaction with acetone $2.3 \times 10^{-13} \text{ cm}^3 \text{ molecules}^{-1} \text{ s}^{-1}$ is reported,⁵⁰⁵ and only for hexafluoroacetone are faster rate coefficients observed,^{477,505} $\sim 3 \times 10^{-11} \text{ cm}^3 \text{ molecules}^{-1} \text{ s}^{-1}$. Despite the lack of entrance barriers, these rate coefficients are thus significantly below the rate coefficients observed for carboxylic acids, which suggests that the rate of reaction is determined to a large extent by the unfavorable change in entropy upon the formation of the rigid, cyclic SOZ adduct; this lends evidence to the hypothesis that carboxylic acids react predominantly by an insertion process. The *a priori* rate coefficients predicted by Jalan *et al.*⁵⁰⁴ for $\text{CH}_2\text{OO} + \text{CH}_3\text{CHO}$ are only about a factor of 3 below the experimental data, and match nearly exactly that for the reaction with acetone, confirming excellent recovery by theory.

6.5.4. The Reaction with Alkenes

Based on earlier theoretical work on the addition of 1,3-dipoles on double bonds,^{432,506} and early experimental work⁵⁰⁷⁻⁵⁰⁹ indicating these reactions might take place, Vereecken *et al.*²¹² theoretically investigated 16 reactions of CI with alkenes. They found that the reactions are very strongly dependent on the alkene and CI substitution, and on the CI conformer, with *a priori* rate coefficients ranging from 4×10^{-20} to $2 \times 10^{-13} \text{ cm}^3 \text{ molecules}^{-1} \text{ s}^{-1}$. Recent combined experimental and theoretical work by Buras *et al.*⁵¹⁰ obtained the rate coefficients for the reaction of CH_2OO with ethene, propene, and three butene isomers. The agreement between the experimental data,⁵¹⁰ and the theoretical work,^{212,510} depends somewhat on the level of theory applied. Unfortunately, the theoretical data do not reliably reproduce

the experimental data, with excellent agreement for some compounds but with discrepancies of up to an order of magnitude in the rate coefficient for other alkenes.

6.5.5. The Reaction with NO_x

Measurement of the reaction of CH₂OO + NO has been attempted several times, leading to upper limits for the rate coefficients of $\leq 6 \times 10^{-14} \text{ cm}^3 \text{ molecules}^{-1} \text{ s}^{-1}$ and $\leq 2 \times 10^{-13} \text{ cm}^3 \text{ molecules}^{-1} \text{ s}^{-1}$.^{8,476} Theoretical work by Vereecken *et al.*¹⁴ finds a fairly high barrier for reaction, $\sim 25 \text{ kJ mol}^{-1}$, predicting a rate coefficient as low as $2 \times 10^{-18} \text{ cm}^3 \text{ molecules}^{-1} \text{ s}^{-1}$, in full agreement with the experiment. Similar rate coefficients were predicted by Sun *et al.*⁴⁶⁵ for limonene-derived CI. For the reaction of CI with NO₂, we are not aware of recent theoretical work improving on the early work by Presto and Donahue.⁵¹¹ This reaction might play a role in the atmosphere, with experimental work finding fast rate coefficients^{8,442,476} of up to $7 \times 10^{-12} \text{ cm}^3 \text{ molecules}^{-1} \text{ s}^{-1}$, and observation of NO₃ as a main reaction product.⁵¹²

6.5.6. The Reaction with CO

Kumar *et al.* report a study on the reaction of several CI with carbon monoxide.⁵¹³ They find that this reaction proceeds by a shallow pre-reactive complex followed by a significant barrier, leading to rate coefficients $\leq 3 \times 10^{-20} \text{ cm}^3 \text{ molecules}^{-1} \text{ s}^{-1}$ at atmospheric temperatures. These results seem to be in discord with experiments, where CO has been used as a CI scavenger with measurable differences in the observed products;^{460,514} this reaction requires further study.

6.5.7. The Reaction with RO₂ and HO₂

The reaction of CI with alkylperoxy radicals has been proposed as a source of oligomers observed in smog chamber experiments.^{509,515} These chains, consisting of multiple CI units, have a low volatility and could contribute to the formation of aerosols, though in the atmosphere the concentration of RO₂ and CI is likely too low for this process to be significant. The chain reaction of CH₂OO with RO₂ has been investigated for the first time by Vereecken *et al.*,¹⁴ confirming the viability of this process and predicting larger chains as products. Recent high-level theoretical work by Anglada *et al.*⁵¹⁶ on the CH₃OO• + CH₂OO reaction improved on these results, finding that these smallest CH₃OOCH₂OO• chain adducts are sufficiently chemically activated in the exothermic addition reaction to decompose to give a ~13% yield of formaldehyde and a hydroperoxide alkoxy radical through a H-migration process. The formation of tetroxide alkyl radicals, CH₃OOOOC•H₂, was found to be negligible, with a large barrier to formation, as was direct H-migration.

The reaction of CI with HO₂ radicals was studied recently by Long *et al.*,⁵⁰² predicting extremely fast rate coefficients exceeding $2 \times 10^{-10} \text{ cm}^3 \text{ molecules}^{-1} \text{ s}^{-1}$, owing to the barrierless association reactions forming hydroperoxide alkylperoxy radicals. No experimental data are available on this reaction.

6.5.8. The Reaction with O₃

The reaction of CI with O₃ has been proposed^{212,517,518} as a potentially important reaction^{212,471} both in experimental conditions and in the free troposphere; the predicted rate coefficients are as high as $1 \times 10^{-12} \text{ cm}^3 \text{ molecules}^{-1} \text{ s}^{-1}$.²¹² The potential energy surfaces predicted by the different authors differ significantly. B3LYP calculations by Kjaergaard *et al.*⁵¹⁷ and Wei *et al.*⁵¹⁸ predict a cycloaddition step; this has a large barrier at the B3LYP level of theory, but which is strongly reduced when higher level

methodologies up to CCSD(T)//CCSD(T) are applied. In contrast, CCSD(T)//M06-2X calculations by Vereecken *et al.*²¹² find a pre-reactive complex and a submerged chain addition transition state; these authors argue that chain addition is preferred as it avoids directly bonding two negatively charged oxygen atoms as in the cycloaddition. The different PES all predict the formation of a carbonyl compounds + 2 O₂ as reaction products, but disagree on the intermediary steps. Experimental data are needed to determine the rate of this reaction.

6.5.9. The CH₂OO+CH₂OO Reaction

The self-reaction of CH₂OO was predicted to be fast by Su *et al.*,⁴²⁸ and was recently measured with a rate coefficient of $4 \times 10^{-10} \text{ cm}^3 \text{ molecules}^{-1} \text{ s}^{-1}$.⁵¹⁹ This extremely high value is in disagreement with the theoretical work by Vereecken *et al.*,²¹² who employed variational microcanonical transition state theory on a M06-2X potential energy surface, obtaining a rate coefficient of $4 \times 10^{-11} \text{ cm}^3 \text{ molecules}^{-1} \text{ s}^{-1}$. Even allowing for a small underprediction of their theoretical rate coefficient owing to the treatment of the transitional degrees of freedom as harmonic oscillators, the order of magnitude discrepancy is unexpected, especially considering the formation of a rigid cyclic adduct that typically imposes an entropic hindrance to the rate of reaction. Recent measurements by Buras *et al.*⁵¹⁰ and Chhantyal-Pun *et al.*⁵²⁰ on the CH₂OO+CH₂OO reaction gave a rate coefficient of $6.0\text{-}7.3 \times 10^{-11} \text{ cm}^3 \text{ molecules}^{-1} \text{ s}^{-1}$, confirming the theoretical predictions.

6.6. The Fate of CI in the Atmosphere

The fate of CI in the atmosphere remains uncertain, though it is clear that it depends on the CI substituents, and conformer considered. The implications of CI on tropospheric chemistry have recently been reviewed,⁵²¹ the analyses on the fate of CI by Novelli *et al.*^{14,212,471} include the most extensive

chemistry. These authors find that CH_2OO and *anti*- CH_3CHOO will essentially only react with water or water dimers throughout the troposphere. For *syn*- CH_3CHOO and $(\text{CH}_3)_2\text{COO}$, in contrast, they find that the water(dimer) reactions are sufficiently slow to allow unimolecular decomposition, forming OH, to compete, as well as the reactions with carboxylic acids and HO-bearing molecules. Reactions of carbonyl compounds, NO_2 , SO_2 and O_3 all contribute as well, but only as a few % of the CI loss. The largest unknown in the assessment of the impact of CI on tropospheric chemistry remains the speciation of the CI, where complex substituents allow for additional reactions and affect the rate of some reactions strongly,¹⁴ as well as the local ambient concentrations of CI. The most important source of CI is expected to be the ozonolysis of terpenoids, in particular mono- and sesquiterpenes. However, few rate coefficients are available for the reactions of these highly substituted CI, nor is it clear how much of these stabilized CI are generated in the different environments ranging from pristine to megacity. More research is clearly needed to quantify the role of CI in the atmosphere.

7. Predictive Correlations and Structure-Activity Relations.

The theory-based techniques described above allow the prediction of the temperature- and pressure-dependent rate coefficients and product distributions for most reactions of importance in atmospheric chemistry. However, the sheer number of elementary reactions in play in the atmosphere prohibits the detailed investigation of each reaction individually, by either experimental or theoretical methods. Based on the available experimental and/or theoretical data, however, it is possible to discover the trends in the reactivity of compounds in a given class of reactions, and summarize them as a structure-activity relationship (SAR) linking the components of the molecular structure to the reactivity. The kinetic parameters for reactions of a new compound can then be estimated by applying

these trends as appropriate for the chemical substitution patterns in the compound studied. Thus, SARs play a critical role in the development of explicit chemical kinetic models for the atmosphere.^{e.g. 522}

Theoretical methods are well-suited for the derivation of SARs. They allow access to systematic series of compounds and substituents, including compounds that are difficult to study by experimental methods such as highly substituted intermediates and radical compounds. Also, a theory-based SAR in principle allows for systematic improvement by increasing the level of theory employed, and is readily expanded to different substituents by increasing the number of compounds in the learning and test sets for the SAR. Some examples of theory-based predictive methods are discussed below.

The reactions of volatile organic compounds (VOC) with ozone, OH and NO₃ radicals, and chlorine atoms have received significant attention, given their role as the initiation reactions for atmospheric oxidation of VOCs. For these reactions, the most widely used SARs remain those developed by Atkinson and coworkers^{3,359,523} for the reaction of OH and Cl with VOCs based on experimental work. The section on OH-addition on unsaturated compounds has been refined recently by Peeters *et al.*,⁵²⁴ and extended to new compounds by Gallego-Iniesta *et al.*⁵²⁵ Carstensen and Dean⁵²⁶ developed an theory-based method to predict the temperature- and pressure-dependent rate coefficients. For NO₃-reactions, SARs are available by Kerdouci *et al.*^{527,528} and Gallego-Iniesta *et al.*⁵²⁵ Theoretical work on the addition of OH, O₃, and NO₃ to unsaturated compounds including alkenes and unsaturated oxygenated compounds correlates the theory-predicted energy of the highest occupied molecular orbital (HOMO) or ionisation potential (IP) of the alkene. The resulting HOMO-energy to rate coefficient correlations have good predictivity,^{525,529–531} especially for OH and NO₃ addition. These have also been recast as SAR expressions^{531–534} using group additivity factors to allow prediction of the rate coefficient based solely on the molecular structure. McGillen *et al.*^{535,536} found

that for the OH and NO₃ reactions, the rate coefficient is predominantly determined by the environment of the reactive site and can thus be discussed in terms of topology. For ozonolysis reactions, however, the correlations based on HOMO or topological indices were less satisfactory.⁵³⁵ Leather *et al.*⁵³⁷ and McGillen *et al.*^{538,539} argue that this is due to effects of steric hindrance that is not accounted for in frontier-orbital SARs; their SAR based on inductive and steric effects indeed has significantly improved predictive capabilities. Some theory-based SARs derive correlations between the experimental rate coefficients and a set of quantum chemical descriptors of the reaction process, such as the LUMO (lowest unoccupied molecular orbital) and HOMO energy, polarizability, dipole moment, atomic charges, tensors, etc. obtained typically at the DFT level of theory. These correlations often include descriptors not just for the reactant, but also for the transition states. Based on advanced statistical analysis such as multiple linear regressions, neural networks, or support vector machines, predictive correlations are derived. Examples are available for the reaction of VOC + OH,^{540–542} VOC + O₃,^{542–544} or VOC + Cl.^{545,546} This later style of SARs is rarely used in the development of models, as they still require quantum chemical calculations to be performed for each and every structure, even if the calculations are significantly less costly than a full theoretical-kinetic analysis. Also, the statistical correlations found are not always conducive to the understanding of the chemical process in itself.

The elementary reactions of radicals are hard to study experimentally, often leading to a dearth of data to describe their kinetics in atmospheric models. A prime example is the chemistry of alkoxy radicals, a critical stage in the oxidation and decomposition of VOCs in the atmosphere. These radicals react slowly with O₂, but usually have faster unimolecular reaction rates for decomposition, and isomerisation by H-migration; only a handful of reaction rate coefficients were measured directly.^{547,548} Extensive theoretical work on these reactions found that the decomposition rate is determined strongly

by the barrier height, in turn affected mostly by the α -substituents around the breaking bond. This has led to the development of several^{4,549–552} easy-to-use SARs based solely on the structure of the alkoxy radical decomposing; the most extensive SAR⁴ accommodates a plethora of substituents and cyclic structures. For H-migration,^{171,553,554} the rate coefficient depends not just on the environment of the alkoxy radical oxygen, but also on the substitution around the migrating H-atom, the span of the H-migration, and the substituents within the ring of the cyclic transition state. These reactions are strongly affected by tunneling, and the TS rigidity caused by the conversion of degrees of freedom for internal rotation in the reactant to rigid skeleton ring vibrations in the TS.

For other radicals, fewer theory-derived SARs are available. King *et al.*⁵⁵⁵ derived a correlation for the reaction of alkylperoxy radicals, RO₂, with co-reactants NO, HO₂ and CH₃O₂, based on the energy of the singly occupied molecular orbital (SOMO) of the RO₂ radical. Shallcross *et al.*⁵⁵⁶ propose a SAR for RO₂ + RO₂ cross-reactions based on the reaction enthalpy as derived from quantum chemical calculations.

8. Construction of Oxidation Mechanisms

The atmospheric oxidation mechanisms for large hydrocarbons, like the ubiquitous isoprene, monoterpene and sesquiterpene molecules, or the aromatics, are highly complex, with explicit mechanisms for a single molecule often comprising thousands of intermediates and reactions.^{395,557} While laboratory investigations, chamber studies, and field measurements have characterized many of the reaction steps involved, as well as their reaction rates and product distributions, the underlying complexity is such that it is nigh impossible to derive the full mechanism in this way. Theoretical work, drawing upon all the techniques discussed in this work, is well suited to help construct a kinetic model;

we give some examples here. One area where theoretical work contributes significantly is in the discovery of novel reactions, and in the confirmation or disproving of a proposed mechanism. In the OH-initiated β -pinene oxidation, for example, the acetone to nopinone product ratio could not be rationally explained by traditional chemistry; theoretical work showed⁵⁵⁸ that including ring closure reactions in unsaturated peroxy radicals can explain the observations. Other novel reactions which were proposed mostly based on theoretical work include H-migrations in peroxy radicals in terpenoids^{368,559} and isoprene,^{5,373,375} now found to be critical in explaining observations on OH regeneration and formation of low-volatility VOCs. In the oxidation of aromatics, theoretical work was able to confirm the importance of a critical bi-cyclic intermediate formed by, again, ring closure reactions of peroxy radicals;³⁹⁶ this was later observed experimentally.^{403,560}

Even for well-known reaction sequences there is often a dearth of experimental data, or data are available only for ambient or laboratory conditions. Theoretical work is very well suited to help extend this to the full range of temperature and pressures encountered in the atmosphere. Experiment and theory are highly complementary in this regard, and their combined application allows for alleviation of some of the shortcomings in both approaches; for theoretical work specifically, even a single experimental datum point often allows for the optimization of the PES or energy transfer parameters to allow T,P-extrapolations with strongly enhanced reliability.

Yet, while *ab initio* and theoretical kinetic methodologies can examine many reactions, the systematic theoretical study of each elementary reaction remains out of reach. The development of Structure-Activity relationships, SARs, as discussed in section 7, is thus another large contribution of theory to the construction of explicit oxidation mechanisms. The MCM, for example,^{394,557} defines its mechanism based on a set of protocols on how each reaction class is to be treated, and future updates of

this style of mechanism creation could incorporate the results of systematic theoretical work. The availability of SARs also supports the computer-aided generation of mechanisms, discussed below, as they allow facile generation of reactions and their rate coefficients, removing tedious manual labor and reducing the possibility of human error.

9. Automated Chemical Process Discovery

The aforementioned techniques for mechanism construction, building both on experimental and theory-based data sets and SARs, can provide well-defined protocols underlying the mechanism, yet due to both size and complexity, creating the mechanism, identifying missing information, and filling these knowledge gaps remains a formidable task. Automation of chemical process discovery could help shape the future of chemical mechanism creation by removing repetitive labor, and aiding in the discovery of pathways and their kinetic parameters.

Automated generation of complete mechanisms, based on a protocol defining SARs as well as criteria for the inclusion or pruning of reactions, seems a natural way forward for explicit chemical models.⁵⁶¹ The GECKO-A system⁵⁶²⁻⁵⁶⁴ (Generator for Explicit Chemistry and Kinetics of Organics in the Atmosphere) by Aumont *et al.*, or RMG⁵⁶⁵ (Reaction Mechanism Generator) by Green *et al.* are such generators, and have each been used successfully to generate mechanisms incorporating tens to hundreds of thousands of reactions. The SARs, predictive correlations, group additivity approaches, or databases used to obtain the rate parameters for some reactions may however not contain the necessary information to provide an accurate temperature- and pressure-dependent rate coefficient and product distribution. For these, explicit theory- and/or experiment-based work remain necessary, as well as for critical reactions that have a strong impact on the predictions and are preferentially treated by the best

methodologies available. Automatically generated asynchronous or on-the-fly quantum chemical and theoretical kinetic analysis of such reactions^{170,566,567} can provide automated solutions that fill in these knowledge gaps. For example, RMG is able to estimate the temperature- and pressure dependence of reaction networks, including the ability to do on-the-fly Master Equation analysis, and links with on-the-fly quantum and force field calculations.¹⁷⁰

10. Future Directions

Computational investigations of topics in tropospheric chemistry is moving forward at a rapid pace. The development of automated protocols for first principles mechanism generation is certainly a ‘holy grail’ in computational chemistry. For the ground state, there is a mature and rich set of tools for calculating the properties of individual molecular structures, and the kinetics of specific elementary steps. However, as the size of the hydrocarbons undergoing oxidation increases, so does the number of distinct minima and reactions available on a given PES. As new research efforts focus more on the oxidation of monoterpenes, sesquiterpenes, and their oxidation products, on the formation of highly-oxidized low-volatility and extremely-low-volatility hydrocarbons (ELVOC), on the formation, growth, and aging of secondary organic aerosols (SOA), and on multi-phase processes, the ability to deal with this increasing complexity efficiently will be critical. It is important to develop systematic sensitivity analysis protocols for identifying the minima and reactions which have the most significant impact on phenomenological observables, and where computational effort should be focussed. The potential combinatorial explosion in the number of structures and reactions involved in any given mechanism also means that we require analytical strategies for course-graining over large numbers of elementary steps in a fashion that preserves important phenomenological kinetic information – i.e., practical

methods for lumping together structures which are characterized by a fast local equilibrium.²⁸⁷ An interesting approach recently proposed by Wang *et al.*⁵⁶⁸ is based on the idea of a ‘nano-Reactor’ simulation protocol. The idea here is that wildly perturbed MD simulations might be used to accelerate the sampling of stationary point structures required to build elementary reaction steps; this approach exploits recent advances in the ability to run fast quantum chemistry (HF and DFT) on graphical processing units (GPUs). Elsewhere, methods typically applied to accelerate rare events in biochemistry have been applied to map out oxidation mechanisms in small molecules. For example, Zheng and Pfaendtner⁵⁶⁹ recently applied meta-dynamics to identify elementary steps in the methanol oxidation pathway. Haag and Reiher⁵⁷⁰ have even developed an interactive haptic framework for interactively discovering minima in a high dimensional potential energy surfaces, which would be interesting to apply to oxidation systems. The aforementioned strategies are all aimed at identifying important minima, pathways, and transition states on rugged ground-state potential energy surfaces. This is a serious problem, amplified by the increasingly high-dimensional PESs being studied.

The accurate theoretical kinetic treatment of these larger systems is problematic with the current tools. Within quantum chemistry, one of the biggest challenges involves the development of efficient methods for accurately recovering electron correlation, which is important for accurately predicting stationary point energies. A great deal of recent effort in this direction is investigating the use of local methods^{571–573} for electron correlation, to reduce the poor scaling of methods like Coupled Cluster theory. Another important area concerns efficient treatment of highly anharmonic molecular modes – particularly torsions, which become increasingly important as molecular sizes increase. Mapping out kinetic networks on excited state PESs also remains a significant challenge for computational investigations of tropospheric chemistry. Finally, turning the structures and reactions which such

methods generate into accurate kinetic networks will inevitably require subsequent refinement steps, where significant challenges also remain.

With the increasing computational power that is becoming available, it seems that a paradigm shift may well be on the horizon: computer-aided mechanisms may finally allow atmospheric scientists to move past the write-once-update-rarely mechanisms of the past. Indeed, these computer-based tools carry great promise to help atmospheric scientists to improve their models, keep them updated, and test their performance, uncertainties and atmospheric implications, without the manual labor or maintenance overheads which constrain mechanism detail and size. This is an exciting area, where progress requires a close link between all the different aspects of the problem.

Author Information

Corresponding Authors

* Tel. +49-6131-3054075. Fax: +49-6131-3054009. E-mail: Luc.Vereecken@mpic.de

* Tel. +1-415-568-1401. E-mail: drglowacki@gmail.com

* Tel. +44-1943-608239. Fax: +44-113-3436401. E-mail: m.j.pilling@leeds.ac.uk

Notes

The authors declare no competing financial interest.

Biographies



Luc Vereecken studied Chemistry at the Katholieke Universiteit Leuven in Belgium, where he later also received his PhD in Chemistry. He remained active at Leuven as a postdoctoral researcher in reaction kinetics. During his time in Leuven, he collaborated with many international research groups, including extended stays at the Academia Sinica in Taiwan, and the University of Leeds in the UK. In 2010, Vereecken moved to the Max Planck Institute for Chemistry in Mainz, Germany, where he heads a research group in Theoretical Atmospheric Chemistry as Junior Staff of the Max Planck Graduate Center.



David Glowacki is a Royal Society Research fellow with broad-ranging interests across theoretical chemistry and computer science. At present, one of his main research emphases is focused on the use of high-performance computing to tackle problems in molecular dynamics and kinetics across both gas and condensed phases. His undergraduate study was carried out at the University of Pennsylvania. After graduating, he obtained his M.A at Manchester University in 2004 and his Ph.D. at the University of Leeds in 2008. He moved to Bristol in 2009 to carry out his

postdoctoral research, and presently holds appointments jointly across the University of Bristol and Stanford University. His work to understand energy transfer in chemical reaction dynamics was recently recognized by the Royal Society of Chemistry's 2014 Harrison-Meldola Memorial Prize.



Mike Pilling did his PhD at Cambridge and then spent 19 years at Oxford before moving to the Chair in Physical Chemistry at the University of Leeds in 1989. His research interests are in radical kinetics and applications in combustion and atmospheric chemistry. He was the Director of Composition Research at the National Centre for Atmospheric Science from 2002 – 2007, Chair of the Air Quality Expert Group, a UK Government advisory body, from 2002 – 2008 and President of the Faraday Division of the Royal Society of Chemistry from 2003 – 2006. He was awarded a CBE in 2008.

Acknowledgements

Luc Vereecken is supported by the Max Planck Graduate Center with the Johannes Gutenberg-Universität Mainz (MPGC), Germany. David Glowacki acknowledges support as a Royal Society research fellow. The authors wish to thank the reviewers for their helpful comments.

References

- (1) Atkinson, R.; Baulch, D. L.; Cox, R. A.; Crowley, J. N.; Hampson, R. F.; Hynes, R. G.; Jenkin, M. E.; Rossi, M. J.; Troe, J.; IUPAC Subcommittee. *Atmospheric Chem. Phys.* **2006**, *6*, 3625.
- (2) Sander, S. P.; Abbatt, J. P. D.; Barker, J. R.; Burkholder, J. B.; Friedl, R. R.; Golden, D. M.; Huie, R. E.; Kolb, C. E.; Kurylo, M. J.; Moortgat, G. K.; Orkin, V. L.; Wine, P. H. *Chemical kinetics and photochemical data for use in atmospheric studies, Evaluation No. 17, JPL Publication 10-6*; Jet Propulsion Laboratory: Pasadena, <http://jpldataeval.jpl.nasa.gov>, 2011.
- (3) Kwok, E.; Atkinson, R. *Atmos. Environ.* **1995**, *29*, 1685.
- (4) Vereecken, L.; Peeters, J. *Phys. Chem. Chem. Phys.* **2009**, *11*, 9062.
- (5) Peeters, J.; Müller, J.-F.; Stavrakou, T.; Nguyen, V. S. *J. Phys. Chem. A* **2014**, *118*, 8625.
- (6) Zádor, J.; Taatjes, C. A.; Fernandes, R. X. *Prog. Energy Combust. Sci.* **2011**, *37*, 371.
- (7) Taatjes, C. A.; Meloni, G.; Selby, T. M.; Trevitt, A. J.; Osborn, D. L.; Percival, C. J.; Shallcross, D. E. *J. Am. Chem. Soc.* **2008**, *130*, 11883.
- (8) Welz, O.; Savee, J. D.; Osborn, D. L.; Vasu, S. S.; Percival, C. J.; Shallcross, D. E.; Taatjes, C. A. *Science* **2012**, *335*, 204.
- (9) Crouse, J. D.; Nielsen, L. B.; Jørgensen, S.; Kjaergaard, H. G.; Wennberg, P. O. *J. Phys. Chem. Lett.* **2013**, *4*, 3513.
- (10) Glowacki, D. R.; Lightfoot, R.; Harvey, J. N. *Mol. Phys.* **2013**, *111*, 631.
- (11) Galano, A.; Alvarez-Idaboy, J. R.; Ruiz-Santoyo, M. E.; Vivier-Bunge, A. *J. Phys. Chem. A* **2005**, *109*, 169.
- (12) Méreau, R.; Rayez, M.-T.; Rayez, J.-C.; Caralp, F.; Lesclaux, R. *Phys. Chem. Chem.*

Phys. **2001**, 3, 4712.

(13) Viskolcz, B.; Bérces, T. *Phys. Chem. Chem. Phys.* **2000**, 2, 5430.

(14) Vereecken, L.; Harder, H.; Novelli, A. *Phys. Chem. Chem. Phys.* **2012**, 14, 14682.

(15) Atkins, P. W. *Quanta - A Handbook of Concepts*; Clarendon Press: Oxford, 1974.

(16) Bartlett, R. J. *Annu. Rev. Phys. Chem.* **1981**, 32, 359.

(17) Hehre, W. J.; Radom, L.; Schleyer, P. von R.; Pople, J. *Ab Initio Molecular Orbital Theory*; Wiley-Interscience: New York, 1986.

(18) Szabo, A.; Ostlund, N. S. *Modern quantum chemistry*; Dover Publications: New York, 1989.

(19) Parr, R. G.; Yang, W. *Density-functional theory of atoms and molecules*; Oxford University Press: Oxford, New York, 1994.

(20) Sherrill, C. D.; Schaefer, H. F. In *Advances in Quantum Chemistry*; Academic Press: New York, 1999; Vol. 34, pp 143–269.

(21) Chalasiniski, G.; Szczesniak, M. M. *Chem. Rev.* **2000**, 100, 4227.

(22) Ziegler, T.; Autschbach, J. *Chem. Rev.* **2005**, 105, 2695.

(23) Jensen, F. *Introduction to computational chemistry*; John Wiley & Sons: Chichester, England, 2007.

(24) Ochsenfeld, C.; Kussmann, J.; Lambrecht, D. S. In *Reviews in Computational Chemistry*; Lipkowitz, K. B., Cundari, T. R., Eds.; John Wiley & Sons, Inc.: Hoboken, NJ, USA, 2007; Vol. 23, pp 1–82.

(25) Helgaker, T.; Klopper, W.; Tew, D. P. *Mol. Phys.* **2008**, 106, 2107.

(26) Atkins, P. W.; Friedman, R. *Molecular quantum mechanics*; Oxford University Press:

Oxford; New York, 2011.

- (27) Perdew, J. P.; Ruzsinszky, A.; Tao, J.; Staroverov, V. N.; Scuseria, G. E.; Csonka, G. I. *J. Chem. Phys.* **2005**, *123*, 062201.
- (28) Baboul, A. G.; Schlegel, H. B. *J. Chem. Phys.* **1997**, *107*, 9413.
- (29) Quapp, W.; Heidrich, D. *Theor. Chim. Acta* **1984**, *66*, 245.
- (30) Liu, B.; Mclean, A. *J. Chem. Phys.* **1973**, *59*, 4557.
- (31) Hariharan, P. C.; Pople, J. A. *Theor. Chim. Acta* **1973**, *28*, 213.
- (32) Dunning, T. H. *J. Chem. Phys.* **1989**, *90*, 1007.
- (33) Dunning, T. H.; Peterson, K. A.; Wilson, A. K. *J. Chem. Phys.* **2001**, *114*, 9244.
- (34) Kendall, R. A.; Dunning, T. H.; Harrison, R. J. *J. Chem. Phys.* **1992**, *96*, 6796.
- (35) Woon, D. E.; Dunning, T. H. *J. Chem. Phys.* **1993**, *98*, 1358.
- (36) Woon, D. E.; Dunning, T. H. *J. Chem. Phys.* **1995**, *103*, 4572.
- (37) Papajak, E.; Leverentz, H. R.; Zheng, J.; Truhlar, D. G. *J. Chem. Theory Comput.* **2009**, *5*, 1197.
- (38) Papajak, E.; Truhlar, D. G. *J. Chem. Theory Comput.* **2011**, *7*, 10.
- (39) Martin, J. M. L. *Chem. Phys. Lett.* **1996**, *259*, 669.
- (40) Martin, J. M. L.; Taylor, P. R. *J. Chem. Phys.* **1997**, *106*, 8620.
- (41) Helgaker, T.; Klopper, W.; Koch, H.; Noga, J. *J. Chem. Phys.* **1997**, *106*, 9639.
- (42) Truhlar, D. G. *Chem. Phys. Lett.* **1998**, *294*, 45.
- (43) Halkier, A.; Klopper, W.; Helgaker, T.; Jorgensen, P.; Taylor, P. R. *J. Chem. Phys.* **1999**, *111*, 9157.
- (44) Halkier, A.; Helgaker, T.; Jorgensen, P.; Klopper, W.; Olsen, J. *Chem. Phys. Lett.* **1999**,

302, 437.

- (45) Varandas, A. J. C. *J. Chem. Phys.* **2007**, *126*, 244105.
- (46) Bakowies, D. *J. Chem. Phys.* **2007**, *127*, 084105.
- (47) Bakowies, D. *J. Chem. Phys.* **2007**, *127*, 164109.
- (48) Purvis, G. D.; Bartlett, R. J. *J. Chem. Phys.* **1982**, *76*, 1910.
- (49) Pople, J. A.; Head-Gordon, M.; Raghavachari, K. *J. Chem. Phys.* **1987**, *87*, 5968.
- (50) Raghavachari, K.; Trucks, G. W.; Pople, J. A.; Head-Gordon, M. *Chem. Phys. Lett.* **1989**,

157, 479.

- (51) Watts, J. D.; Gauss, J.; Bartlett, R. J. *J. Chem. Phys.* **1993**, *98*, 8718.
- (52) Roos, B. O. In *Theory and Applications of Computational Chemistry*; Elsevier:

Amsterdam ; Boston, 2005; pp 725–764.

- (53) Salem, L.; Rowland, C. *Angew. Chem.-Int. Ed.* **1972**, *11*, 92.
- (54) Slipchenko, L. V.; Krylov, A. I. *J. Chem. Phys.* **2002**, *117*, 4694.
- (55) Roos, B. O.; Taylor, P. R.; Siegbahn, P. E. M. *Chem. Phys.* **1980**, *48*, 157.
- (56) Olsen, J.; Roos, B. O.; Jorgensen, P.; Jensen, H. J. A. *J. Chem. Phys.* **1988**, *89*, 2185.
- (57) Malmqvist, P. A.; Rendell, A.; Roos, B. O. *J. Phys. Chem.* **1990**, *94*, 5477.
- (58) Sauri, V.; Serrano-Andres, L.; Shahi, A. R. M.; Gagliardi, L.; Vancoillie, S.; Pierloot, K.

J. Chem. Theory Comput. **2011**, *7*, 153.

- (59) Tishchenko, O.; Zheng, J.; Truhlar, D. G. *J. Chem. Theory Comput.* **2008**, *4*, 1208.
- (60) Yang, K. R.; Jalan, A.; Green, W. H.; Truhlar, D. G. *J. Chem. Theory Comput.* **2013**, *9*,

418.

- (61) Lee, T. J.; Taylor, P. R. *Int. J. Quantum Chem.* **1989**, *36*, 199.

- (62) Lee, T. J. *Chem. Phys. Lett.* **2003**, 372, 362.
- (63) Rienstra-Kiracofe, J. C.; Allen, W. D.; Schaefer, H. F. *J. Phys. Chem. A* **2000**, 104, 9823.
- (64) Tao, J.; Perdew, J.; Staroverov, V.; Scuseria, G. *Phys. Rev. Lett.* **2003**, 91, 146401.
- (65) Zhao, Y.; Truhlar, D. G. *Theor. Chem. Acc.* **2008**, 120, 215.
- (66) Grimme, S.; Ehrlich, S.; Goerigk, L. *J. Comput. Chem.* **2011**, 32, 1456.
- (67) Hujó, W.; Grimme, S. *Phys. Chem. Chem. Phys.* **2011**, 13, 13942.
- (68) Thiel, W. *Wiley Interdiscip. Rev. Comput. Mol. Sci.* **2014**, 4, 145.
- (69) Hoffmann, R. *J. Chem. Phys.* **1963**, 39, 1397.
- (70) Elstner, M. *Theor. Chem. Acc.* **2006**, 116, 316.
- (71) Greaves, S. J.; Rose, R. A.; Abou-Chahine, F.; Glowacki, D. R.; Troya, D.; Orr-Ewing, A. J. *Phys. Chem. Chem. Phys.* **2011**, 13, 11438.
- (72) Otte, N.; Scholten, M.; Thiel, W. *J. Phys. Chem. A* **2007**, 111, 5751.
- (73) Tirado-Rives, J.; Jorgensen, W. L. *J. Chem. Theory Comput.* **2008**, 4, 297.
- (74) Curtiss, L. A.; Raghavachari, K.; Trucks, G. W.; Pople, J. A. *J. Chem. Phys.* **1991**, 94, 7221.
- (75) Pople, J. A.; Head-Gordon, M.; Fox, D. J.; Raghavachari, K.; Curtiss, L. A. *J. Chem. Phys.* **1989**, 90, 5622.
- (76) Curtiss, L. A.; Raghavachari, K.; Redfern, P. C.; Rassolov, V.; Pople, J. A. *J. Chem. Phys.* **1998**, 109, 7764.
- (77) Curtiss, L. A.; Redfern, P. C.; Raghavachari, K.; Pople, J. A. *J. Chem. Phys.* **2001**, 114, 108.
- (78) Curtiss, L. A.; Redfern, P. C.; Raghavachari, K. *J. Chem. Phys.* **2007**, 126, 084108.

- (79) Curtiss, L. A.; Raghavachari, K.; Redfern, P. C.; Baboul, A. G.; Pople, J. A. *Chem. Phys. Lett.* **1999**, *314*, 101.
- (80) Curtiss, L. A.; Raghavachari, K.; Redfern, P. C.; Pople, J. A. *J. Chem. Phys.* **2000**, *112*, 1125.
- (81) Curtiss, L. A.; Redfern, P. C.; Raghavachari, K.; Pople, J. A. *Chem. Phys. Lett.* **1999**, *313*, 600.
- (82) Curtiss, L. A.; Redfern, P. C.; Raghavachari, K. *J. Chem. Phys.* **2007**, *127*, 124105.
- (83) Curtiss, L. A.; Redfern, P. C.; Raghavachari, K.; Rassolov, V.; Pople, J. A. *J. Chem. Phys.* **1999**, *110*, 4703.
- (84) Petersson, G. A.; Bennett, A.; Tensfeldt, T. G.; Al-Laham, M. A.; Shirley, W. A.; Mantzaris, J. J. *J. Chem. Phys.* **1988**, *89*, 2193.
- (85) Petersson, G. A.; Tensfeldt, T. G.; Montgomery, J. A. *J. Chem. Phys.* **1991**, *94*, 6091.
- (86) Montgomery, J. A.; Ochterski, J. W.; Petersson, G. A. *J. Chem. Phys.* **1994**, *101*, 5900.
- (87) Ochterski, J. W.; Petersson, G. A.; Montgomery, J. A. *J. Chem. Phys.* **1996**, *104*, 2598.
- (88) Montgomery, J. A.; Frisch, M. J.; Ochterski, J. W.; Petersson, G. A. *J. Chem. Phys.* **1999**, *110*, 2822.
- (89) Martin, J. M. L.; de Oliveira, G. *J. Chem. Phys.* **1999**, *111*, 1843.
- (90) Boese, A. D.; Oren, M.; Atasoylu, O.; Martin, J. M. L.; Kállay, M.; Gauss, J. *J. Chem. Phys.* **2004**, *120*, 4129.
- (91) Karton, A.; Rabinovich, E.; Martin, J. M. L.; Ruscic, B. *J. Chem. Phys.* **2006**, *125*, 144108.
- (92) Karton, A.; Martin, J. M. L. *J. Chem. Phys.* **2012**, *136*, 124114.

- (93) Tajti, A.; Szalay, P. G.; Császár, A. G.; Kállay, M.; Gauss, J.; Valeev, E. F.; Flowers, B. A.; Vázquez, J.; Stanton, J. F. *J. Chem. Phys.* **2004**, *121*, 11599.
- (94) Bomble, Y. J.; Vázquez, J.; Kállay, M.; Michauk, C.; Szalay, P. G.; Császár, A. G.; Gauss, J.; Stanton, J. F. *J. Chem. Phys.* **2006**, *125*, 064108.
- (95) East, A.; Johnson, C.; Allen, W. *J. Chem. Phys.* **1993**, *98*, 1299.
- (96) Schuurman, M. S.; Muir, S. R.; Allen, W. D.; Schaefer, H. F. *J. Chem. Phys.* **2004**, *120*, 11586.
- (97) Serrano-Andrés, L.; Merchán, M. *J. Mol. Struct. THEOCHEM* **2005**, *729*, 99.
- (98) Schreiber, M.; Silva-Junior, M. R.; Sauer, S. P. A.; Thiel, W. *J. Chem. Phys.* **2008**, *128*, 134110.
- (99) Silva-Junior, M. R.; Schreiber, M.; Sauer, S. P. A.; Thiel, W. *J. Chem. Phys.* **2008**, *129*, 104103.
- (100) Sauer, S. P. A.; Schreiber, M.; Silva-Junior, M. R.; Thiel, W. *J. Chem. Theory Comput.* **2009**, *5*, 555.
- (101) Silva-Junior, M. R.; Schreiber, M.; Sauer, S. P. A.; Thiel, W. *J. Chem. Phys.* **2010**, *133*, 174318.
- (102) González, L.; Escudero, D.; Serrano-Andrés, L. *ChemPhysChem* **2012**, *13*, 28.
- (103) Roca-Sanjuán, D.; Aquilante, F.; Lindh, R. *Wiley Interdiscip. Rev.-Comput. Mol. Sci.* **2012**, *2*, 585.
- (104) Sneskov, K.; Christiansen, O. *Wiley Interdiscip. Rev.-Comput. Mol. Sci.* **2012**, *2*, 566.
- (105) Helgaker, T.; Coriani, S.; Jorgensen, P.; Kristensen, K.; Olsen, J.; Ruud, K. *Chem. Rev.* **2012**, *112*, 543.

- (106) Oddershede, J. In *Advances in Chemical Physics*; Lawley, K. P., Ed.; John Wiley & Sons, Inc.: Hoboken, NJ, USA, 1987; Vol. 69, pp 201–239.
- (107) Adamo, C.; Jacquemin, D. *Chem. Soc. Rev.* **2013**, *42*, 845.
- (108) Ullrich, C. A.; Yang, Z. *Braz. J. Phys.* **2014**, *44*, 154.
- (109) Ezra, G. S.; Waalkens, H.; Wiggins, S. *J. Chem. Phys.* **2009**, *130*, 164118.
- (110) Carpenter, B. K. In *Annual Review of Physical Chemistry*; Annual Reviews: Palo Alto, 2005; Vol. 56, pp 57–89.
- (111) Newton, I. *Philosophiæ Naturalis Principia Mathematica*; 1687.
- (112) Greenwald, E. E.; North, S. W.; Georgievskii, Y.; Klippenstein, S. J. *J. Phys. Chem. A* **2005**, *109*, 6031.
- (113) Greenwald, E. E.; North, S. W.; Georgievskii, Y.; Klippenstein, S. J. *J. Phys. Chem. A* **2007**, *111*, 5582.
- (114) Senosiain, J. P.; Klippenstein, S. J.; Miller, J. A. *J. Phys. Chem. A* **2005**, *109*, 6045.
- (115) Barker, J. R.; Weston, R. E., Jr. *J. Phys. Chem. A* **2010**, *114*, 10619.
- (116) Zhu, L.; Hase, W. L. *Chem. Phys. Lett.* **1990**, *175*, 117.
- (117) Aubanel, E. E.; Wardlaw, D. M.; Zhu, L.; Hase, W. L. *Int. Rev. Phys. Chem.* **1991**, *10*, 249.
- (118) Golden, D. M.; Barker, J. R. *Combust. Flame* **2011**, *158*, 602.
- (119) Ghaderi, N.; Marcus, R. A. *J. Phys. Chem. A* **2014**, *118*, 10166.
- (120) Beyer, T.; Swinehart, D. F. *Commun. Acm* **1973**, *16*, 379.
- (121) Stein, S. E.; Rabinovitch, B. S. *J. Chem. Phys.* **1973**, *58*, 2438.
- (122) Stein, S. E.; Rabinovitch, B. S. *Chem. Phys. Lett.* **1977**, *49*, 183.

- (123) Barone, V. *J. Chem. Phys.* **2004**, *120*, 3059.
- (124) Knyazev, V. D.; Tsang, W. *J. Phys. Chem. A* **1998**, *102*, 9167.
- (125) Katzer, G.; Sax, A. F. *J. Phys. Chem. A* **2002**, *106*, 7204.
- (126) Katzer, G.; Sax, A. F. *J. Comput. Chem.* **2005**, *26*, 1438.
- (127) Katzer, G.; Sax, A. F. *J. Chem. Phys.* **2002**, *117*, 8219.
- (128) Varshni, Y. P. *Rev. Mod. Phys.* **1957**, *29*, 664.
- (129) Klippenstein, S. J.; Khundkar, L. R.; Zewail, A. H.; Marcus, R. A. *J. Chem. Phys.* **1988**, *89*, 4761.
- (130) Miller, J.; Klippenstein, S. J. *J. Phys. Chem. A* **2000**, *104*, 2061.
- (131) Murrell, J. N.; Sorbie, K. S. *J. Chem. Soc.-Faraday Trans. 2 Mol. Chem. Phys.* **1974**, *70*, 1552.
- (132) Pitzer, K. S.; Gwinn, W. D. *J. Chem. Phys.* **1942**, *10*, 428.
- (133) Marston, C. C.; Balint-Kurti, G. G. *J. Chem. Phys.* **1989**, *91*, 3571.
- (134) Balint-Kurti, G. G.; Dixon, R. N.; Marston, C. C. *Int. Rev. Phys. Chem.* **1992**, *11*, 317.
- (135) Meyer, R. *J. Chem. Phys.* **1970**, *52*, 2053.
- (136) Dutta, P.; Adhikari, S.; Bhattacharyya, S. P. *Chem. Phys. Lett.* **1993**, *212*, 677.
- (137) Barone, V.; Bloino, J.; Guido, C. A.; Lipparini, F. *Chem. Phys. Lett.* **2010**, *496*, 157.
- (138) Basire, M.; Parneix, P.; Calvo, F. *J. Chem. Phys.* **2008**, *129*, 081101.
- (139) Calvo, F.; Basire, M.; Parneix, P. *Chem. Phys. Lett.* **2010**, *496*, 196.
- (140) Nguyen, T. L.; Barker, J. R. *J. Phys. Chem. A* **2010**, *114*, 3718.
- (141) Kamarchik, E.; Jasper, A. W. *J. Chem. Phys.* **2013**, *138*, 194109.
- (142) Kamarchik, E.; Jasper, A. W. *J. Phys. Chem. Lett.* **2013**, *4*, 2430.

- (143) Irikura, K. K. *J. Chem. Thermodyn.* **2014**, *73*, 183.
- (144) Ellingson, B. A.; Lynch, V. A.; Mielke, S. L.; Truhlar, D. G. *J. Chem. Phys.* **2006**, *125*, 084305.
- (145) Pfaendtner, J.; Yu, X.; Broadbelt, L. J. *Theor. Chem. Acc.* **2007**, *118*, 881.
- (146) Kilpatrick, J. E.; Pitzer, K. S. *J. Chem. Phys.* **1949**, *17*, 1064.
- (147) Pitzer, K. S. *J. Chem. Phys.* **1946**, *14*, 239.
- (148) Pitzer, K. S.; Gwinn, W. D. *J. Chem. Phys.* **1941**, *9*, 485.
- (149) Harthcock, M. A.; Laane, J. *J. Mol. Spectrosc.* **1982**, *91*, 300.
- (150) Chuang, Y.-Y.; Truhlar, D. G. *J. Chem. Phys.* **2000**, *112*, 1221.
- (151) Truhlar, D. G. *J. Comput. Chem.* **1991**, *12*, 266.
- (152) Ayala, P. Y.; Schlegel, H. B. *J. Chem. Phys.* **1998**, *108*, 2314.
- (153) Zheng, J.; Yu, T.; Papajak, E.; Alecu, I. M.; Mielke, S. L.; Truhlar, D. G. *Phys. Chem. Chem. Phys.* **2011**, *13*, 10885.
- (154) Barker, J. R.; Shovlin, C. N. *Chem. Phys. Lett.* **2004**, *383*, 203.
- (155) McClurg, R. B.; Flagan, R. C.; Goddard, W. A. I. *J. Chem. Phys.* **1997**, *106*, 6675.
- (156) Knyazev, V. D. *J. Phys. Chem. A* **1998**, *102*, 3916.
- (157) East, A. L. L.; Radom, L. *J. Chem. Phys.* **1997**, *106*, 6655.
- (158) Katzer, G.; Sax, A. F. *Chem. Phys. Lett.* **2003**, *368*, 473.
- (159) Lin, C. Y.; Izgorodina, E. I.; Coote, M. L. *J. Phys. Chem. A* **2008**, *112*, 1956.
- (160) Sharma, S.; Raman, S.; Green, W. H. *J. Phys. Chem. A* **2010**, *114*, 5689.
- (161) Strekalov, M. L. *Chem. Phys.* **2009**, *355*, 62.
- (162) Strekalov, M. L. *Chem. Phys.* **2009**, *362*, 75.

- (163) Sturdy, Y. K.; Clary, D. C. *Phys. Chem. Chem. Phys.* **2007**, *9*, 2397.
- (164) Vansteenkiste, P.; Van Speybroeck, V.; Marin, G. B.; Waroquier, M. *J. Phys. Chem. A* **2003**, *107*, 3139.
- (165) Vansteenkiste, P.; Van Neck, D.; Van Speybroeck, V.; Waroquier, M. *J. Chem. Phys.* **2006**, *124*, 044314.
- (166) Witschel, W.; Hartwigsen, C. *Chem. Phys. Lett.* **1997**, *273*, 304.
- (167) Troe, J. *J. Chem. Phys.* **1977**, *66*, 4758.
- (168) McClurg, R. B. *J. Chem. Phys.* **1999**, *111*, 7165.
- (169) Gang, J.; Pilling, M. J.; Robertson, S. H. *Chem. Phys.* **1998**, *231*, 183.
- (170) Magoon, G. R.; Green, W. H. *Comput. Chem. Eng.* **2013**, *52*, 35.
- (171) Vereecken, L.; Peeters, J. *J. Chem. Phys.* **2003**, *119*, 5159.
- (172) Vansteenkiste, P.; Van Speybroeck, V.; Pauwels, E.; Waroquier, M. *Chem. Phys.* **2005**, *314*, 109.
- (173) Lewis, J.; Malloy, T.; Chao, T.; Laane, J. *J. Mol. Struct.* **1972**, *12*, 427.
- (174) Lee, A.; Kalotas, T.; Mellor, W. *Chem. Phys. Lett.* **1995**, *243*, 341.
- (175) Mellor, W. E.; Kalotas, T. M.; Lee, A. R. *J. Chem. Phys.* **1997**, *106*, 6825.
- (176) Fernández-Ramos, A. *J. Chem. Phys.* **2013**, *138*, 134112.
- (177) Reinisch, G.; Leyssale, J.-M.; Vignoles, G. L. *J. Chem. Phys.* **2010**, *133*, 154112.
- (178) Forst, W. *Theory of unimolecular reactions.*; Academic Press: New York, 1973.
- (179) Benson, S. *The foundations of chemical kinetics*; R.E. Krieger: Malabar Fla., 1982.
- (180) Truhlar, D. G.; Garrett, B. C. *Annu. Rev. Phys. Chem.* **1984**, *35*, 159.
- (181) Truhlar, D. G.; Garrett, B. C.; Klippenstein, S. J. *J. Phys. Chem.* **1996**, *100*, 12771.

- (182) Holbrook, K.; Pilling, M. J.; Robertson, S. H. *Unimolecular reactions*, 2nd ed.; Wiley: Chichester, 1996.
- (183) Steinfeld, J.; Francisco, J. S.; Hase, W. L. *Chemical kinetics and dynamics*, 2nd ed.; Prentice Hall: Upper Saddle River N.J., 1999.
- (184) Forst, W. *Unimolecular reactions : a concise introduction*; Cambridge University Press: Cambridge U.K., 2003.
- (185) Fernández-Ramos, A.; Miller, J. A.; Klippenstein, S. J.; Truhlar, D. G. *Chem. Rev.* **2006**, *106*, 4518.
- (186) Pilling, M.; Seakins, P. W. *Reaction kinetics*; Oxford Univ. Press: Oxford, 2007.
- (187) Coulson, D. *J. Am. Chem. Soc.* **1978**, *100*, 2992.
- (188) Pollak, E.; Pechukas, P. *J. Am. Chem. Soc.* **1978**, *100*, 2984.
- (189) Fernández-Ramos, A.; Ellingson, B. A.; Meana-Pañeda, R.; Marques, J. M. C.; Truhlar, D. G. *Theor. Chem. Acc.* **2007**, *118*, 813.
- (190) Newton, G.; Lewis, M. R. *Thermodynamics. Revised by Kenneth S. Pitzer and Leo Brewer.*, 2nd. edition.; McGraw-Hill: New York, 1965.
- (191) Miller, W. H. *J. Chem. Phys.* **1975**, *62*, 1899.
- (192) Miller, W. H. *Faraday Discuss.* **1977**, *62*, 40.
- (193) Miller, W. H.; Hernandez, R.; Handy, N. C.; Jayatilaka, D.; Willetts, A. *Chem. Phys. Lett.* **1990**, *172*, 62.
- (194) Hernandez, R.; Miller, W. H. *Chem. Phys. Lett.* **1993**, *214*, 129.
- (195) Nguyen, T. L.; Stanton, J. F.; Barker, J. R. *Chem. Phys. Lett.* **2010**, *499*, 9.
- (196) Gilbert, R.; Smith, S. C. *Theory of unimolecular and recombination reactions*;

Blackwell Scientific Publications: Oxford, 1990.

- (197) Rice, O. K.; Ramsperger, H. C. *J. Am. Chem. Soc.* **1927**, *49*, 1617.
- (198) Kassel, L. S. *J. Phys. Chem.* **1927**, *32*, 225.
- (199) Marcus, R. A. *J. Chem. Phys.* **1952**, *20*, 359.
- (200) Maranzana, A.; Barker, J. R.; Tonachini, G. *Phys. Chem. Chem. Phys.* **2007**, *9*, 4129.
- (201) Green, N. J. B.; Robertson, S. H. *Chem. Phys. Lett.* **2014**, *605*, 44.
- (202) Olzmann, M. *Phys. Chem. Chem. Phys.* **2002**, *4*, 3614.
- (203) Pfeifle, M.; Olzmann, M. *Int. J. Chem. Kinet.* **2014**, *46*, 231.
- (204) Davies, J. W.; Green, N. J. B.; Pilling, M. J. *Chem. Phys. Lett.* **1986**, *126*, 373.
- (205) Klippenstein, S. *J. Chem. Phys.* **1992**, *96*, 367.
- (206) Garrett, B. C.; Truhlar, D. G. In *Theory and Applications of Computational Chemistry*; Elsevier: Amsterdam ; Boston, 2005; pp 67–87.
- (207) Corchado, J. C.; Coitiño, E. L.; Chuang, Y.-Y.; Fast, P. L.; Truhlar, D. G. *J. Phys. Chem. A* **1998**, *102*, 2424.
- (208) Masgrau, L.; González-Lafont, À.; Lluch, J. M. *J. Phys. Chem. A* **2002**, *106*, 11760.
- (209) Meana-Pañeda, R.; Truhlar, D. G.; Fernández-Ramos, A. *J. Chem. Phys.* **2011**, *134*, 094302.
- (210) Vereecken, L.; Peeters, J. *J. Phys. Chem. A* **1999**, *103*, 5523.
- (211) Xu, X.; Papajak, E.; Zheng, J.; Truhlar, D. G. *Phys. Chem. Chem. Phys.* **2012**, *14*, 4204.
- (212) Vereecken, L.; Harder, H.; Novelli, A. *Phys. Chem. Chem. Phys.* **2014**, *16*, 4039.
- (213) Kuwata, K. T.; Dibble, T. S.; Sliz, E.; Petersen, E. B. *J. Phys. Chem. A* **2007**, *111*, 5032.
- (214) Klippenstein, S. *J. Phys. Chem.* **1994**, *98*, 11459.

- (215) Smith, S. C. *J. Phys. Chem.* **1994**, *98*, 6496.
- (216) Taatjes, G. A.; Klippenstein, S. J. *J. Phys. Chem. A* **2001**, *105*, 8567.
- (217) Davis, M. J.; Klippenstein, S. J. *J. Phys. Chem. A* **2002**, *106*, 5860.
- (218) Georgievskii, Y.; Klippenstein, S. J. *J. Phys. Chem. A* **2003**, *107*, 9776.
- (219) Klippenstein, S. J.; Georgievskii, Y.; Harding, L. B. *Phys. Chem. Chem. Phys.* **2006**, *8*, 1133.
- (220) Pritchard, H. O. *The quantum theory of unimolecular reactions*; Cambridge University Press: Cambridge ; New York, 1984.
- (221) Glowacki, D. R.; Liang, C. H.; Morley, C.; Pilling, M. J.; Robertson, S. H. *J. Phys. Chem. A* **2012**, *116*, 9545.
- (222) Eskola, A. J.; Carr, S. A.; Shannon, R. J.; Wang, B.; Blitz, M. A.; Pilling, M. J.; Seakins, P. W. *J. Phys. Chem. A* **2014**, *118*, 6773.
- (223) Wigner, E. Z. *Phys. Chem.-Abt. B-Chem. Elem. Aufbau Mater.* **1932**, *19*, 203.
- (224) Eckart, C. *Phys. Rev.* **1930**, *35*, 1303.
- (225) Johnston, H. S.; Heicklen, J. *J. Phys. Chem.* **1962**, *66*, 532.
- (226) Truhlar, D. G.; Kuppermann, A. *J. Am. Chem. Soc.* **1971**, *93*, 1840.
- (227) Marcus, R.; Coltrin, M. *J. Chem. Phys.* **1977**, *67*, 2609.
- (228) Liu, Y.; Lu, D.; Gonzalez-lafont, A.; Truhlar, D.; Garrett, B. *J. Am. Chem. Soc.* **1993**, *115*, 7806.
- (229) Skodje, R. T.; Truhlar, D. G.; Garrett, B. C. *J. Phys. Chem.* **1981**, *85*, 3019.
- (230) Fernandez-Ramos, A.; Truhlar, D. G. *J. Chem. Phys.* **2001**, *114*, 1491.
- (231) Wagner, A. F. *J. Phys. Chem. A* **2013**, *117*, 13089.

- (232) Wagner, A. F.; Dawes, R.; Continetti, R. E.; Guo, H. *J. Chem. Phys.* **2014**, *141*, 054304.
- (233) Tully, J. C. *J. Chem. Phys.* **1990**, *93*, 1061.
- (234) Tapavicza, E.; Bellchambers, G. D.; Vincent, J. C.; Furche, F. *Phys. Chem. Chem. Phys.* **2013**, *15*, 18336.
- (235) Shemesh, D.; Lan, Z.; Gerber, R. B. *J. Phys. Chem. A* **2013**, *117*, 11711.
- (236) Lignell, H.; Epstein, S. A.; Marvin, M. R.; Shemesh, D.; Gerber, B.; Nizkorodov, S. *J. Phys. Chem. A* **2013**, *117*, 12930.
- (237) Shemesh, D.; Gerber, R. B. *Mol. Phys.* **2012**, *110*, 605.
- (238) Fu, B.; Han, Y.-C.; Bowman, J. M.; Angelucci, L.; Balucani, N.; Leonori, F.; Casavecchia, P. *Proc. Natl. Acad. Sci.* **2012**, *109*, 9733.
- (239) Plane, J. M. C.; Whalley, C. L.; Frances-Soriano, L.; Goddard, A.; Harvey, J. N.; Glowacki, D. R.; Viggiano, A. A. *J. Chem. Phys.* **2012**, *137*, 014310.
- (240) Schinke, R.; McBane, G. C. *J. Chem. Phys.* **2010**, *132*, 044305.
- (241) McBane, G. C.; Nguyen, L. T.; Schinke, R. *J. Chem. Phys.* **2010**, *133*, 144312.
- (242) Tully, J. C. *J. Chem. Phys.* **2012**, *137*, 22A301.
- (243) Zener, C. *Proc. R. Soc. Math. Phys. Eng. Sci.* **1932**, *137*, 696.
- (244) Harvey, J. N. *Phys. Chem. Chem. Phys.* **2007**, *9*, 331.
- (245) Levine, B. G.; Martinez, T. J. In *Annual Review of Physical Chemistry*; Annual Reviews: Palo Alto, 2007; Vol. 58, pp 613–634.
- (246) Beck, M. H.; Jackle, A.; Worth, G. A.; Meyer, H. D. *Phys. Rep.-Rev. Sect. Phys. Lett.* **2000**, *324*, 1.
- (247) Wolfe, G. M.; Crouse, J. D.; Parrish, J. D.; St. Clair, J. M.; Beaver, M. R.; Paulot, F.;

Yoon, T. P.; Wennberg, P. O.; Keutsch, F. N. *Phys. Chem. Chem. Phys.* **2012**, *14*, 7276.

(248) Nehr, S.; Bohn, B.; Dorn, H.-P.; Fuchs, H.; Haeseler, R.; Hofzumahaus, A.; Li, X.;

Rohrer, F.; Tillmann, R.; Wahner, A. *Atmospheric Chem. Phys.* **2014**, *14*, 6941.

(249) Nikitin, E. E.; Troe, J. *Phys. Chem. Chem. Phys.* **2008**, *10*, 1483.

(250) Hirschfelder, J. O.; Curtiss, C. F.; Bird, R. B. *Molecular theory of gases and liquids*;

Wiley: London, 1954.

(251) Jasper, A. W.; Miller, J. A. *Combust. Flame* **2014**, *161*, 101.

(252) Tardy, D. C.; Rabinovitch, B. S. *Chem. Rev.* **1977**, *77*, 369.

(253) Oref, I.; Tardy, D. C. *Chem. Rev.* **1990**, *90*, 1407.

(254) Flynn, G. W.; Parmenter, C. S.; Wodtke, A. M. *J. Phys. Chem.* **1996**, *100*, 12817.

(255) Barker, J. R.; Yoder, L. M.; King, K. D. *J. Phys. Chem. A* **2001**, *105*, 796.

(256) Hold, U.; Lenzer, T.; Luther, K.; Reihls, K.; Symonds, A. *Berichte Bunsen-Ges.-Phys.*

Chem. Chem. Phys. **1997**, *101*, 552.

(257) Troe, J. *J. Chem. Phys.* **1977**, *66*, 4745.

(258) Smith, S. C.; Gilbert, R. G. *Int. J. Chem. Kinet.* **1988**, *20*, 979.

(259) Miller, J. A.; Klippenstein, S. J.; Raffy, C. *J. Phys. Chem. A* **2002**, *106*, 4904.

(260) Barker, J. R. *Int. J. Chem. Kinet.* **2009**, *41*, 748.

(261) Lenzer, T.; Luther, K. *Phys. Chem. Chem. Phys.* **2004**, *6*, 955.

(262) Hold, U.; Lenzer, T.; Luther, K.; Reihls, K.; Symonds, A. C. *J. Chem. Phys.* **2000**, *112*,

4076.

(263) Hold, U.; Lenzer, T.; Luther, K.; Symonds, A. C. *J. Chem. Phys.* **2003**, *119*, 11192.

(264) Paul, A. K.; Kohale, S. C.; Pratihar, S.; Sun, R.; North, S. W.; Hase, W. L. *J. Chem.*

Phys. **2014**, *140*, 194103.

(265) Conte, R.; Houston, P. L.; Bowman, J. M. *J. Phys. Chem. A* **2014**, *118*, 7742.

(266) Houston, P. L.; Conte, R.; Bowman, J. M. *J. Phys. Chem. A* **2014**, *118*, 7758.

(267) Grigoleit, U.; Lenzer, T.; Luther, K. *Z. Phys. Chem.-Int. J. Res.* **2000**, *214*, 1065.

(268) Grigoleit, U.; Lenzer, T.; Luther, K.; Mutzel, M.; Takahara, A. *Phys. Chem. Chem. Phys.* **2001**, *3*, 2191.

(269) Lenzer, T.; Luther, K.; Troe, J.; Gilbert, R. G.; Lim, K. F. *J. Chem. Phys.* **1995**, *103*, 626.

(270) Lenzer, T.; Luther, K. *J. Chem. Phys.* **1996**, *105*, 10944.

(271) Jasper, A. W.; Oana, C. M.; Miller, J. A. *Proc. Combust. Inst.* **2014**, *35*, 197.

(272) Jasper, A. W.; Pelzer, K. M.; Miller, J. A.; Kamarchik, E.; Harding, L. B.; Klippenstein, S. J. *Science* **2014**, *346*, 1212.

(273) Nilsson, D.; Nordholm, S. *J. Chem. Phys.* **2002**, *116*, 7040.

(274) Nilsson, D.; Nordholm, S. *J. Chem. Phys.* **2003**, *119*, 11212.

(275) Lenzer, T.; Luther, K.; Nilsson, D.; Nordholm, S. *J. Phys. Chem. B* **2005**, *109*, 8325.

(276) Nilsson, D.; Nordholm, S. *J. Phys. Chem. A* **2006**, *110*, 3289.

(277) Jasper, A. W.; Miller, J. A. *J. Phys. Chem. A* **2009**, *113*, 5612.

(278) Jasper, A. W.; Miller, J. A. *J. Phys. Chem. A* **2011**, *115*, 6438.

(279) Lindemann, F. A.; Arrhenius, S.; Langmuir, I.; Dhar, N. R.; Perrin, J.; Lewis, W. C. M. *Trans. Faraday Soc.* **1922**, *17*, 598.

(280) Hinshelwood, C. N. *Proc. R. Soc. Lond. Ser. -Contain. Pap. Math. Phys. Character* **1926**, *113*, 230.

(281) McKee, K. W.; Blitz, M. A.; Cleary, P. A.; Glowacki, D. R.; Pilling, M. J.; Seakins, P.

W.; Wang, L. *J. Phys. Chem. A* **2007**, *111*, 4043.

(282) Klippenstein, S. J.; Miller, J. A. *J. Phys. Chem. A* **2002**, *106*, 9267.

(283) Georgievskii, Y.; Miller, J. A.; Burke, M. P.; Klippenstein, S. J. *J. Phys. Chem. A* **2013**, *117*, 12146.

(284) Bartis, J.; Widom, B. *J. Chem. Phys.* **1974**, *60*, 3474.

(285) Miller, J. A.; Klippenstein, S. J. *J. Phys. Chem. A* **2006**, *110*, 10528.

(286) Robertson, S. H.; Pilling, M. J.; Jitariu, L. C.; Hillier, I. H. *Phys. Chem. Chem. Phys.* **2007**, *9*, 4085.

(287) Miller, J. A.; Klippenstein, S. J. *Phys. Chem. Chem. Phys.* **2013**, *15*, 4744.

(288) Gillespie, D. T.; Hellander, A.; Petzold, L. R. *J. Chem. Phys.* **2013**, *138*, 170901.

(289) Gillespie, D. T. *J. Phys. Chem.* **1977**, *81*, 2340.

(290) Baldwin, A. C.; Barker, J. R.; Golden, D. M.; Duperrex, R.; Vandenberg, H. *Chem. Phys. Lett.* **1979**, *62*, 178.

(291) Barker, J. R. *Chem. Phys.* **1983**, *77*, 301.

(292) Vereecken, L.; Huyberechts, G.; Peeters, J. *J. Chem. Phys.* **1997**, *106*, 6564.

(293) In *Methods in Biomolecular Simulations*; Monticelli, L., Salonon, E., Eds.; Methods in Molecular Biology; Humana Press: Totowa, NJ, 2013; Vol. 924, pp 197–213.

(294) Demerdash, O.; Yap, E.-H.; Head-Gordon, T. *Annu. Rev. Phys. Chem. Vol 65* **2014**, *65*, 149.

(295) Kamerlin, S. C. L.; Warshel, A. *Wiley Interdiscip. Rev.-Comput. Mol. Sci.* **2011**, *1*, 30.

(296) Glowacki, D. R.; Orr-Ewing, A. J.; Harvey, J. N. *J. Chem. Phys.* **2011**, *134*, 214508.

(297) Yockel, S.; Schatz, G. C. In *Multiscale Molecular Methods in Applied Chemistry*;

Kirchner, B., Vrabec, J., Eds.; Springer-Verlag Berlin: Berlin, 2012; Vol. 307, pp 43–67.

(298) Braams, B. J.; Bowman, J. M. *Int. Rev. Phys. Chem.* **2009**, *28*, 577.

(299) Miller, Y.; Chaban, G. M.; Finlayson-Pitts, B. J.; Gerber, R. B. *J. Phys. Chem. A* **2006**, *110*, 5342.

(300) Miller, Y.; Gerber, R. B. *J. Am. Chem. Soc.* **2006**, *128*, 9594.

(301) Glowacki, D. R.; Reed, S. K.; Pilling, M. J.; Shalashilin, D. V.; Martínez-Núñez, E. *Phys. Chem. Chem. Phys.* **2009**, *11*, 963.

(302) Vaida, V.; Donaldson, D. J. *Phys. Chem. Chem. Phys.* **2014**, *16*, 827.

(303) Bowman, J. M.; Shepler, B. C. *Annu. Rev. Phys. Chem.* **2011**, *62*, 531.

(304) Bowman, J. M.; Suits, A. G. *Phys. Today* **2011**, *64*, 33.

(305) Bowman, J. M. *Mol. Phys.* **2014**, *112*, 2516.

(306) Mauguière, F. A. L.; Collins, P.; Ezra, G. S.; Farantos, S. C.; Wiggins, S. *J. Chem. Phys.* **2014**, *140*, 134112.

(307) Townsend, D.; Lahankar, S. A.; Lee, S. K.; Chambreau, S. D.; Suits, A. G.; Zhang, X.; Rheinecker, J.; Harding, L. B.; Bowman, J. M. *Science* **2004**, *306*, 1158.

(308) Herath, N.; Suits, A. G. *J. Phys. Chem. Lett.* **2011**, *2*, 642.

(309) Harding, L. B.; Georgievskii, Y.; Klippenstein, S. J. *J. Phys. Chem. A* **2010**, *114*, 765.

(310) Goncharov, V.; Herath, N.; Suits, A. G. *J. Phys. Chem. A* **2008**, *112*, 9423.

(311) Dey, A.; Fernando, R.; Abeysekera, C.; Homayoon, Z.; Bowman, J. M.; Suits, A. G. *J. Chem. Phys.* **2014**, *140*, 054305.

(312) Joalland, B.; Shi, Y.; Kamasah, A.; Suits, A. G.; Mebel, A. M. *Nat. Commun.* **2014**, *5*, 4064.

- (313) Klippenstein, S. J.; Georgievskii, Y.; Harding, L. B. *J. Phys. Chem. A* **2011**, *115*, 14370.
- (314) Harding, L. B.; Klippenstein, S. J.; Jasper, A. W. *J. Phys. Chem. A* **2012**, *116*, 6967.
- (315) Iyengar, S. S.; Li, X.; Sumner, I. In *Advances in Quantum Chemistry, Vol 55: Applications of Theoretical Methods to Atmospheric Science*; Sabin, J. R., Brandas, E., Eds.; Elsevier Academic Press Inc: San Diego, 2008; Vol. 55, pp 333–353.
- (316) Dietrick, S. M.; Pacheco, A. B.; Phatak, P.; Stevens, P. S.; Iyengar, S. S. *J. Phys. Chem. A* **2012**, *116*, 399.
- (317) Jubb, A. M.; Hua, W.; Allen, H. C. *Acc. Chem. Res.* **2012**, *45*, 110.
- (318) Tobias, D. J.; Stern, A. C.; Baer, M. D.; Levin, Y.; Mundy, C. J. *Annu. Rev. Phys. Chem. Vol 64* **2013**, *64*, 339.
- (319) Simpson, W. R.; von Glasow, R.; Riedel, K.; Anderson, P.; Ariya, P.; Bottenheim, J.; Burrows, J.; Carpenter, L. J.; Friess, U.; Goodsite, M. E.; Heard, D.; Hutterli, M.; Jacobi, H.-W.; Kaleschke, L.; Neff, B.; Plane, J.; Platt, U.; Richter, A.; Roscoe, H.; Sander, R.; Shepson, P.; Sodeau, J.; Steffen, A.; Wagner, T.; Wolff, E. *Atmospheric Chem. Phys.* **2007**, *7*, 4375.
- (320) Finlayson-Pitts, B. J. *Anal. Chem.* **2010**, *82*, 770.
- (321) Jungwirth, P.; Tobias, D. J. *J. Phys. Chem. B* **2002**, *106*, 6361.
- (322) Ottosson, N.; Heyda, J.; Wernersson, E.; Pokapanich, W.; Svensson, S.; Winter, B.; Ohrwall, G.; Jungwirth, P.; Bjorneholm, O. *Phys. Chem. Chem. Phys.* **2010**, *12*, 10693.
- (323) Gladich, I.; Roeselova, M. *Phys. Chem. Chem. Phys.* **2012**, *14*, 11371.
- (324) Liyana-Arachchi, T. P.; Valsaraj, K. T.; Hung, F. R. *J. Phys. Chem. A* **2012**, *116*, 2519.
- (325) Liyana-Arachchi, T. P.; Stevens, C.; Hansel, A. K.; Ehrenhauser, F. S.; Valsaraj, K. T.; Hung, F. R. *Phys. Chem. Chem. Phys.* **2013**, *15*, 3583.

- (326) Martins-Costa, M. T. C.; Anglada, J. M.; Francisco, J. S.; Ruiz-Lopez, M. F. *J. Am. Chem. Soc.* **2012**, *134*, 11821.
- (327) Murdachaew, G.; Varner, M. E.; Phillips, L. F.; Finlayson-Pitts, B. J.; Gerber, R. B. *Phys. Chem. Chem. Phys.* **2013**, *15*, 204.
- (328) Habartova, A.; Obisesan, A.; Minofar, B.; Roeselova, M. *Theor. Chem. Acc.* **2014**, *133*, 1455.
- (329) Nadykto, A. B.; Al Natsheh, A.; Yu, F.; Mikkelsen, K. V.; Herb, J. In *Advances in Quantum Chemistry, Vol 55: Applications of Theoretical Methods to Atmospheric Science*; Sabin, J. R., Brandas, E., Eds.; Elsevier Academic Press Inc: San Diego, 2008; Vol. 55, pp 449–478.
- (330) Loukonen, V.; Kuo, I.-F. W.; McGrath, M. J.; Vehkamaki, H. *Chem. Phys.* **2014**, *428*, 164.
- (331) Hammerich, A. D.; Finlayson-Pitts, B. J.; Gerber, R. B. *J. Phys. Chem. Lett.* **2012**, *3*, 3405.
- (332) Vayner, G.; Addepalli, S. V.; Song, K.; Hase, W. L. *J. Chem. Phys.* **2006**, *125*, 014317.
- (333) Xu, L.; Doubleday, C. E.; Houk, K. N. *J. Am. Chem. Soc.* **2010**, *132*, 3029.
- (334) Baeza-Romero, M. T.; Glowacki, D. R.; Blitz, M. A.; Heard, D. E.; Pilling, M. J.; Rickard, A. R.; Seakins, P. W. *Phys. Chem. Chem. Phys.* **2007**, *9*, 4114.
- (335) Pechukas, P.; Light, J. *J. Chem. Phys.* **1965**, *42*, 3281.
- (336) Pechukas, P.; Light, J.; Rankin, C. *J. Chem. Phys.* **1966**, *44*, 794.
- (337) Quack, M.; Troe, J. *Berichte Bunsen-Ges.-Phys. Chem. Chem. Phys.* **1974**, *78*, 240.
- (338) Quack, M.; Troe, J. *Berichte Bunsen-Ges.-Phys. Chem. Chem. Phys.* **1975**, *79*, 469.
- (339) Wittig, C.; Nadler, I.; Reisler, H.; Noble, M.; Catanzarite, J.; Radhakrishnan, G. *J. Chem.*

Phys. **1985**, 83, 5581.

(340) Nguyen, T. L.; Peeters, J.; Vereecken, L. *Phys. Chem. Chem. Phys.* **2009**, 11, 5643.

(341) Drozd, G. T.; Donahue, N. M. *J. Phys. Chem. A* **2011**, 115, 4381.

(342) Ruscic, B.; Pinzon, R. E.; Laszewski, G. von; Kodeboyina, D.; Burcat, A.; Leahy, D.;

Montoy, D.; Wagner, A. F. *J. Phys. Conf. Ser.* **2005**, 16, 561.

(343) Ruscic, B. *Int. J. Quantum Chem.* **2014**, 114, 1097.

(344) Ruscic, B.; Feller, D.; Peterson, K. A. *Theor. Chem. Acc.* **2014**, 133.

(345) Feller, D.; Peterson, K. A.; Ruscic, B. *Theor. Chem. Acc.* **2014**, 133, 1407.

(346) Baulch, D. L. *J. Phys. Chem. Ref. Data* **2005**, 34, 757.

(347) Nguyen, T. L.; Stanton, J. F.; Barker, J. R. *J. Phys. Chem. A* **2011**, 115, 5118.

(348) Nguyen, T. L.; Xue, B. C.; Weston, R. E.; Barker, J. R.; Stanton, J. F. *J. Phys. Chem.*

Lett. **2012**, 3, 1549.

(349) Weston, R. E.; Nguyen, T. L.; Stanton, J. F.; Barker, J. R. *J. Phys. Chem. A* **2013**, 117,

821.

(350) Miller, W. H. *J. Chem. Phys.* **1976**, 65, 2216.

(351) Miller, W. H. *J. Phys. Chem.* **1983**, 87, 21.

(352) Troe, J. *J. Chem. Soc.-Faraday Trans.* **1994**, 90, 2303.

(353) Golden, D. M. *J. Phys. Chem. A* **2012**, 116, 4259.

(354) Vandenberk, S.; Vereecken, L.; Peeters, J. *Phys. Chem. Chem. Phys.* **2002**, 4, 461.

(355) Henon, E.; Canneaux, S.; Bohr, F.; Dóbé, S. *Phys. Chem. Chem. Phys.* **2003**, 5, 333.

(356) Caralp, F.; Forst, W.; Hénon, E.; Bergeat, A.; Bohr, F. *Phys. Chem. Chem. Phys.* **2006**, 8,

1072.

- (357) Shannon, R. J.; Blitz, M. A.; Goddard, A.; Heard, D. E. *Nat. Chem.* **2013**, *5*, 745.
- (358) Xu, S.; Lin, M. C. *Proc. Combust. Inst.* **2007**, *31*, 159.
- (359) Atkinson, R. *Chem. Rev.* **1986**, *86*, 69.
- (360) Peeters, J.; Vandenberk, S.; Piessens, E.; Pultau, V. *Chemosphere* **1999**, *38*, 1189.
- (361) Vereecken, L.; Peeters, J. *Chem. Phys. Lett.* **2001**, *333*, 162.
- (362) Vereecken, L.; Peeters, J. *Phys. Chem. Chem. Phys.* **2002**, *4*, 467.
- (363) Vereecken, L.; Peeters, J. *J. Phys. Chem. A* **2000**, *104*, 11140.
- (364) Peeters, J.; Vereecken, L.; Fantechi, G. *Phys. Chem. Chem. Phys.* **2001**, *3*, 5489.
- (365) Capouet, M.; Peeters, J.; Nozière, B.; Müller, J.-F. *Atmospheric Chem. Phys.* **2004**, *4*, 2285.
- (366) Capouet, M.; Müller, J.-F.; Ceulemans, K.; Compernelle, S.; Vereecken, L.; Peeters, J. *J. Geophys. Res.* **2008**, *113*, D02308.
- (367) Ceulemans, K.; Compernelle, S.; Peeters, J.; Müller, J.-F. *Atmos. Environ.* **2010**, *44*, 5434.
- (368) Vereecken, L.; Peeters, J. *Phys. Chem. Chem. Phys.* **2012**, *14*, 3802.
- (369) Fantechi, G.; Vereecken, L.; Peeters, J. *Phys. Chem. Chem. Phys.* **2002**, *4*, 5795.
- (370) Lelieveld, J.; Butler, T. M.; Crowley, J. N.; Dillon, T. J.; Fischer, H.; Ganzeveld, L.; Harder, H.; Lawrence, M. G.; Martinez, M.; Taraborrelli, D.; Williams, J. *Nature* **2008**, *452*, 737.
- (371) Hofzumahaus, A.; Rohrer, F.; Lu, K. D.; Bohn, B.; Brauers, T.; Chang, C. C.; Fuchs, H.; Holland, F.; Kita, K.; Kondo, Y.; Li, X.; Lou, S. R.; Shao, M.; Zeng, L. M.; Wahner, A.; Zhang, Y. H. *Science* **2009**, *324*, 1702.
- (372) Whalley, L. K.; Edwards, P. M.; Furneaux, K. L.; Goddard, A.; Ingham, T.; Evans, M. J.;

Stone, D.; Hopkins, J. R.; Jones, C. E.; Karunaharan, A.; Lee, J. D.; Lewis, A. C.; Monks, P. S.; Moller, S. J.; Heard, D. E. *Atmospheric Chem. Phys.* **2011**, *11*, 7223.

(373) Peeters, J.; Nguyen, T. L.; Vereecken, L. *Phys. Chem. Chem. Phys.* **2009**, *11*, 5935.

(374) Peeters, J.; Muller, J. F. *Phys. Chem. Chem. Phys.* **2010**, *12*, 14227.

(375) Nguyen, T. L.; Vereecken, L.; Peeters, J. *ChemPhysChem* **2010**, *11*, 3996.

(376) Da Silva, G.; Graham, C.; Wang, Z.-F. *Environ. Sci. Technol.* **2010**, *44*, 250.

(377) Crouse, J. D.; Paulot, F.; Kjaergaard, H. G.; Wennberg, P. O. *Phys. Chem. Chem. Phys.* **2011**, *13*, 13607.

(378) Miller, J. A.; Klippenstein, S. J.; Robertson, S. H. *Proc Combust Inst* **2000**, *28*, 1479.

(379) Miller, J. A.; Klippenstein, S. J. *Int J Chem Kinet* **2001**, *33*, 654.

(380) Hatakeyama, S.; Washida, N.; Akimoto, H. *J. Phys. Chem.* **1986**, *90*, 173.

(381) Bohn, B.; Siese, M.; Zetzsch, C. *J. Chem. Soc.-Faraday Trans.* **1996**, *92*, 1459.

(382) Bohn, B.; Zetzsch, C. *J. Chem. Soc.-Faraday Trans.* **1998**, *94*, 1203.

(383) Glowacki, D. R.; Pilling, M. J. *ChemPhysChem* **2010**, *11*, 3836.

(384) Maranzana, A.; Ghigo, G.; Tonachini, G.; Barker, J. R. *J. Phys. Chem. A* **2008**, *112*, 3656.

(385) Maranzana, A.; Barker, J. R.; Tonachini, G. *J. Phys. Chem. A* **2008**, *112*, 3666.

(386) Glowacki, D. R.; Lockhart, J.; Blitz, M. A.; Klippenstein, S. J.; Pilling, M. J.; Robertson, S. H.; Seakins, P. W. *Science* **2012**, *337*, 1066.

(387) Tyndall, G. *Science* **2012**, *337*, 1046.

(388) Dibble, T. S.; Sha, Y.; Thornton, W. F.; Zhang, F. *J. Phys. Chem. A* **2012**, *116*, 7603.

(389) Schneider, W. F.; Wallington, T. J.; Barker, J. R.; Stahlberg, E. A. *Berichte Bunsen-Ges.-*

Phys. Chem. Chem. Phys. **1998**, *102*, 1850.

(390) Orlando, J. J.; Tyndall, G. S.; Bilde, M.; Ferronato, C.; Wallington, T. J.; Vereecken, L.; Peeters, J. *J. Phys. Chem. A* **1998**, *102*, 8116.

(391) Vereecken, L.; Peeters, J.; Orlando, J. J.; Tyndall, G. S.; Ferronato, C. *J. Phys. Chem. A* **1999**, *103*, 4693.

(392) Orlando, J. J.; Tyndall, G. S.; Vereecken, L.; Peeters, J. *J. Phys. Chem. A* **2000**, *104*, 11578.

(393) Caralp, F.; Forst, W.; Bergeat, A. *Phys. Chem. Chem. Phys.* **2008**, *10*, 5746.

(394) Bloss, C.; Wagner, V.; Jenkin, M. E.; Volkamer, R.; Bloss, W. J.; Lee, J. D.; Heard, D. E.; Wirtz, K.; Martin-Reviejo, M.; Rea, G.; Wenger, J. C.; Pilling, M. J. *Atmospheric Chem. Phys.* **2005**, *5*, 641.

(395) Carter, W. P. L.; Heo, G. *Atmos. Environ.* **2013**, *77*, 404.

(396) Glowacki, D. R.; Wang, L.; Pilling, M. J. *J. Phys. Chem. A* **2009**, *113*, 5385.

(397) Lay, T. H.; Bozzelli, J. W.; Seinfeld, J. H. *J. Phys. Chem.* **1996**, *100*, 6543.

(398) Ghigo, G.; Tonachini, G. *J. Am. Chem. Soc.* **1998**, *120*, 6753.

(399) Ghigo, G.; Tonachini, G. *J. Am. Chem. Soc.* **1999**, *121*, 8366.

(400) Motta, F.; Ghigo, G.; Tonachini, G. *J. Phys. Chem. A* **2002**, *106*, 4411.

(401) Bohn, B.; Zetzsch, C. *Phys. Chem. Chem. Phys.* **1999**, *1*, 5097.

(402) Raoult, S.; Rayez, M. T.; Rayez, J. C.; Lesclaux, R. *Phys. Chem. Chem. Phys.* **2004**, *6*, 2245.

(403) Birdsall, A. W.; Elrod, M. J. *J. Phys. Chem. A* **2011**, *115*, 5397.

(404) Wang, L.; Wu, R.; Xu, C. *J. Phys. Chem. A* **2013**, *117*, 14163.

(405) Wu, R.; Pan, S.; Li, Y.; Wang, L. *J. Phys. Chem. A* **2014**, *118*, 4533.

(406) Jimenez, J. L.; Canagaratna, M. R.; Donahue, N. M.; Prevot, A. S. H.; Zhang, Q.; Kroll, J. H.; DeCarlo, P. F.; Allan, J. D.; Coe, H.; Ng, N. L.; Aiken, A. C.; Docherty, K. S.; Ulbrich, I. M.; Grieshop, A. P.; Robinson, A. L.; Duplissy, J.; Smith, J. D.; Wilson, K. R.; Lanz, V. A.; Hueglin, C.; Sun, Y. L.; Tian, J.; Laaksonen, A.; Raatikainen, T.; Rautiainen, J.; Vaattovaara, P.; Ehn, M.; Kulmala, M.; Tomlinson, J. M.; Collins, D. R.; Cubison, M. J.; E.; Dunlea, J.; Huffman, J. A.; Onasch, T. B.; Alfarra, M. R.; Williams, P. I.; Bower, K.; Kondo, Y.; Schneider, J.; Drewnick, F.; Borrmann, S.; Weimer, S.; Demerjian, K.; Salcedo, D.; Cottrell, L.; Griffin, R.; Takami, A.; Miyoshi, T.; Hatakeyama, S.; Shimono, A.; Sun, J. Y.; Zhang, Y. M.; Dzepina, K.; Kimmel, J. R.; Sueper, D.; Jayne, J. T.; Herndon, S. C.; Trimborn, A. M.; Williams, L. R.; Wood, E. C.; Middlebrook, A. M.; Kolb, C. E.; Baltensperger, U.; Worsnop, D. R. *Science* **2009**, *326*, 1525.

(407) Riccobono, F.; Schobesberger, S.; Scott, C. E.; Dommen, J.; Ortega, I. K.; Rondo, L.; Almeida, J.; Amorim, A.; Bianchi, F.; Breitenlechner, M.; David, A.; Downard, A.; Dunne, E. M.; Duplissy, J.; Ehrhart, S.; Flagan, R. C.; Franchin, A.; Hansel, A.; Junninen, H.; Kajos, M.; Keskinen, H.; Kupc, A.; Kurten, A.; Kvashin, A. N.; Laaksonen, A.; Lehtipalo, K.; Makhmutov, V.; Mathot, S.; Nieminen, T.; Onnela, A.; Petaja, T.; Praplan, A. P.; Santos, F. D.; Schallhart, S.; Seinfeld, J. H.; Sipila, M.; Spracklen, D. V.; Stozhkov, Y.; Stratmann, F.; Tome, A.; Tsagkogeorgas, G.; Vaattovaara, P.; Viisanen, Y.; Vrtala, A.; Wagner, P. E.; Weingartner, E.; Wex, H.; Wimmer, D.; Carslaw, K. S.; Curtius, J.; Donahue, N. M.; Kirkby, J.; Kulmala, M.; Worsnop, D. R.; Baltensperger, U. *Science* **2014**, *344*, 717.

(408) Criegee, R.; Wenner, G. *Justus Liebigs Ann. Chem.* **1949**, *564*, 9.

(409) Criegee, R. *Angew. Chem. Int. Ed. Engl.* **1975**, *14*, 745.

- (410) Eskola, A. J.; Wojcik-Pastuszka, D.; Ratajczak, E.; Timonen, R. S. *Phys. Chem. Chem. Phys.* **2006**, *8*, 1416.
- (411) Sander, W. *Angew. Chem. Int. Ed. Engl.* **1990**, *29*, 344.
- (412) Bunnelle, W. H. *Chem. Rev.* **1991**, *91*, 335.
- (413) Anglada, J. M.; Bofill, J. M.; Olivella, S.; Solé, A. *J. Am. Chem. Soc.* **1996**, *118*, 4636.
- (414) Anglada, J. M.; Bofill, J. M. *J. Org. Chem.* **1997**, *62*, 2720.
- (415) Chen, B.-Z.; Anglada, J. M.; Huang, M.-B.; Kong, F. *J. Phys. Chem. A* **2002**, *106*, 1877.
- (416) Aplin-court, P.; Henon, E.; Bohr, F.; Ruiz-López, M. F. *Chem. Phys.* **2002**, *285*, 221.
- (417) Cremer, D.; Gauss, J.; Kraka, E.; Stanton, J. F.; Bartlett, R. J. *Chem. Phys. Lett.* **1993**, *209*, 547.
- (418) Fang, D.-C.; Fu, X.-Y. *J. Phys. Chem. A* **2002**, *106*, 2988.
- (419) Kalinowski, J.; Räsänen, M.; Heinonen, P.; Kilpeläinen, I.; Gerber, R. B. *Angew. Chem. Int. Ed.* **2014**, *53*, 265.
- (420) Ahrens, J.; Carlsson, P. T. M.; Hertl, N.; Olzmann, M.; Pfeifle, M.; Wolf, J. L.; Zeuch, T. *Angew. Chem. Int. Ed.* **2014**, *53*, 715.
- (421) Beames, J. M.; Liu, F.; Lu, L.; Lester, M. I. *J. Am. Chem. Soc.* **2012**, *134*, 20045.
- (422) Beames, J. M.; Liu, F.; Lu, L.; Lester, M. I. *J. Chem. Phys.* **2013**, *138*, 244307.
- (423) Lee, E. P. F.; Mok, D. K. W.; Shallcross, D. E.; Percival, C. J.; Osborn, D. L.; Taatjes, C. A.; Dyke, J. M. *Chem. - Eur. J.* **2012**, *18*, 12411.
- (424) Lehman, J. H.; Li, H.; Beames, J. M.; Lester, M. I. *J. Chem. Phys.* **2013**, *139*, 141103.
- (425) Liu, F.; Beames, J. M.; Green, A. M.; Lester, M. I. *J. Phys. Chem. A* **2014**, *118*, 2298.
- (426) Nakajima, M.; Endo, Y. *J. Chem. Phys.* **2013**, *139*, 101103.

- (427) Nakajima, M.; Endo, Y. *J. Chem. Phys.* **2014**, *140*, 011101.
- (428) Su, Y.-T.; Huang, Y.-H.; Witek, H. A.; Lee, Y.-P. *Science* **2013**, *340*, 174.
- (429) Sheps, L. *J. Phys. Chem. Lett.* **2013**, *4*, 4201.
- (430) Wheeler, S. E.; Ess, D. H.; Houk, K. N. *J. Phys. Chem. A* **2008**, *112*, 1798.
- (431) Zhao, Y.; Tishchenko, O.; Gour, J. R.; Li, W.; Lutz, J. J.; Piecuch, P.; Truhlar, D. G. *J. Phys. Chem. A* **2009**, *113*, 5786.
- (432) Lan, Y.; Zou, L.; Cao, Y.; Houk, K. N. *J. Phys. Chem. A* **2011**, *115*, 13906.
- (433) Huang, H.; Eskola, A. J.; Taatjes, C. A. *J. Phys. Chem. Lett.* **2012**, *3*, 3399.
- (434) Huang, H.; Rotavera, B.; Eskola, A. J.; Taatjes, C. A. *J. Phys. Chem. Lett.* **2013**, *4*, 3824.
- (435) Stone, D.; Blitz, M.; Daubney, L.; Ingham, T.; Seakins, P. *Phys. Chem. Chem. Phys.* **2013**, *15*, 19119.
- (436) McCarthy, M. C.; Cheng, L.; Crabtree, K. N.; Martinez, O.; Nguyen, T. L.; Womack, C. C.; Stanton, J. F. *J. Phys. Chem. Lett.* **2014**, *4*, 4133.
- (437) Nguyen, T. L.; McCarthy, M. C.; Stanton, J. F. *J. Phys. Chem. A* **2014**, DOI: 10.1021/jp510554g.
- (438) Bossolasco, A.; Farago, E. P.; Schoemaeker, C.; Fittschen, C. *Chem. Phys. Lett.* **2014**, *593*, 7.
- (439) Asatryan, R.; Bozzelli, J. W. *Phys. Chem. Chem. Phys.* **2008**, *10*, 1769.
- (440) Andersen, A.; Carter, E. A. *J. Phys. Chem. A* **2003**, *107*, 9463.
- (441) Andersen, A.; Carter, E. A. *Mol. Phys.* **2008**, *106*, 367.
- (442) Taatjes, C. A.; Welz, O.; Eskola, A. J.; Savee, J. D.; Scheer, A. M.; Shallcross, D. E.; Rotavera, B.; Lee, E. P. F.; Dyke, J. M.; Mok, D. K. W.; Osborn, D. L.; Percival, C. J. *Science* **2013**,

340, 177.

(443) Sheps, L.; Scully, A. M.; Au, K. *Phys. Chem. Chem. Phys.* **2014**, *16*, 26701.

(444) Smith, M. C.; Ting, W.-L.; Chang, C.-H.; Takahashi, K.; Boering, K. A.; Lin, J. J.-M. *J. Chem. Phys.* **2014**, *141*, 074302.

(445) Li, J.; Carter, S.; Bowman, J. M.; Dawes, R.; Xie, D.; Guo, H. *J. Phys. Chem. Lett.* **2014**, *5*, 2364.

(446) Meng, Q.; Meyer, H.-D. *J. Chem. Phys.* **2014**, *141*, 124309.

(447) Liu, F.; Beames, J. M.; Petit, A. S.; McCoy, A. B.; Lester, M. I. *Science* **2014**, *345*, 1596.

(448) Samanta, K.; Beames, J. M.; Lester, M. I.; Subotnik, J. E. *J. Chem. Phys.* **2014**, *141*, 134303.

(449) Kuwata, K. T.; Hermes, M. R.; Carlson, M. J.; Zogg, C. K. *J. Phys. Chem. A* **2010**, *114*, 9192.

(450) Kuwata, K. T.; Kujala, B. J.; Morrow, Z. W.; Tonc, E. *Comput. Theor. Chem.* **2011**, *965*, 305.

(451) Nguyen, T. L.; Winterhalter, R.; Moortgat, G.; Kanawati, B.; Peeters, J.; Vereecken, L. *Phys. Chem. Chem. Phys.* **2009**, *11*, 4173.

(452) Vereecken, L.; Francisco, J. S. *Chem. Soc. Rev.* **2012**, *41*, 6259.

(453) Ryzhkov, A. B.; Ariya, P. A. *Phys. Chem. Chem. Phys.* **2004**, *6*, 5042.

(454) Anglada, J. M.; González, J.; Torrent-Sucarrat, M. *Phys. Chem. Chem. Phys.* **2011**, *13*, 13034.

(455) Gutbrod, R.; Schindler, R. N.; Kraka, E.; Cremer, D. *Chem. Phys. Lett.* **1996**, *252*, 221.

(456) Olzmann, M.; Kraka, E.; Cremer, D.; Gutbrod, R.; Andersson, S. *J. Phys. Chem. A* **1997**,

101, 9421.

(457) Kroll, J. H.; Sahay, S. R.; Anderson, J. G.; Demerjian, K. L.; Donahue, N. M. *J. Phys.*

Chem. A **2001**, *105*, 4446.

(458) Selçuki, C.; Aviyente, V. *J. Mol. Model.* **2001**, *7*, 70.

(459) Zhang, D.; Zhang, R. *J. Am. Chem. Soc.* **2002**, *124*, 2692.

(460) Gutbrod, R.; Kraka, E.; Schindler, R. N.; Cremer, D. *J. Am. Chem. Soc.* **1997**, *119*, 7330.

(461) Leonardo, T.; Baptista, L.; da Silva, E. C.; Arbilla, G. *J. Phys. Chem. A* **2011**, *115*, 7709.

(462) Chuong, B.; Zhang, J.; Donahue, N. M. *J. Am. Chem. Soc.* **2004**, *126*, 12363.

(463) Kuwata, K. T.; Templeton, K. L.; Hasson, A. S. *J. Phys. Chem. A* **2003**, *107*, 11525.

(464) Zhang, D.; Zhang, R. *J. Chem. Phys.* **2005**, *122*, 114308.

(465) Sun, T.; Wang, Y.; Zhang, C.; Sun, X.; Wang, W. *Atmos. Environ.* **2011**, *45*, 1725.

(466) Berndt, T.; Voigtländer, J.; Stratmann, F.; Junninen, H.; Mauldin, R. L.; Sipilä, M.;

Kulmala, M.; Herrmann, H. *Phys. Chem. Chem. Phys.* **2014**, *16*, 19130.

(467) Fenske, J. D.; Hasson, A. S.; Ho, A. W.; Paulson, S. E. *J. Phys. Chem. A* **2000**, *104*,

9921.

(468) Berndt, T.; Jokinen, T.; Mauldin, R. L.; Petäjä, T.; Herrmann, H.; Junninen, H.;

Paasonen, P.; Worsnop, D. R.; Sipilä, M. *J. Phys. Chem. Lett.* **2012**, *3*, 2892.

(469) Horie, O.; Schafer, C.; Moortgat, G. K. *Int. J. Chem. Kinet.* **1999**, *31*, 261.

(470) Horie, O.; Neeb, P.; Moortgat, G. K. *Int. J. Chem. Kinet.* **1997**, *29*, 461.

(471) Novelli, A.; Vereecken, L.; Lelieveld, J.; Harder, H. *Phys. Chem. Chem. Phys.* **2014**, *16*,

19941.

(472) Newland, M. J.; Rickard, A. R.; Alam, M. S.; Vereecken, L.; Muñoz, A.; Ródenas, M.;

Bloss, W. J. *Phys. Chem. Chem. Phys.* **2015**, *17*, 4076.

(473) Kurtén, T.; Donahue, N. M. *J. Phys. Chem. A* **2012**, *116*, 6823.

(474) Vereecken, L.; Nguyen, T. L.; Hermans, I.; Peeters, J. *Chem. Phys. Lett.* **2004**, *393*, 432.

(475) Winterhalter, R.; Herrmann, F.; Kanawati, B.; Nguyen, T. L.; Peeters, J.; Vereecken, L.;

Moortgat, G. K. *Phys. Chem. Chem. Phys.* **2009**, *11*, 4152.

(476) Stone, D.; Blitz, M.; Daubney, L.; Howes, N. U. M.; Seakins, P. *Phys. Chem. Chem.*

Phys. **2014**, *16*, 1139.

(477) Liu, Y.; Bayes, K. D.; Sander, S. P. *J. Phys. Chem. A* **2014**, *118*, 741.

(478) Berndt, T.; Jokinen, T.; Sipilä, M.; Mauldin, R. L.; Herrmann, H.; Stratmann, F.;

Junninen, H.; Kulmala, M. *Atmos. Environ.* **2014**, *89*, 603.

(479) Carlsson, P. T. M.; Keunecke, C.; Krüger, B. C.; Maaß, M.-C.; Zeuch, T. *Phys. Chem.*

Chem. Phys. **2012**, *14*, 15637.

(480) Cox, R. A.; Penkett, S. A. *Nature* **1971**, *230*, 321.

(481) Hatakeyama, S.; Kobayashi, H.; Akimoto, H. *J. Phys. Chem.* **1984**, *88*, 4736.

(482) Hatakeyama, S.; Kobayashi, H.; Lin, Z. Y.; Takagi, H.; Akimoto, H. *J. Phys. Chem.*

1986, *90*, 4131.

(483) Jiang, L.; Lan, R.; Xu, Y.-S.; Zhang, W.-J.; Yang, W. *Int. J. Mol. Sci.* **2013**, *14*, 5784.

(484) Berresheim, H.; Adam, M.; Monahan, C.; O'Dowd, C.; Plane, J. M. C.; Bohn, B.;

Rohrer, F. *Atmospheric Chem. Phys. Discuss.* **2014**, *14*, 1159.

(485) Boy, M.; Mogensen, D.; Smolander, S.; Zhou, L.; Nieminen, T.; Paasonen, P.; Plass-

Dülmer, C.; Sipilä, M.; Petäjä, T.; Mauldin, L.; Berresheim, H.; Kulmala, M. *Atmospheric Chem. Phys.*

2013, *13*, 3865.

- (486) Mauldin, R. L.; Berndt, T.; Sipilä, M.; Paasonen, P.; Petäjä, T.; Kim, S.; Kurtén, T.; Stratmann, F.; Kerminen, V.-M.; Kulmala, M. *Nature* **2012**, *488*, 193.
- (487) Percival, C.; Welz, O.; Eskola, A. J.; Savee, J. D.; Osborn, D. L.; Topping, D. O.; Lowe, D.; Utembe, S.; Bacak, A.; McFiggans, G.; Cooke, M.; Archibald, A. T.; Jenkin, M.; Derwent, R. G.; Riipinen, I.; Mok, D.; Lee, E. P. F.; Dyke, J.; Taatjes, C. A.; Shallcross, D. E. *Faraday Discuss.* **2013**, *165*, 45.
- (488) Sarwar, G.; Fahey, K.; Kwok, R.; Gilliam, R. C.; Roselle, S. J.; Mathur, R.; Xue, J.; Yu, J.; Carter, W. P. L. *Atmos. Environ.* **2013**, *68*, 186.
- (489) Sarwar, G.; Simon, H.; Fahey, K.; Mathur, R.; Goliff, W. S.; Stockwell, W. R. *Atmos. Environ.* **2014**, *85*, 204.
- (490) Aplincourt, P.; Ruiz-López, M. F. *J. Phys. Chem. A* **2000**, *104*, 380.
- (491) Kurtén, T.; Bonn, B.; Vehkamäki, H.; Kulmala, M. *J. Phys. Chem. A* **2007**, *111*, 3394.
- (492) Kurtén, T.; Lane, J. R.; Jørgensen, S.; Kjaergaard, H. G. *J. Phys. Chem. A* **2011**, *115*, 8669.
- (493) Chao, W.; Hsieh, J.-T.; Chang, C.-H.; Lin, J. J.-M. *Science* **2015**, *347*, 751.
- (494) Huang, D.; Chen, Z. M.; Zhao, Y.; Liang, H. *Atmospheric Chem. Phys.* **2013**, *13*, 5671.
- (495) Ryzhkov, A. B.; Ariya, P. A. *Chem. Phys. Lett.* **2003**, *367*, 423.
- (496) Ryzhkov, A. B.; Ariya, P. A. *Chem. Phys. Lett.* **2006**, *419*, 479.
- (497) Lewis, T. R.; Blitz, M. A.; Heard, D. E.; Seakins, P. W. *Phys. Chem. Chem. Phys.* **2015**, *17*, 4859.
- (498) Welz, O.; Eskola, A. J.; Sheps, L.; Rotavera, B.; Savee, J. D.; Scheer, A. M.; Osborn, D. L.; Lowe, D.; Murray Booth, A.; Xiao, P.; Anwar H. Khan, M.; Percival, C. J.; Shallcross, D. E.;

Taatjes, C. A. *Angew. Chem.* **2014**, *126*, 4635.

(499) Neeb, P.; Sauer, F.; Horie, O.; Moortgat, G. K. *Atmos. Environ.* **1997**, *31*, 1417.

(500) Tobias, H. J.; Ziemann, P. J. *J. Phys. Chem. A* **2001**, *105*, 6129.

(501) Sipila, M.; Jokinen, T.; Berndt, T.; Richters, S.; Makkonen, R.; Donahue, N. M.;

Mauldin, R. L.; Kurten, T.; Paasonen, P.; Sarnela, N.; Ehn, M.; Junninen, H.; Rissanen, M. P.;

Thornton, J.; Stratmann, F.; Herrmann, H.; Worsnop, D. R.; Kulmala, M.; Kerminen, V.-M.; Petaja, T.

Atmospheric Chem. Phys. **2014**, *14*, 12143.

(502) Long, B.; Cheng, J.-R.; Tan, X.; Zhang, W. *J. Mol. Struct. THEOCHEM* **2009**, *916*, 159.

(503) Kumar, M.; Busch, D. H.; Subramaniam, B.; Thompson, W. *Phys Chem Chem Phys*

2014, *16*, 22968.

(504) Jalan, A.; Allen, J. W.; Green, W. H. *Phys. Chem. Chem. Phys.* **2013**, *15*, 16841.

(505) Taatjes, C. A.; Welz, O.; Eskola, A. J.; Savee, J. D.; Osborn, D. L.; Lee, E. P. F.; Dyke, J.

M.; Mok, D. W. K.; Shallcross, D. E.; Percival, C. J. *Phys. Chem. Chem. Phys.* **2012**, *14*, 10391.

(506) Crehuet, R.; Anglada, J. M.; Cremer, D.; Bofill, J. M. *J. Phys. Chem. A* **2002**, *106*, 3917.

(507) Story, P. R.; Burgess, J. R. *J. Am. Chem. Soc.* **1967**, *89*, 5726.

(508) Keul, H.; Choi, H.; Kuczkowski, R. *J. Org. Chem.* **1985**, *50*, 3365.

(509) Sadezky, A.; Chaimbault, P.; Mellouki, A.; Römpf, A.; Winterhalter, R.; Le Bras, G.;

Moortgat, G. K. *Atmospheric Chem. Phys.* **2006**, *6*, 5009.

(510) Buras, Z. J.; Elsamra, R. M. I.; Jalan, A.; Middaugh, J. E.; Green, W. H. *J. Phys. Chem.*

A **2014**, *118*, 1997.

(511) Presto, A. A.; Donahue, N. M. *J. Phys. Chem. A* **2004**, *108*, 9096.

(512) Ouyang, B.; McLeod, M. W.; Jones, R. L.; Bloss, W. J. *Phys. Chem. Chem. Phys.* **2013**,

15, 17070.

(513) Kumar, M.; Busch, D. H.; Subramaniam, B.; Thompson, W. H. *J. Phys. Chem. A* **2014**, *118*, 1887.

(514) Su, F.; Calvert, J. G.; Shaw, J. H. *J. Phys. Chem.* **1980**, *84*, 239.

(515) Sadezky, A.; Winterhalter, R.; Kanawati, B.; Römpp, A.; Spengler, B.; Mellouki, A.; Le Bras, G.; Chaimbault, P.; Moortgat, G. K. *Atmospheric Chem. Phys.* **2008**, *8*, 2667.

(516) Anglada, J. M.; Olivella, S.; Solé, A. *Phys. Chem. Chem. Phys.* **2013**, *15*, 18921.

(517) Kjaergaard, H. G.; Kurtén, T.; Nielsen, L. B.; Jørgensen, S.; Wennberg, P. O. *J. Phys. Chem. Lett.* **2013**, 2525.

(518) Wei, W.; Zheng, R.; Pan, Y.; Wu, Y.; Yang, F.; Hong, S. *J. Phys. Chem. A* **2014**, *118*, 1644.

(519) Su, Y.-T.; Lin, H.-Y.; Putikam, R.; Matsui, H.; Lin, M. C.; Lee, Y.-P. *Nat. Chem.* **2014**, *6*, 477.

(520) Chhantyal-Pun, R.; Davey, A.; Shallcross, D. E.; Percival, C. J.; Orr-Ewing, A. J. *Phys. Chem. Chem. Phys.* **2014**, *17*, 3617.

(521) Taatjes, C. A.; Shallcross, D. E.; Percival, C. *Phys. Chem. Chem. Phys.* **2014**, *16*, 1704.

(522) Jenkin, M. E.; Saunders, S. M.; Pilling, M. J. *Atmos. Environ.* **1997**, *31*, 81.

(523) Aschmann, S.; Atkinson, R. *Int. J. Chem. Kinet.* **1995**, *27*, 613.

(524) Peeters, J.; Boullart, W.; Pultau, V.; Vandenberg, S.; Vereecken, L. *J. Phys. Chem. A* **2007**, *111*, 1618.

(525) Gallego-Iniesta, M. P.; Cabanas, B.; Salgado, S.; Martinez, E.; Martin, P. *Atmos. Environ.* **2014**, *90*, 133.

- (526) Carstensen, H.-H.; Dean, A. M. *J. Phys. Chem. A* **2009**, *113*, 367.
- (527) Kerdouci, J.; Picquet-Varrault, B.; Doussin, J.-F. *ChemPhysChem* **2010**, *11*, 3909.
- (528) Kerdouci, J.; Picquet-Varrault, B.; Doussin, J.-F. *Atmos. Environ.* **2014**, *84*, 363.
- (529) King, M. D.; Canosa-Mas, C. E.; Wayne, R. P. *Phys. Chem. Chem. Phys.* **1999**, *1*, 2231.
- (530) Pfrang, C.; King, M. D.; Canosa-Mas, C. E.; Wayne, R. P. *Atmos. Environ.* **2006**, *40*, 1170.
- (531) Pfrang, C.; King, M.; Braeckevelt, M.; Canosamas, C.; Wayne, R. *Atmos. Environ.* **2008**, *42*, 3018.
- (532) King, M. D.; Canosa-Mas, C. E.; Wayne, R. P. *Phys. Chem. Chem. Phys.* **1999**, *1*, 2239.
- (533) Pfrang, C.; King, M. D.; Canosa-Mas, C. E.; Wayne, R. P. *Atmos. Environ.* **2006**, *40*, 1180.
- (534) Pfrang, C.; King, M. D.; Canosa-Mas, C. E.; Flugge, M.; Wayne, R. P. *Atmos. Environ.* **2007**, *41*, 1792.
- (535) McGillen, M. R.; Crosier, J.; Percival, C. J.; Sanchez-Reyna, G.; Shallcross, D. E. *Chemosphere* **2006**, *65*, 2035.
- (536) McGillen, M. R.; Percival, C. J.; Raventos-Duran, T.; Sanchez-Reyna, G.; Shallcross, D. E. *Atmos. Environ.* **2006**, *40*, 2488.
- (537) Leather, K. E.; McGillen, M. R.; Percival, C. J. *Phys. Chem. Chem. Phys.* **2010**, *12*, 2935.
- (538) McGillen, M. R.; Carey, T. J.; Archibald, A. T.; Wenger, J. C.; Shallcross, D. E.; Percival, C. J. *Phys. Chem. Chem. Phys.* **2008**, *10*, 1757.
- (539) McGillen, M. R.; Archibald, A. T.; Carey, T.; Leather, K. E.; Shallcross, D. E.; Wenger,

J. C.; Percival, C. J. *Phys. Chem. Chem. Phys.* **2011**, *13*, 2842.

(540) Fatemi, M. H.; Baher, E. *SAR QSAR Environ. Res.* **2009**, *20*, 77.

(541) Huang, X.; Yu, X.; Yi, B.; Zhang, S. *J. Atmospheric Chem.* **2012**, *69*, 201.

(542) Xu, Y.; Yu, X.; Zhang, S. *J. Braz. Chem. Soc.* **2013**, *24*, 1781.

(543) Li, X.; Zhao, W.; Li, J.; Jiang, J.; Chen, J.; Chen, J. *Chemosphere* **2013**, *92*, 1029.

(544) Yu, X.; Yi, B.; Wang, X.; Chen, J. *Atmos. Environ.* **2012**, *51*, 124.

(545) Senkan, S. M.; Quam, D. *J. Phys. Chem.* **1992**, *96*, 10837.

(546) Poutsma, M. L. *J. Phys. Chem. A* **2013**, *117*, 687.

(547) Orlando, J. J.; Tyndall, G. S.; Wallington, T. J. *Chem. Rev.* **2003**, *103*, 4657.

(548) Falgayrac, G.; Caralp, F.; Sokolowski-Gomez, N.; Devolder, P.; Fittschen, C. *Phys.*

Chem. Chem. Phys. **2004**, *6*, 4127.

(549) Johnson, D.; Cassanelli, P.; Cox, R. A. *Atmos. Environ.* **2004**, *38*, 1755.

(550) Méreau, R.; Rayez, M.-T.; Caralp, F.; Rayez, J.-C. *Phys. Chem. Chem. Phys.* **2000**, *2*, 3765.

(551) Somnitz, H.; Zellner, R. *Phys. Chem. Chem. Phys.* **2000**, *2*, 4319.

(552) Peeters, J.; Fantechi, G.; Vereecken, L. *J. Atmospheric Chem.* **2004**, *48*, 59.

(553) Méreau, R.; Rayez, M.-T.; Caralp, F.; Rayez, J.-C. *Phys. Chem. Chem. Phys.* **2003**, *5*, 4828.

(554) Vereecken, L.; Peeters, J. *Phys. Chem. Chem. Phys.* **2010**, *12*, 12608.

(555) King, M. D.; Canosa-Mas, C. E.; Wayne, R. P. *Atmos. Environ.* **2001**, *35*, 2081.

(556) Shallcross, D.; Raventos-duran, M. T.; Bardwell, M.; Bacak, A.; Solman, Z.; Percival, C. *J. Atmos. Environ.* **2005**, *39*, 763.

- (557) Jenkin, M. E.; Saunders, S. M.; Wagner, V.; Pilling, M. J. *Atmospheric Chem. Phys.* **2003**, *3*, 181.
- (558) Vereecken, L.; Peeters, J. *J. Phys. Chem. A* **2004**, *108*, 5197.
- (559) Vereecken, L.; Müller, J.-F.; Peeters, J. *Phys. Chem. Chem. Phys.* **2007**, *9*, 5241.
- (560) Birdsall, A. W.; Andreoni, J. F.; Elrod, M. J. *J. Phys. Chem. A* **2010**, *114*, 10655.
- (561) Blurock, E.; Battin-Leclerc, F.; Faravelli, T.; Green, W. H. In *Cleaner Combustion: Developing Detailed Chemical Kinetic Models*; BattinLeclerc, F., Simmie, J. M., Blurock, E., Eds.; Springer-Verlag Berlin: Berlin, 2013; pp 59–92.
- (562) Aumont, B.; Szopa, S.; Madronich, S. *Atmospheric Chem. Phys.* **2005**, *5*, 2497.
- (563) Camredon, M.; Aumont, B.; Lee-Taylor, J.; Madronich, S. *Atmospheric Chem. Phys.* **2007**, *7*, 5599.
- (564) Aumont, B.; Valorso, R.; Mouchel-Vallon, C.; Camredon, M.; Lee-Taylor, J.; Madronich, S. *Atmospheric Chem. Phys.* **2012**, *12*, 7577.
- (565) Green, W. H.; Allen, J. W.; Buesser, B. A.; Ashcraft, R. W.; Beran, G. J. O.; Class, C. A.; Gao, C.; Goldsmith, C. F.; Harper, M. R.; Jalan, A.; Keceli, M.; Magoon, G. R.; Matheu, D. M.; Merchant, S. S.; Mo, J. D.; Petway, S.; Raman, S.; Sharma, S.; Song, J.; Suleymanov, Y.; Van Geem, K. M.; Wen, J.; West, R. H.; Wong, A.; Wong, H.-W.; Yelvington, P. E.; Yee, N.; Yu, J. *RMG - Reaction Mechanism Generator v4.0.1*; <http://rmg.sourceforge.net/>, 2013.
- (566) Zádor, J.; Nahm, H. N. In *Joint meeting - US Sections of the Combustion Institute*; Curran Associates, Inc. , Red Hook, NY: Parc City, Utah, 2013; Vol. 2, pp 1693–1697.
- (567) Rappoport, D.; Galvin, C. J.; Zubarev, D. Y.; Aspuru-Guzik, A. *J. Chem. Theory Comput.* **2014**, *10*, 897.

- (568) Wang, L.-P.; Titov, A.; McGibbon, R.; Liu, F.; Pande, V. S.; Martinez, T. J. *Nat. Chem.* **2014**, *6*, 1044.
- (569) Zheng, S.; Pfaendtner, J. *J. Phys. Chem. C* **2014**, *118*, 10764.
- (570) Haag, M. P.; Vaucher, A. C.; Bosson, M.; Redon, S.; Reiher, M. *Chemphyschem* **2014**, *15*, 3301.
- (571) Saebo, S.; Pulay, P. *Annu. Rev. Phys. Chem.* **1993**, *44*, 213.
- (572) Ziólkowski, M.; Jansík, B.; Kjærgaard, T.; Jørgensen, P. *J. Chem. Phys.* **2010**, *133*, 014107.
- (573) Kats, D.; Manby, F. R. *J. Chem. Phys.* **2013**, *138*, 144101.

List of captions

Figure 1. Simplified potential energy surface for the reaction of glycolaldehyde with OH radicals, based on Galano *et al.*,¹¹ Méreau *et al.*,¹² and Viskolcz and Bérces.¹³

Figure 2. Simplified potential energy surface for the reaction of carbonyl oxides, CH₂OO, with SO₂, based on Vereecken *et al.*¹⁴

Figure 3. Singlet biradicals, a functionality present in some molecules or in the transition states of homolytical dissociation, are two-electron two-orbital systems that require multireference wavefunctions consisting of multiple configurations Φ to describe the ground state wavefunction.

Figure 4. The interaction of a chemical reaction, and the collisional energy transfer between reactant A and product P with bath gas M.

Figure 5. Schematic representation of the set up of a master equation model for dissociation. The bold horizontal lines represent the ground state energies of the reactant, AB and the products, A + B. The fine horizontal lines represent the edges of the energy grains. Microcanonical first order rate constants are shown for dissociation from the grain at energy E and for energy transfer between the grains at energy E and E'.

Figure 6. Bimolecular rate constants, $k(T)$, for OH + C₂H₂ at 210 K (circle), 233 K (square), 253 K (triangle), 298 K (diamond) and 373 K (star) in He. Also included as full lines are the Troe format rate coefficients obtained by fitting to a master equation fit to the experimental data. Based with permission on McKee *et al.*²⁸¹ Copyright 2007 American Chemical Society.

Figure 7. Schematic reaction for formation of AB from A+B, isomerisation to AB', and disssociation to fragments C+D.

Figure 8. Phenomenological reactions and rate coefficients for methoxymethyl + O₂, as an example of a typical R + O₂ reaction.

Figure 9. (a) Chemically significant eigenvalues (CSEs) for the methoxymethyl + O₂ reaction system: λ_1 , blue; λ_2 , red; λ_3 , black. **(b)** Phenomenological rate constants for the system as shown in Figure 8. Reaction for R (+ O₂) are shown as full lines, for RO₂ as short dashed lines and for QOOH as long dashed lines. For both figures [O₂] = 1 × 10¹⁶ molecule cm⁻³ and the nitrogen pressure is 500 Torr. Reprinted with permission from Eskola *et al.*²²² Copyright 2014, American Chemical Society

Figure 10. Stationary points on the potential energy surface for HO-C₂H₂ + O₂, obtained using B3LYP/6-311+G(3df,2p) geometry optimizations and subsequent G3X single-point energy calculations. CT is the *trans* β -hydroxyvinyl radical and CC is the *cis* radical. Reprinted with permission from Glowacki and Pilling.³⁸³ Copyright 2010 Wiley.

Figure 11. The reaction of acetylene with OH, followed by reaction with O₂ prior to thermalization. Reprinted with permission from Glowacki *et al.*³⁸⁶ Copyright 2012, American Association for the Advancement of Science.

Figure 12. Main stationary points on the potential energy surface for reaction of the OH_benzene adduct with O₂. Energies in kJ mol⁻¹. Reprinted with permission from Glowacki *et al.*³⁹⁶ Copyright 2009 Wiley.

Figure 13. Formation of the hydroperoxy allyl radical **3** via O₂ addition on the allylic OH adduct followed by a 1,6-H-migration.

Figure 14. OH formation from QOOH radicals after O₂ addition and 1,5-H-migration.

Figure 15. Reaction scheme for the ozonolysis of alkenes and subsequent reactions of the Criegee intermediates. Product yields of fragments and thermalized intermediates depends strongly on

the competition between collisional energy transfer and chemically activated reactions.

Figure 16. Non-traditional reactions of Criegee intermediates

Table 1. Barrier heights for unimolecular processes of stabilized Criegee intermediates. The alkyl substituent studied is a methyl group unless the number of carbons in the substituent is indicated, where prefix “c” indicates a cyclic substituent. Vereecken and Francisco⁴⁵² review a larger set of substituents studied in the literature.

Table 2. Rate coefficients for unimolecular decomposition of Criegee intermediates

Table 3. Rate coefficients ($\text{cm}^3 \text{ molecule}^{-1} \text{ s}^{-1}$) for the reaction of small Criegee intermediates with H_2O and $(\text{H}_2\text{O})_2$, including experimental data (exp.). For more extensive results, see refs. ^{449,452–454}